SEISMIC PERFORMANCE EVALUATION OF SWITCHBOARD

CABINETS USING NONLINEAR NUMERICAL MODELS

A Dissertation
Presented to
The Academic Faculty

by

Jieun Hur

In Partial Fulfillment
of the Requirements for the Degree
Doctor of Philosophy in the
School of Civil and Environmental Engineering

Georgia Institute of Technology

December, 2012

SEISMIC PERFORMANCE EVALUATION OF SWITCHBOARD

CABINETS USING NONLINEAR NUMERICAL MODELS

Approved by:

Dr. Barry J. Goodno, Co-Advisor
School of Civil and Environmental
Engineering
Georgia Institute of Technology

Dr. Reginald DesRoches
School of Civil and Environmental
Engineering
Georgia Institute of Technology

Dr. Roberto T. Leon
Department of Civil and Environmental
Engineering
*Virginia Polytechnic Institute and State
University*

Dr. James I. Craig, Co-Advisor
School of Aerospace Engineering
Georgia Institute of Technology

Dr. Bruce R. Ellingwood
School of Civil and Environmental
Engineering
Georgia Institute of Technology

Date Approved: 6/29/2012

ACKNOWLEDGEMENTS

I would like to show my appreciation for my thesis advisors, Dr. Barry J. Goodno and Dr. James I. Craig, for their decisive guidance and support from the beginning to the end of this study. Also I would like to thank the members of thesis committee, Dr. Reginald DesRoches, Dr. Bruce R. Ellingwood, and Dr. Roberto T. Leon for their helpful advice and valuable recommendations.

I must also acknowledge the support of Mr. Philip J. Caldwell and Mr. Jeffrey A. Gatscher at Square D. They provided me valuable information as well as chances to enhance my understanding about switchboard cabinets.

I would like to give my special thanks to my colleagues and best friends, Karthik, Tim, Nathan, and Stephanie for the memorable times we had together. Also, I would like to thank my former and current officemates at 522A Mason and my research fellows.

Most of all, I have to express all gratitude to my family who are praying for me every day in my country. In addition, I would like to thank my husband, Abdollah Shafieezadeh, for his endless support, encouragement, and love.

TABLE OF CONTENTS

Page

iii

LIST OF TABLES

LIST OF FIGURES

x

SUMMARY

Past earthquake events have shown that seismic damage to electrical power systems in commercial buildings, hospitals, and other systems such as public service facilities can cause serious economic losses as well as operational problems. A methodology for evaluation of the seismic vulnerability of electrical power systems is needed and all essential components of the system must be included. A key system component is the switchboard cabinet which houses many different elements which control and monitor electrical power usage and distribution within a building. Switchboard cabinets vary in size and complexity and are manufactured by a number of different suppliers; a typical cabinet design was chosen for detailed evaluation in this investigation.

This study presents a comprehensive framework for the evaluation of the seismic performance of electrical switchboard cabinets. This framework begins with the introduction and description of the essential equipment in building electrical power systems and explains possible seismic damage to this equipment. The shortcomings of previous studies are highlighted and advanced finite element models are developed to aid in their vulnerability estimation. Unlike previous research in this area, this study proposes practical, computationally efficient, and versatile numerical models, which can capture the critical nonlinear behavior of switchboard cabinets subjected to seismic excitations. A major goal of the current study was the development of nonlinear numerical models that can accommodate various support boundary conditions ranging from fixed, elasto-plastic to free.

Using both linear and nonlinear dynamic analyses, this study presents an enhanced evaluation of the seismic behavior of switchboard cabinets. First the dynamic characteristics of switchboard cabinets are determined and then their seismic performance is assessed through nonlinear time history analysis using an expanded suite of ground motions. The seismic responses and associated ground motions are described and analyzed using probabilistic seismic demand models (PSDMs). Based on the PSDMs, the effectiveness and practicality of common intensity measures are discussed for different components. Correlation of intensity measures and seismic responses are then estimated for each component, and their seismic performance and uncertainties are quantified in terms of engineering demand parameters. The results of this study are intended for use in the seismic vulnerability assessment of essential electrical equipment in order to achieve more reliable electrical power systems resulting in reduced overall risk of both physical and operational failures of this important class of nonstructural components.

CHAPTER I

INTRODUCTION

1.1   Problem Description

Earthquake damage to nonstructural components not only degrades their performance and can cause their normal functioning to cease but it also can lead to disruption in critical facilities such as hospitals, gas and electricity distribution stations, and nuclear power plants. As a consequence, damage to nonstructural components has been observed to cause the majority of economic losses after many seismic events. Among various nonstructural components, critical equipment functioning as part of electrical and mechanical systems is especially important to consider in estimating economic losses due to earthquakes. These observations have prompted more studies to investigate the seismic behavior of nonstructural equipment. The studies include 1) collecting empirical data pertaining to the damage and vulnerability of nonstructural components during specific seismic events, 2) developing fragility functions for these components using shake table tests, and 3) developing analytical models of equipment for dynamic analyses.

Past earthquake data and expert opinions comprise the empirical data which is often used to evaluate the seismic vulnerability of nonstructural components. A main problem with the empirical data, however, is the lack of adequate and objective observations to define the correlation between the dynamic response of nonstructural components and the characteristics of earthquakes. As a result, this approach can only be applied to limited

regions for which the correlation between the dynamic response of nonstructural components and characteristics of earthquake is clearly indicated. On the other hand, shake table tests help in understanding the linear and nonlinear seismic behavior of nonstructural components and the relationships between limit states and response measures. However, the abundance of these components in buildings, the wide variation in their configurations which depends on the manufacturer, and the range of support boundary conditions make it impractical to evaluate their seismic vulnerability through expensive shake table tests alone. Hence, the key to obtaining sufficiently accurate estimates of the vulnerability of such nonstructural components is through the development of analytical or numerical models and performance of sophisticated response analyses.

Although analytical models for nonstructural components have been developed to estimate their seismic response, such models may be limited by their application to specific cases such as components modeled as rigid blocks characterized by pure sliding or pure rocking with a simple symmetric structure and mass distribution. These analytical models cannot be used for electrical or mechanical equipment which have complex configurations and diverse combinations of devices and instruments contained within them. Furthermore, a single analytical model cannot capture the range of dynamic behaviors of complicated configurations as well as the nonlinear behavior of the entire nonstructural component under large seismic events. Most currently existing analytical models are based on detailed finite element representations that are costly and time-consuming to develop and cannot easily be adapted to the wide range of component configurations encountered in buildings. Nor do generic models of standard

configurations yield reliable estimates of the seismic vulnerability of complex or irregular nonstructural equipment.

Numerical models for nonstructural equipment generally are formulated using finite element (FE) techniques. The dynamic response results from detailed FE models have been shown to be quite accurate at providing results that agree well with those obtained from shake table tests, and FE models are far more economical and practical than conducting shake table tests. Additionally, FE models because of their higher fidelity are more capable than analytical models in evaluating various types of structures. A shortcoming of most numerical models for nonstructural equipment in previous studies is their inability to capture the full nonlinear behavior of equipment arising from the boundary conditions at the supports. The dynamic behavior of nonstructural equipment mounted on floors is quite different from that of the building itself during seismic events because the response of nonstructural equipment is quite sensitive to their support boundary conditions and the material properties of the contacting elements such as steel plate and concrete. The response of unrestrained equipment depends heavily on the material properties of the ground surface, while for restrained components the response depends on the type and properties of the restraints. In other words, the boundary conditions for nonstructural components play a significant role in determining the dominant dynamic behavior of the equipment, and therefore the associated seismic vulnerabilities can be starkly different depending on the boundary conditions. As a result, it is necessary to develop numerical models capable of capturing the complete nonlinear behavior of various types of nonstructural equipment including the effect of boundary conditions during time history analyses.

1.2 Objectives and Scope of Research

The goal of this study is to develop using nonlinear numerical models a framework for the seismic response assessment of nonstructural equipment mounted on building floors. Information about the seismic response of electrical and mechanical equipment is essential to assess the functional and physical damage to buildings during seismic events and to estimate their overall vulnerability. This study develops a practical and effective methodology for evaluation of the seismic response of certain nonstructural equipment in buildings. Among the various types of nonstructural equipment, this study focuses on electrical switchboard cabinets. Electrical switchboard cabinets are responsible for distributing electricity and therefore are an essential component in electrical power system used in buildings ranging from office buildings to commercial manufacturing or distribution facilities, healthcare facilities, and electrical power or nuclear power plant facilities at the largest scales. The typical type of electrical equipment is a complex structure assembled from steel frame members and flat plates supporting various electrical components, bus bars, wiring and instruments. For seismic vulnerability assessment, several limit states should be considered such as the displacement response at the connection between the switchboard cabinet and connecting electrical conduit, the acceleration at electrical circuit breakers, and the failure of the restraints. This study of electrical switchboard cabinets demonstrates an efficient modeling procedure to numerically evaluate the seismic response of complex nonstructural equipment. Such procedures are a fundamental part of seismic vulnerability assessments which must be carried out to estimate the performance of such equipment in buildings.

The specific tasks comprising this research are as follows:

1. Identify limitations of previous approaches in determining the seismic response of nonstructural components and present the necessity for developing detailed numerical models of nonstructural components and using advanced analyses techniques.

2. Generate simplified numerical models of switchboard cabinets using finite element methods, and evaluate the dynamic characteristics of switchboard cabinets using the numerical models

3. Assess the dynamic characteristics of linear finite element models by calculating their modal sensitivity to frame and panel connection stiffnesses.

4. Construct and validate finite element models for switchboard cabinets, and validate the boundary conditions of the numerical models by comparing the results of nonlinear time history analysis with those obtained using analytical solutions.

5. Conduct time history analyses using finite element models that account for nonlinear boundary conditions, and evaluate the dynamic characteristics of simplified nonlinear numerical models for switchboard cabinets to provide enhanced understanding of their behavior during seismic events.

6. Illustrate how these models can be used to generate probabilistic seismic demand models for switchboard cabinets considering different engineering demands such as displacements or accelerations at different locations. Also illustrate how the models can be employed to evaluate the seismic vulnerability of switchboard cabinets using selected suites of ground motions and compare them with those obtained using empirical data.

1.3 Outline of Thesis

This thesis is organized into eight chapters, outlined as follows:

Chapter 2 describes possible seismic damage to electrical equipment and presents previous research in the area of assessing the seismic vulnerability of electrical equipment through three different approaches.

Chapter 3 begins with an introduction to switchboard cabinets as one type of electrical equipment. Typical switchboards are selected, and their physical features are explained. Finite element models are then generated and validated by comparing their dynamic characteristics with the resonance search test data.

Chapter 4 presents different analytical models describing the nonlinear behavior of nonstructural components arising from boundary support conditions. Numerical models using finite element analysis are compared to the analytical models, and boundary conditions for the numerical models are validated.

Chapter 5 describes how to generate nonlinear finite element models combined with different boundary conditions for switchboard cabinets, and their dynamic characteristics are investigated using a time history analysis.

Chapter 6 describes an application using the finite element models developed in Chapter 5 to develop probabilistic seismic demand models (PSDMs) for switchboard cabinets using selected suites of ground motions. Based on the PSDMs, the seismic vulnerability of switchboard cabinets is evaluated.

Finally, in Chapter 7 summary and conclusions are drawn from the research and future research needs are outlined.

CHAPTER II

OVERVIEW OF SEISMIC VULNERABILITY OF ELECTRICAL EQUIPMENT

2.1   Seismic Damage to Electrical Equipment

Earthquake ground motions cause physical as well as functional damage to electrical equipment, and the damage to even one type of essential component can lead to the operational failure of the entire electrical power system in buildings, commercial/industrial facilities, and special facilities such as nuclear power plants and hospitals. Under strong earthquake shaking, the enclosure of electrical equipment which includes plates and frames can be damaged, the anchor bolts or connecting fasteners can be loosened, and electrical conduits can be deformed or ruptured. This type of physical damage can also lead to operational failure as well.

Moderate seismic shakings with lower acceleration levels still can induce the operational failure of electrical equipment without outward physical damage. Electrical equipment such as switchboard cabinets contains many different electrical devices, some of which are sensitive to high-frequency acceleration. Depending on the spectral content of earthquake ground motions, electrical components can be exposed to accelerations with high frequencies arising from resonance effects in the equipment housing, which may result in important components becoming inoperable and partial or total loss of system functionality. For example, an electrical relay is a common device in a large

number of electrical distribution and control systems, and relay chatter is a common functional problem that can develop under high-frequency seismic acceleration (NUREG, 1987).

Figures 2.1(a) and (b) show electrical cabinets that overturned after being subjected to strong seismic shakings that induced the physical damage as well as operational failure. Note that in Figure 2.1(a), the cabinets were initially anchored to the floor, while in Figure 2.1(b), the cabinets were unrestrained.

| (a) Seismic damage to anchored cabinets in 1985 Mexico Earthquake (Magnitude 8), FEMA 74 (2011), | (b) Seismic damage to unanchored cabinets in 2010 Haiti Earthquake (Magnitude 7), FEMA 74 (2011). |

Figure 2.1 Seismic Damage to Electrical Cabinets

Figure 2.2 illustrates seismic damage caused by the 2010 Haiti earthquake to electrical equipment located on the roof of the U.S. Embassy building in Port-au-Prince. Here the equipment was anchored but displaced approximately 2 inches during in the earthquake. This sliding behavior resulted from insufficient restraint, and such movement can cause physical damage to the connecting conduits as well as functional damage to the electrical system.
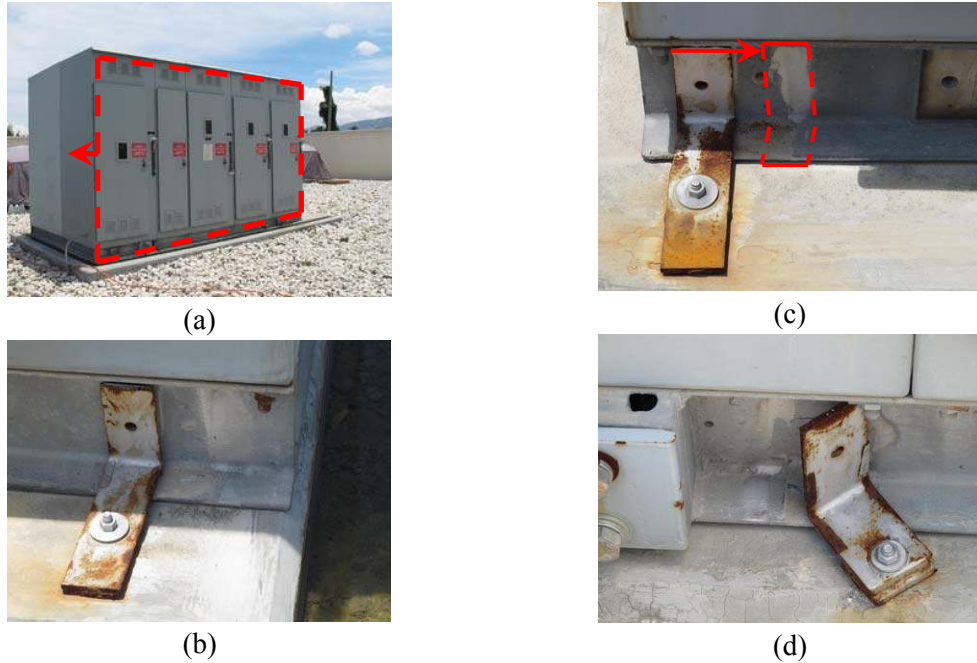
Figure 2.2 Seismic Damage to Electrical Equipment in the 2010 Haiti Earthquake (1)
Goodno et. al. (2011).

Additional seismic damage to electrical equipment located in the U.S. Embassy building in Port-au-Prince is presented in Figure 2.3. Anchor bolts have pulled out and localized failure has occurred at the corner of the concrete pad (Figures 2.3 (a)-(c)) as these electrical switchgear units moved back and forth during the earthquake. Note that the rocking behavior shown here may increase the acceleration, displacement, and drift of cabinets and cause physical as well as operational damage.

Figures 2.4 (a) and (b) illustrate typical conduits feeding electrical equipment, which continued working at the U.S. Embassy building and the Digicel building, respectively, after the 2010 Haiti Earthquake. Figure 2.4(a) shows a rigid feeder busway which showed no evidence of physical damage due to the provision of sufficient lateral restraints. In contrast, Figure 2.4(b) shows the significant deformation that occurred in the absence of restraint to conduits feeding an uninterruptable power supply (UPS)

system. As a result of the lack of restraint, these UPS cabinets slid as much as 5 inches during the earthquakes.

(a)

(b)

(c)
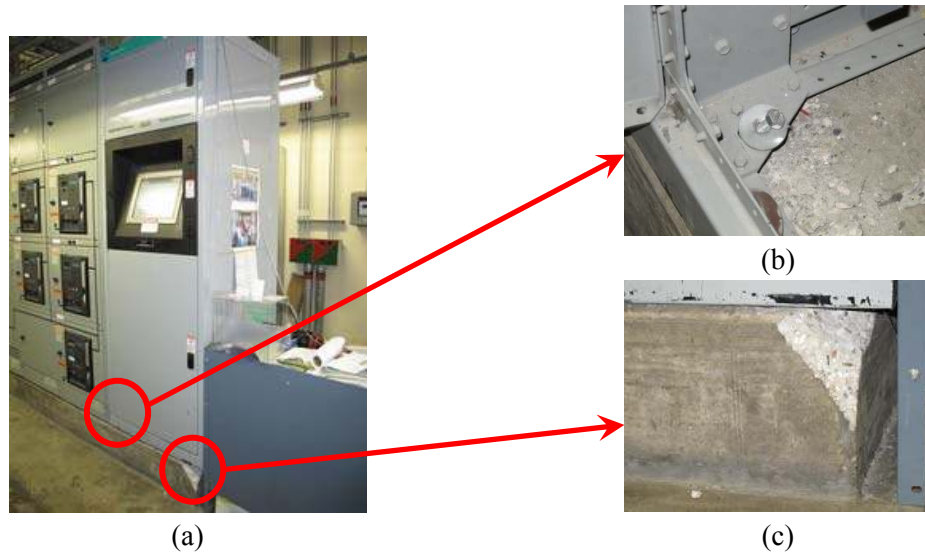
Figure 2.3 Seismic Damage to Electrical Equipment in the 2010 Haiti Earthquake (2)
Source: Goodno et. al. (2011)

(a) Busway at the U.S. Embassy

(b) Conduit at top of UPS at Digicel

Figure 2.4 Conduits attached to Electrical Equipment
Source: Goodno et. al. (2011)

2.2 Classification of the Seismic Vulnerability of Electrical Equipment

The study of the seismic vulnerability of electrical equipment in electric power systems requires the classification of the vulnerability of electrical components. Electrical equipment refers to any device powered by electricity, ranging from various household appliances to the essentials in a power distribution system such as an electric switchboard, a circuit breaker, or a transformer. For the seismic damage assessment associated with electrical equipment and electric power distribution systems, categorization of electrical equipment is necessary so that a fragility function can be defined for each category. This necessity stems from the fact that there are many different types of electrical equipment and the seismic vulnerability of a particular type of electrical equipment depends on its specific boundary conditions and mechanical configurations. A number of factors influence the seismic response of a specific type of equipment, such as its internal and external configurations, installed locations, support conditions, and the characteristics of the seismic excitation. As a result, this can lead to significant differences in the limit states used to define different damage states. Further, the seismic intensity measures correlated with the response of these complex electrical components should be developed specifically for each component for more accurate damage assessments.

For example, an electric switchboard typically consists of stacks of circuit breakers or fusible switches associated with control as well as relays, instrumentation, small control transformers, and distribution buses mounted in cabinets assembled using light metal framing enclosed by sheet metal panels. Failure of any of these switchboard components can lead to operational failure of the equipment. Electric devices such as circuit breakers

or fusible switches are sensitive to acceleration response, while the bus connections are sensitive to relative drift, and the connecting conduits are sensitive to the displacement at the top or bottom of the switchboard. More complex electrical equipment requires more detailed classifications or descriptions to define their seismic vulnerability.

Studies of the seismic damage assessment of nonstructural components have included damage to electrical equipment. However, there is a lack of research that focuses on the classification of seismic vulnerability for electrical components.

Scholl (1981) assessed the seismic damage to high-rise buildings and classified nonstructural components, but the categorization for electrical equipment was not studied in detail. The study assumed that mechanical and electrical equipment fall in the same category for which the same motion parameters such as the peak floor acceleration or velocity can describe the behavior of equipment.

Electrical components such as motor control centers, switchboards, or transformers are commonly used in buildings as essential elements in a power system. However, their seismic vulnerability and classification have been investigated only for the seismic damage assessment of special facilities, such as nuclear power plants and hospitals. It should be noted that the main functionality of these facilities relies on the performance of their electrical components in power systems. Therefore, the seismic damage of such equipment should be minimized for the sound operation of the facilities during and following strong earthquakes.

The Nuclear Regulatory Commission (NUREG, 1987) investigated the seismic fragility of various electrical components in nuclear power plants, including motor control centers, switchboards, panel boards, and power supplies. Shake table tests on

different specimens were conducted to define the seismic fragility of each component. As shown in Table 2.1, this study considered different damage states for each type of electrical equipment such as operational failure due to power loss and structural loosening. For the seismic intensity measure, ground accelerations as an input excitation were measured, but the acceleration or displacement responses of the components were not measured. Therefore, the dynamic response of electrical equipment was not defined in terms of engineering demands.

Table 2.1 Recommended Probabilistic Fragility Levels
(NUREG, 1987)

Equipment	Failure Mode	ZPA[*] (g)	ASA[**](g) @ 2% damping
Motor Control Center	Contact chatter	0.8	1.7
	Change of state of starter:		
	a) auxiliary contact	1.0	2.1
	b) main contact	1.1	2.4
	Major structural damage:		
	a) without seismic stiffeners	1.6	3.2
	b) with seismic stiffeners	1.9	4.6
Switchboard	Breaker tripping	1.8	3.9
Panel board	Breaker tripping:		
	a) possibly recoverable	1.0	3.2
	b) unrecoverable	2.1	4.2
DC Power Supply	Power loss for 0.5ms	2.6	6.5
	Output level variation:		
	a) 2%	3.5	8.2
	b) 10%	4.3	9.4

  * ZPA: Peak (zero-period) acceleration of the test input of the time history
  **APA: Average spectral acceleration for electrical equipment from a frequency range of
      4~16 Hz

Swan and Kassawara (1998) categorized industrial equipment in detail and presented a number of equipment seismic fragilities, as shown in Table 2.2. These fragility

functions are based on empirical and survey data from 25 earthquakes. Peak diaphragm acceleration (PDA) was used as the intensity measure instead of peak ground acceleration (PGA), with the assumption that PDA and PGA would be the same for components at ground level and PDA would be twice the PGA for components at the roof level. Furthermore, the seismic response of each electrical component was assumed based on the PGA without detailed classification of the damage state of each part of the equipment. Therefore, only the operational failure of each electrical component and the PDA of the installed location were considered. In addition, it was assumed that all of the components are fairly rugged without considering the nonlinear behavior of the electrical equipment under seismic loadings.

Table 2.2 Miscellaneous mechanical and electrical component fragilities
(Swan and Kassawara, 1998)

Component	x_m*	β**
Unanchored cabinet	0.52 g	0.62 g
Motor control center	0.79 g	0.52 g
Transformer	1.23 g	0.62 g
Low voltage switchgear	1.12 g	0.64 g
Med voltage switchgear	1.60 g	0.80 g
Distribution panel	1.75 g	0.68 g
Diesel generator	0.87 g	0.51 g
Inventor	1.20 g	0.57 g
Fan	2.69 g	0.93 g

*x_m: Median
**β: Logarithmic standard deviation

Porter and Kiremidjian (2001) and an Applied Technology Council report (ATC-58, 2007) refer to the data from the work by Swan and Kassawara (1998). The study by Porter and Kiremidjian (2001) summarized previous data for fragility functions of structural and nonstructural components and developed probabilistic and statistical

14

methods to evaluate the seismic vulnerability of individual buildings. This study formed the basis of the ATC-58 report, which deals with the performance based seismic design of structural and nonstructural components of a building.

The final report on Project SE-3 of the Mid-America Earthquake Center (Goodno et al, 2007), entitled "Nonstructural Seismic Evaluation of the Memphis Light, Gas, Water(MLGW) Operations Center", classified nonstructural components in the MLGW Operations Center and assigned seismic fragility functions to each component based on a literature review. Table 2.3 illustrates the fragility functions of electrical equipment presented in the SE-3 report. The fragility functions include the median (x_m) and logarithmic standard deviation (β) of peak diaphragm acceleration to reach the operational failure of each component. The data provides a useful reference that can be used to assess the economic losses due to the operational failure of electrical equipment. However, the study does not consider the dynamic characteristics of electrical equipment and therefore cannot model the seismic vulnerability of electrical equipment with different configurations and installation conditions accurately.

Table 2.3 Fragility Functions of Electrical Equipment
(Goodno et al, 2007)

Electrical Equipment	x_m	β	Reference
Switchgear, low volt.	1.1g	0.64g	Porter and Kiremidjian (2001), Table B-4 Assembly fragility & ATC-58(75%draft)
Switchgear, med. volt.	1.6g	0.8g	Porter and Kiremidjian (2001), Table B-4 Assembly fragility & ATC-58 (75%draft)
Switch gear	0.85g	0.5g	ATC 29-2 Seismic Risk Assessment of Nonstructural Components in Hospitals Table 2 Values of Components for Electric Power System
Load transfer switch	1.49g	0.56g	ATC 29-2 Seismic Risk Assessment of Nonstructural Components in Hospitals Table 2 Values of Components for Electric Power System
Transformer	1.23g	0.62g	ATC-58 (75% draft) Table E-11
12kV Transformers	0.65g	0.4g	ATC 29-2 Seismic Risk Assessment of Nonstructural Components in Hospitals Table 2 Values of Components for Electric Power System
Motor installation Motor control center	0.79g	0.52g	Porter and Kiremidjian (2001), Table B-4 Assembly fragility & ATC-58 (75%draft)
Motor control center	0.67g	0.43g	ATC 29-2 Seismic Risk Assessment of Nonstructural Components in Hospitals Table 2 Values of Components for Electric Power System
Elec. Cabinet	0.52g	0.62g	ATC-58 (75% draft) Table E-11
Distribution panel	1.75g	0.68g	ATC-58 (75% draft) Table E-11
Inverter	1.2g	0.57g	ATC-58 (75% draft) Table E-11
Battery Unit	0.9g	0.56g	ATC 29-2 Seismic Risk Assessment of Nonstructural Components in Hospitals Table 2 Values of Components for Electric Power System
Generator Diesel generator	0.87g	0.51g	Porter and Kiremidjian (2001), Table B-4 Assembly fragility & ATC-58 (75%draft)
New emergency generator	0.68g	0.24g	ATC 29-2 Seismic Risk Assessment of Nonstructural Components in Hospitals Table 1 Values of Components for Water System
Diesel generator	1.25g	0.36g	ATC 29-2 Seismic Risk Assessment of Nonstructural Components in Hospitals Table 2 Values of Components for Electric Power System
Start system	0.78g	0.21g	ATC 29-2 Seismic Risk Assessment of Nonstructural Components in Hospitals Table 1 Values of Components for Water System

Based on previous work, the classification for the seismic fragilities of electrical equipment has a number of limitations that prevent a more general seismic damage assessment of this type of equipment.

(1) Previous classifications do not incorporate detailed information about the equipment to evaluate its dynamic characteristics. Electrical equipment such as switchboards is configured in different sizes, weights, and layouts depending on the demands of customers as well as available designs of manufacturers. These characteristics determine the dynamic response under earthquake excitations. Therefore, more detailed information needs to be collected for accurate damage assessments.

(2) Previous fragility assessments were conducted under the assumption that the equipment is fully anchored. However, the support boundary conditions for the equipment cannot be perfectly fixed. In addition, empirical and experimental data show that the connection of the equipment to its supports can deform and behave nonlinearly even before reaching the operational failure stage especially during large seismic events. As a consequence, the classifications should consider more accurate representation and nonlinear characteristics of the equipment-support boundary condition (i.e., base interface) for accurate damage assessments.

(3) Although NUREC (1987) considers different damage states of a switchboard, most previous fragility data did not account for these different limit/damage states. Complex electrical equipment such as switchboards can reach the operational failure stage through a variety of paths, such as malfunctioning of electrical components and possible physical damage. In order to classify electrical

17

equipment appropriately, the different damage states should be properly accounted for and considered to achieve reasonable estimates of damage after a seismic event.

2.3   Approaches to Determine Seismic Vulnerability of Electrical Equipment

2.3.1   Empirical Data and Survey

Following most earthquakes, damage investigations and surveys are conducted to assess economic loss to electrical equipment through empirical data collection. However, most of these studies are limited to loss estimation at a macroscopic scale. They classified a large number of equipment into restricted groups according to the operational features rather than the dynamic characteristics of individual equipment. For instance, ATC-13 (1984) and Hazards U.S. (HAZUS) Standard Methodology (NIBS, 2003) present methods of evaluating seismic damage from inventory data by focusing on loss to buildings in an area rather than loss at the component level within a building. Therefore, electrical and mechanical components were not classified and henceforth not considered in the assessment of overall seismic vulnerability. The damage states for electrical and mechanical equipment considered in HAZUS (2003) are discussed in detail in Table 2.4.

Table 2.4 Damage States for Electrical or Mechanical Equipment
(HAZUS Manual, 2003)

Slight	In unanchored or on spring isolators, movement of the device and the consequent damage in attached piping or ducts
Moderate	Larger movements and more extensive damage, such as leakage of piping at few locations and derailment of machinery
Extensive	Toppling and falling of equipment on spring isolators; sliding or falling of unanchored equipment that may follow by breaking connections to piping and ducts; leakage at many locations;
Complete	Damage to equipment by sliding, overturning or failure of their supports leading to inoperability of the device; leakage of piping at many locations (some pipe and duct supports have failed causing pipes and ducts to fall down); bucking of the rails of elevator or failure of the supports and derailment of counterweights.

With more detailed classification, Swan and Kassawara (1998) categorized nonstructural components and collected fragility functions of electrical equipment based on the empirical data as previously shown in Table 2.2. Saeki, Tsubokawa, and Midorikawa (2000) also conducted surveys to collect the damage data of nonstructural components resulting from the 1995 Kobe earthquake. Based on the survey data, probabilistic fragility functions of nonstructural components including electrical equipment were derived. However, the JMA intensity (Japan Meteorological Agency seismic intensity scale) was used as the earthquake intensity measure for developing fragility functions, and therefore it could be subjective depending on the surveyed respondents. This is because JMA intensity does not state the scientific correlation between the earthquake intensity and the seismic responses of nonstructural components in terms of engineering parameters. Based on the JMA intensity, for example, the peak ground acceleration is approximated, and there is no simple and linear relationship between them.

19

The major limitation associated with empirically developed fragility functions is that, for several reasons, they tend to provide subjective and incomplete information without detailed classification and explicit observations. First, it is a complicated and difficult task to collect the damage data through survey and investigation. There are many different types of electrical components, and a particular type of equipment can also have different inner configurations despite the same exterior size and shape. The diversity and complexity of electrical equipment lead to differences in response and damage under the same seismic event. Second, it is difficult to judge the damage (or limit) states of each component from the empirical data. Malfunctioning of large and complex electrical equipment under different conditions could occur due to a variety of reasons. Through observations, it is hard to capture the process reaching different damage states as well as the correlation between the limits states and the seismic intensity measure. Finally, the determination of the critical engineering demand (response parameter) for each component may be difficult. This is because electrical devices and structural frames can be sensitive to different response parameters, such as displacement, drift, velocity, or acceleration depending on the location and installation condition. Furthermore, electrical devices such as circuit breakers are sensitive to acceleration amplitude as well as frequency. It is almost impossible to estimate the seismic response of various pieces of equipment through observations, and therefore it is necessary to assume intensity measures and response parameters for each component.

The end result is that the development of fragility functions for electrical components using empirical data and survey results has its own limitations, as stated above, due to the large variety and inherent complexity of the systems.

2.3.2 Shake Table Tests

Shake table tests are often used to define the seismic vulnerability of specific electrical equipment due to the limitations in the usage of empirical and survey data. The tests provide a medium for: 1) observing the process and the associated damage states; 2) recording objective data on engineering demands in order to correlate the seismic intensity measure to the response of the equipment; and 3) generating fragility functions for various levels of ground shaking.

The U.S. Nuclear Regulatory Commission document entitled Seismic Fragility Nuclear Power Plant Components (NUREG, 1987) illustrates how to determine the respective probabilistic fragility levels of electrical equipment using shake table tests of nonstructural components in nuclear power plants. The electrical equipment includes switchboards, motor control centers, panel boards, and power supplies. As shown in Table 2.2, the study considered several limit states such as malfunction and physical damage, and also suggested effective engineering demands (response demands) for the fragility functions such as zero-period acceleration and average spectral acceleration. The seismic response of electrical equipment was estimated using statistical methods and the resulting fragility functions are presented in terms of a median and lognormal standard deviation.

Shake table tests are also used as seismic qualification tests. Through these tests the seismic vulnerability of specific electrical components can be evaluated under the required seismic conditions suggested by standards such as IEEE 693 Recommended Practice for Seismic Design of Substations (2005) or AC156 (2010). The manufacturers that produce electrical equipment conduct the seismic qualification test to define the seismic vulnerability of their products. Figure 2.5 shows the required response spectrum

(RRS) for electrical equipment such as switchboards suggested by IEEE 693 and AC156, respectively. IEEE 693 describes the seismic qualification for various types of electrical components and evaluates each of them with three seismic qualification levels (high, moderate, and low). Figure 2.5(a) shows the high level of RRS for a switchboard suggested by IEEE 693-2005.

(a) IEEE 693-2005 (High Level RRS)   (b) ICBOES AC156
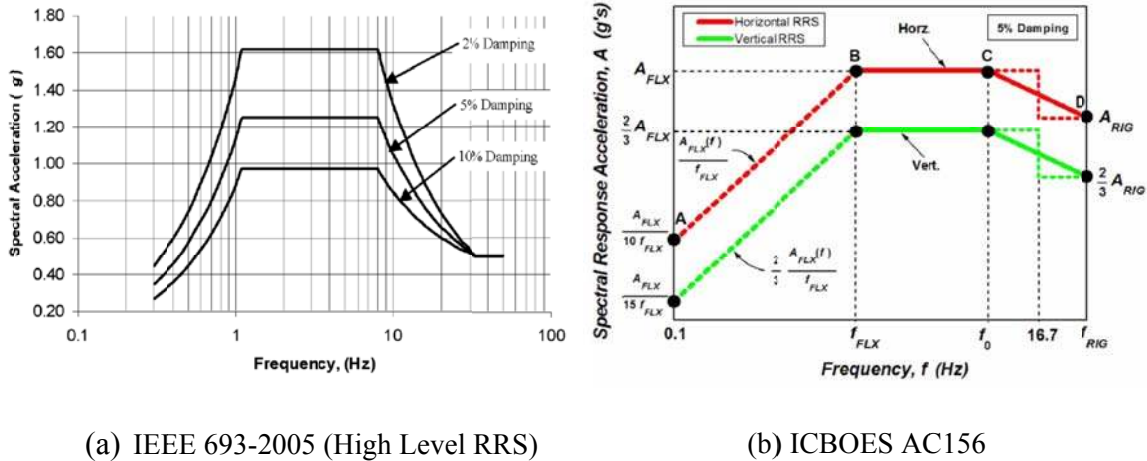
Figure 2.5 Required Response Spectrum for Electrical Equipment

Based on the Standard IEEE 693 (2005), Gatscher et al. (2006) developed a generic dynamic qualification test method for the seismic validation of electrical equipment for commercial applications. The method is consistent with the lateral force design requirements for nonstructural components presented in the U.S. building codes such as IBC (2009) and ASCE 7(2010). Procedures related to the seismic demand requirements for secondary systems and nonstructural components from the U.S. building codes were adopted and the RRS (Required Response Spectrum) from AC156 (2010) was modified to consider the installation condition of electrical equipment and building dynamic characteristics. In this study, several issues were addressed including: 1) the importance of the rationalization criteria of the test specimens; 2) the definition of lateral force for

nonstructural components attached to buildings; 3) the derivation of the seismic qualifications such as RRS in terms of acceleration and frequency; and 4) the vertical RRS for the future code. Furthermore, the study suggested a Pass/Fail acceptance criterion through a comparison of the seismic capacity of a particular nonstructural component and the seismic demand, considering the importance factor for the nonstructural component defined in the building code.

However, these seismic shaking table tests for seismic qualification have limitations when used to define the dynamic characteristics of electrical equipment under seismic excitation. The RRS does not provide the acceleration or displacement responses of each component attached to the electrical equipment but directly defines the relationship of the ground acceleration and the operational failure. Therefore, the seismic responses of each component cannot be compared with calculated responses, and the seismic vulnerability of the tested electrical equipment cannot be used for the same type of equipment with different configurations of components. Furthermore, the suggested required response spectrum can be conservative for general types and yet may not be sufficient for abnormal types which have different frequency characteristics or eccentric stiffness and mass distribution. That is, qualification testing using the RRS requires many different specimens to accurately capture the seismic vulnerability of one type of electrical equipment with various configurations.

In summary, determining the seismic vulnerability of electrical equipment using the shake table tests induces practical and cost issues that future studies should take into account. Some of these issues are as follows:

(1) Shake table tests can be impractical and expensive due to the great diversity of electrical equipment. There are various types of electrical equipment with different configurations which are produced by different manufacturers. Not only are these products different, the specifications of similar products of one manufacturer may change from year to year. It is also a daunting task to trouble-shoot all the devices attached to the equipment for their operational and physical integrity at a specific ground motion. Therefore, it is impossible to test all types of electrical equipment with different configurations. For practical reasons, the specifications of equipment should be more thoroughly examined, and their seismic characteristics determined in order for these studies to be used in a seismic vulnerability database.

(2) Application of recorded test data can be impractical as well as inconsistent due to the complexity and diversity of electrical equipment. For more accurate evaluation of equipment vulnerability, critical devices and locations on frames should be determined, and enough measuring devices such as accelerometers should be attached to the critical parts. Acquisition of more recorded data from complex equipment enables more accurate evaluation of its vulnerability. Despite the large number of devices attached to the equipment as well as their large amount of record data, it may not be easy to determine the cause of malfunction in electrical equipment. For example, contact chatter is a common example of malfunctioning of electrical devices, because it is sensitive to acceleration response and depends on excitation frequencies. Furthermore, it is impractical to use a large number of measuring devices and also difficult to obtain consistent

data from the large records through shake table tests for a complex electrical component.

(3) Many tests and specimens are required for a single type of electrical equipment as the input excitations should cover various magnitudes as well as a large range of frequency content. Both magnitude and frequency of input accelerations can influence the malfunction of the equipment. Electrical devices attached to complex equipment can be sensitive to high frequencies at low magnitudes of acceleration, while a high magnitude of accelerations can cause physical damage to the frame which would consequently cause an operational failure. Therefore, various input excitations are required to evaluate the seismic vulnerability of the equipment, resulting in the need for many different tests using many different specimens.

2.3.3 Numerical Modeling

The numerous limitations of using empirical data and the limited feasibility of testing a large number of specimens on a shake table leads to the alternative of using numerical techniques such as the finite element (FE) method to evaluate the seismic vulnerability of electrical equipment. FE models can be generated to significant levels of complexity in accordance with the needs of developers and analyzed with significant savings in time and money.

Gupta et al (1999) developed FE models of 16 types of electrical cabinets. The FE models were generated using the ANSYS software. One of the cabinets, DGLSB, represents one type of switchboard cabinet including instruments mounted on the doors and internal frames shown in Figure 2.6. The FE model for this equipment was validated

and the results were presented by Rustogi and Gupta (2004), who compared the results of the analytical model and experimental data. Shake table testing was performed using six sets of accelerometers mounted on the DGLSB cabinet to measure the acceleration response. In the experiments, four accelerometers were attached to the doors and two accelerometers to the internal frames. The numbers in Figure 2.6 represent the locations of the accelerometers. Frequency response functions (FRF) were recorded during the tests, and the recorded data were analyzed to obtain the dynamic characteristics of the electrical cabinets. The spectral accelerations of the structure from the recorded data were compared to the FE analysis results to evaluate the significant frequencies and modal participation factors of the cabinets. Figure 2.3 shows a comparison of the FE results and recorded data from two accelerometers.
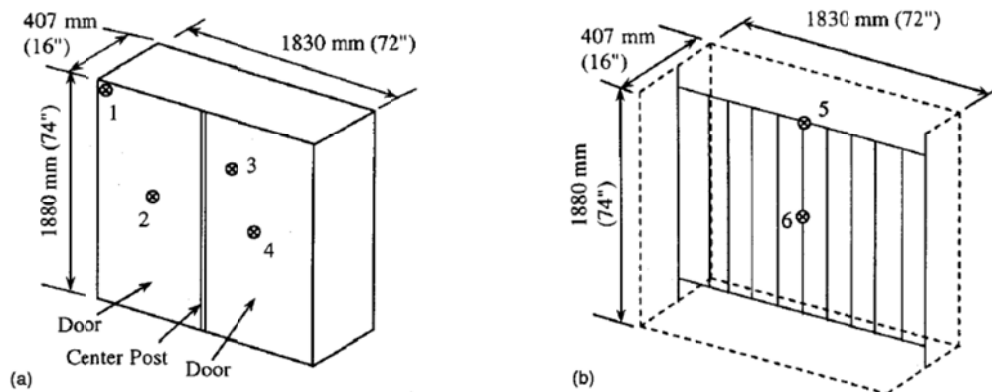
Figure 2.6 Cabinet DGLSB (a) Outer box structure (b) Internal frame
(Rustogi and Gupta, 2004)

The study presented the following important results:

(1) As shown in Figure 2.7, the test data of one mode is very close to the test data of all modes. It means that a single degree of freedom (SDOF) model appears to be sufficient to define accurate spectra for instruments located on the door at accelerometer locations 1 and 4.

26

(2) The local modes of the steel panels significantly affect the behavior of the critical locations of the cabinet when compared to the global modes.

(3) The type of the electrical equipment considered in this study has a distinct global mode (the cantilever behavior of the box) and a local mode (the steel panel behavior of the doors and walls).

(4) The support boundary conditions of the FE models are assumed to be fixed. From the experimental tests, however, it was observed that the anchor bolt at the support boundary can reach the local nonlinear behavior range. It means that an elastic model of the global system is no longer adequate.

(5) In addition, this nonlinear behavior at the support boundary of the equipment affects the fundamental frequency and global mode shape of equipment.

(b) Accelerometer at Location 1
(Front-Top of Door)

(b) Accelerometer at Location 4
(Front-Center of Door)
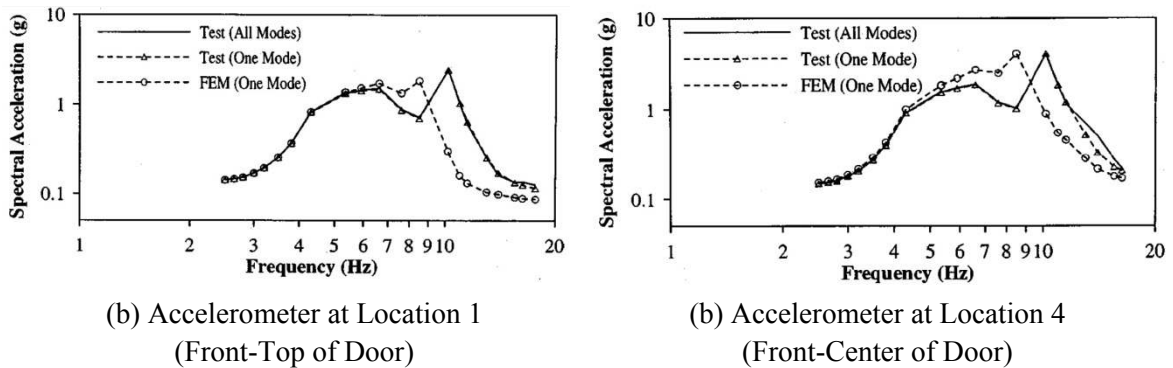
Figure 2.7 Spectral Acceleration (Rustogi and Gupta, 2004)

However, it is also important to recognize the limitations of numerical techniques. Techniques like finite element analysis can produce serious errors due to inexperience on the part of users. Furthermore, despite correct applications based on in-depth knowledge, it is also computationally impractical to construct and analyze FE models that include all electrical devices and joint details for large and complex electrical equipment. If a 3D-

FE model for one type of switchboard cabinets is generated with a large number of elements, it would take a long time to perform the linear modal analysis using a supercomputer, and therefore it is possible but not practical to conduct nonlinear time history analysis with this complex a FE model. Therefore, for practical reasons, FE models must be simplified and constructed for the specific purposes of the analysis. In addition, simplified numerical models should be validated to accurately capture fundamental dynamic characteristics, such as frequencies, mode shapes, and damping ratios.

2.4   Closure

1. This chapter reviewed past studies of the seismic vulnerability of electrical equipment in electric power systems to assess the seismic performance and possible damage states of these components in buildings and public service facilities. This review of the state of the art has identified the following factors required to properly classify advance vulnerability assessment of electrical equipment. The studies involved classification of the vulnerability of electrical components, seismic vulnerability data collection, and evaluation and analysis of their performance and damage during earthquakes.

2. For the seismic vulnerability of electrical equipment, the classification should be detailed to the extent that it facilitates the recognition of interior and exterior specifications as well as the damage states of each component for the seismic vulnerability database due to the diversity and complexity of electrical equipment.

3. Three different approaches have been pursued to define the seismic vulnerability of electrical equipment: empirical data and survey, shake table tests, and numerical models.

4. Empirical data and post-earthquake surveys of damage, as well as shake table tests, better define the damage states of electrical equipment.

5. It is impractical to conduct shake table tests on all of the various types of complex electrical equipment under different loading conditions to estimate their seismic vulnerability.

6. Numerical models are the most practical and viable option to estimate the seismic vulnerability of electrical equipment in terms of engineering demands considering the correlation between damage states and earthquake intensity measures.

7. Simplified numerical models should be developed and validated in order to achieve reliable estimates of their vulnerability.

Based on this review, it is clear that significant challenges remain in developing and improving the seismic vulnerability of complex electrical equipment with different configurations, various parameters, and correlated earthquake intensity measures. Furthermore, improvements are required in the process of finite element models of complex electrical equipment considering various ways in which they could be rendered inoperable. The following chapters build upon these conclusions.

CHAPTER III

NUMERICAL MODELS FOR SWITCHBOARD CABINETS

This chapter describes the functionality of electric switchboards in power systems. Simplified numerical structural models are constructed using a finite element approach to describe their dynamic response. The bolted joints between frame members and the screw connections between the infill panels and the frames are modeled with discrete stiffness elements to represent the elastic interaction between these members.

3.1   Introduction

3.1.1   Functionality of Electric Switchboard

Since early in the 20th century, most modern buildings have been equipped with electric power distribution systems housed in substations. A substation functions as the electrical "nervous system" of a building and includes a variety of equipment, such as transformers, switchboards, and panel boards. The electrical power delivered from a power utility company enters the building at a relatively high voltage characteristic of the transmission system. Typically, a transformer reduces the high voltage to a lower voltage which is then distributed by a switchboard to panel boards at each floor level or region in a building where it may be further reduced to match the end loads. Figure 3.1 shows an example of the power flow in the Georgia Center for Advanced Telecommunications Technology (GCATT) building at the Georgia Institute of Technology in Atlanta.

When an electrical system sustains even partial damage due to seismic shaking, the supply of electrical power is interrupted, resulting in economic losses and possibly serious disruptions in critical facilities such as hospitals, water distribution stations, nuclear power plants, or radio and television stations. The proper functioning of the electrical system is therefore crucial to many facilities, and the seismic vulnerability of each electrical component such as a switchboard is needed to evaluate the vulnerability of the full electrical power system.
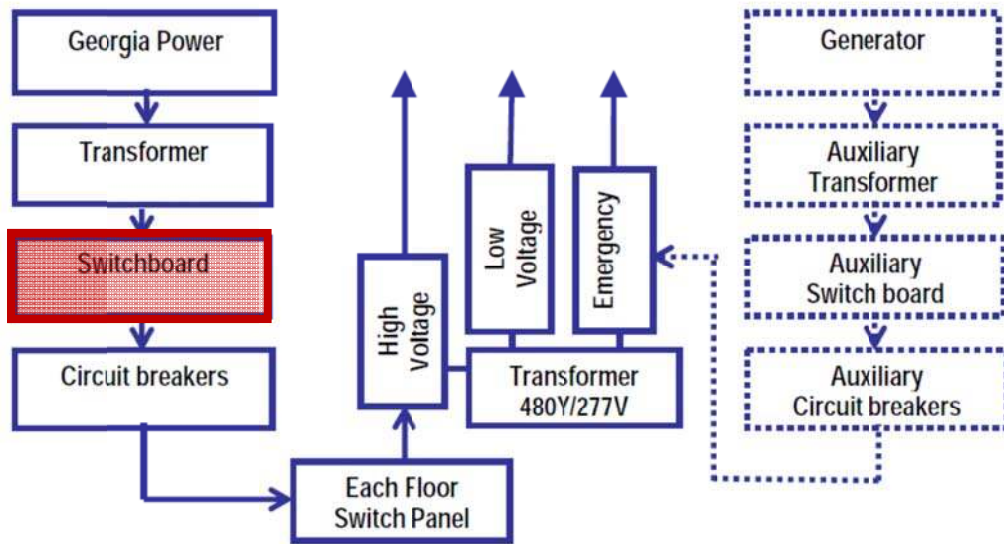
Figure 3.1 Power Flow in the GCATT building

3.1.2   Complexity of Electric Switchboard

Switchboard cabinets consist of many different components such as a steel enclosure consisting of steel frames and thin steel panels (plates), as well as interior components such as switchgear, electrical control boxes, and distribution wiring and bus bars. These components are both structurally and electrically interconnected. The steel plates and frame members are connected by bolts or screws, and the electrical devices such as

switchgear, transformers, control systems and control monitors are attached to the structural frames and in some cases to the steel plates. These components in a switchboard are electrically interconnected, and the switchboard is also electrically connected to other electrical equipment through conduits shown in Figure 3.1. The complexity of electric switchboards complicates their seismic response and vulnerability assessment

Malfunction of any one of the electrical devices can cause the operational failure of a switchboard, while minor structural damage to the cabinet may not affect the operation of the equipment at all. Moreover, the electrical devices and the structural frame have different damage states under seismic excitation. Steel structural frames can behave linearly or nonlinearly depending on the magnitude of the excitation, while the electrical devices can shut down intermittently. Therefore, a parametric study is required to define the events that cause the operational failure of the equipment under seismic loading.

Furthermore, the variation in the combinations of components directly affects the dynamic behavior of the equipment because the weight and location of the electrical devices as well as the distribution of horizontal and vertical members are related to the mass and stiffness distribution in switchboard cabinets. Therefore, it is imperative to identify the parameters that have the largest effects on the dynamic response characteristics of the equipment and include these in the numerical models that are generated.

3.1.3   Necessity of Numerical Models

All electrical equipment used in power distribution systems in buildings and infrastructure facilities is required to withstand some level of environmental vibrations during shipping, delivery, and installation. Most are also required to meet seismic qualifications to operate during ground shakings, usually in essential facilities such as hospitals or in many industrial facilities and always in certain critical facilities such as nuclear power plants. Most previous studies reviewed in Chapter 2 have focused on evaluating dynamic amplifications for limited types of equipment by conducting shake table tests or by developing simple analytical models.

A major shortcoming of previous studies discussed in Chapter 2 has been their failure to address the seismic fragility of diversified and complex electrical equipment. This issue is immensely important because even one generic type of equipment can have vastly different structural characteristics, depending on installation conditions alone. Figure 3.2 shows switchboard units produced by major manufacturers in the United States. The four units are similar in function, but their appearances and modular frames depend on the manufacturer. Furthermore, each manufacturer produces units containing different combinations of electrical components, devices and instruments. Due to the very large number of possible configurations, it is impractical to use vibration tests or to perform detailed finite element analysis for every configuration of switchboard cabinets. Consequently, both analytical and simple numerical models must be developed to evaluate the dynamic behavior of the full range of electrical equipment. Simplifications to basic analytical models can achieve significant reductions in modeling complexity, but important dynamic characteristics such as mass and structural asymmetry, local mode shapes, and nonlinear behavior are not captured.

While numerical models using the finite element method are more capable of overcoming the shortcomings of analytical models, they invariably lead to large and highly complicated formulations to achieve higher fidelity. The required detail for numerical models of electrical equipment is determined by the needed level of accuracy for their dynamic response. The challenge is not simply to increase the number of elements or degrees of freedom achieve this with consequent increase in complexity. Rather, simplified numerical models must include the critical parameters affecting the dynamic response in order to provide a more realistic representation of their true behavior without increased model complexity and cost.

| Square D | General Electric | Westinghouse | Siemens |

Figure 3.2 Electric Switchboards by Four Major Manufactures

3.2   Numerical models of switchboard cabinets

3.2.1   Previous works on finite element analysis of switchboard cabinets

Finite Element (FE) analysis is employed in this research for the development of numerical models of electrical switchboard cabinets. It is also more economical than shake table tests as discussed in Chapter 2. Finite element models can be easily

constructed, and they can be analyzed under various loading configurations, boundary conditions, and excitations to predict the structural response at any point of interest.

Gupta et al. (1999) generated finite element models of several types of electrical cabinets and identified the significant features of the cabinet dynamic behavior. One of these models is the Diesel Generator Load Sequencer Board (DGLSB) shown in Figure 3.3. This equipment has a box type of structure rigidly anchored to the floor through the base plate. In order to construct a finite element model, four-node quadrilateral elements were used for the steel plates, and beam elements with six degrees of freedom per node were employed for the frame members. Each of two front doors is hinged at one edge and tightly secured to a center post on the opposite edge. These doors are also connected to top and base of the frames by wing screws. For the connection by screws, one rotational degree of freedom was considered to be free for the rotational axis, and five degrees of freedom were considered at each node to connect the doors and frames. The electrical instruments were assumed to be mounted on the front door panels and on an internal frame consisting of horizontal and vertical channels.

Using the same FE model of the DGLSB, Rustogi and Gupta (2004) conducted a modal analysis, and they compared their results to shake table test results. The modal analysis results showed that the local modes tend to be dominant due to the box-type structure with exterior plates and an internal frame. A global cabinet bending mode for this box type cabinet was not indicated in the non-rigid frequency region. This means that the global box-type structure is much stiffer than the individual door plate or internal frame members. The steel plates forming the doors led a local door mode with the fundamental frequency of 8.6 Hz, while a significant modal contribution from the internal

frame occurred at a frequency of 10.8 Hz. The study also concludes that a single local mode is sufficient to evaluate accurate in-cabinet spectra for instruments located on the door as well as for those located on the frame. That is, the fundamental frequencies of local components, such as doors or internal frames shown in Figure 3.3, provide the most significant components of the spectra for instruments attached to these members.

(a) Local door mode shape   (b) Local frame mode shape

Figure 3.3 Local mode shapes for a DGLSB Cabinet (Rustogi and Gupta, 2004)

Spectral Accelerations (SA) computed from the FE analyses were compared to Spectral Accelerations (SA) measured during the shake table tests. For the comparison, six accelerometers at six different locations in the DGLSB were monitored under the acceleration excitation and compared to the FE analysis results. Figure 3.4 shows one of the test results plotting the variation of SA over a range of frequencies. As seen in the figure, the test results consistently underestimate the computed spectral acceleration at frequencies greater than 8 Hz. The discrepancy was attributed to the inaccuracies in the stiffness, magnitude and/or distribution of mass, and improper representation of the force-deformation behavior of the connections and joints.
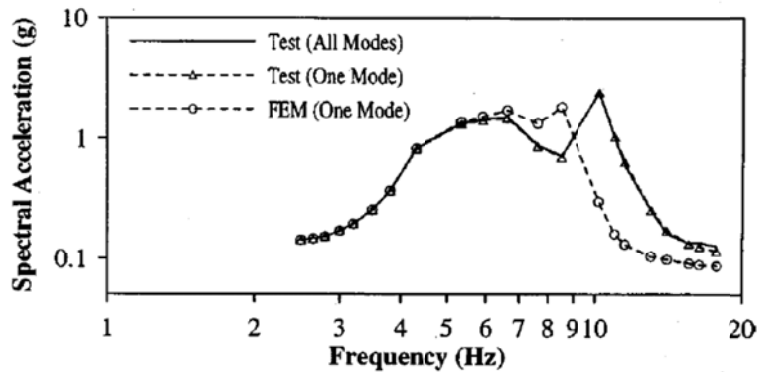
Figure 3.4 In-cabinet spectra at accelerometer 1 attached to the front top of the cabinet
(Rustogi and Gupta, 2004)

Llambias et al. (1989) also found that the results from shake table tests can be sensitive to the mounting arrangements of the cabinet since the nonlinear behavior exhibited at the boundaries can have a large influence on the total response behavior of the equipment. A wide disparity in the response can be observed between FE analysis results where the base is typically assumed to be perfectly fixed and shake table tests in which the base fixity is less rigid. This can be further compounded by the fact that the bolt connections of the frames tend to loosen during the shake table tests and contribute to discrepancies between the measured test response and FE analysis results.

These previous FE studies provide a basis upon which to develop improved FE models for switchboard cabinets which address the following factors:

1) FE models for electrical cabinets are generated with two-node beam and four-node quadrilateral thin plate elements, in which six-degrees of freedom are considered at each node.

2) FE models need to be simplified with reduced degrees of freedom but with the ability to capture the most important dynamic behavior of the cabinet structure.

3) In box-type steel cabinets, the local modes dominate over the global modes. FE models must be capable of capturing any significant mode shapes caused by the local modes such as the steel door plates or internal frames.

4) The complexity of the equipment will make it difficult to achieve a good match between shake table tests and analytical results but general behavior and trends must be captured.

5) If the electrical devices or instruments are located on the local structural components such as steel panels or internal frames, the local mode shapes from the local structures will be more important than the global mode shape, and therefore their dynamic response should be included.

6) Support boundary conditions can directly affect the global behavior of the structure and must be incorporated in the models.

3.2.2 Descriptions of switchboard cabinets for the finite element models

This section introduces the configurations of switchboards and describes the procedure to generate their FE models. The configurations of switchboard units were provided by one of the major manufacturers in the United States. (Wyle, 2008)

3.2.2.1 General description of switchboard cabinets

As mentioned in the previous section, switchboard cabinets are composed of steel structural frames and panels, electrical devices, conductors, and electrical conduits. Their dimensions vary depending on the type, current and voltage capability, quantity of bussing, and combination of electrical devices installed.

Structural frames are built up with L-shape and C-shape steel sections for vertical (column) and horizontal (beam) members, respectively, and they are covered on all four sides and top with thin sheet steel exterior panels to form a box. Figure 3.5 (a) and (b) show internal components in switchboard cabinets before they are enclosed by the exterior panels.

The frame members are usually bolted together while the steel plates are usually attached to the frames with self-tapping, hardened screws which have rolled threads that exhibit superior torque and strip-out resistant performance. Lockable doors with a hinge at one edge can be substituted on the front side of cabinets for monitoring systems, while the rear plates of cabinets are generally removable for maintenance purposes.

Electrical devices and instruments mounted on a switchboard are diverse and include circuit breakers, switches, metering devices, relays and other components. Instruments are usually mounted on the front side of cabinets and record and display the frequency, current, and voltage of the electrical power.

The conductors transmitting electrical power usually consist of one of two types: busbars and cables, as shown in Figure 3.5. Busbars are thick strips of solid copper or aluminum, while cables contain multi-stranded copper wires insulted with poly-vinyl chloride (PVC). Busbars are more commonly used in switchboard cabinets because they are more practical and versatile than cables of comparable capacity. They are placed on the inside of cabinets and carry large currents into other electrical equipment. Control signals are fed through instrument grade wiring of much lower gauge that is often bundled into harnesses.

| (a) Copper busbars | (b) Cables |

Figure 3.5 Conductors inside of Switchboard Cabinets

Electrical conduit is a piping system which connects switchboards to other electrical equipment. Conduit can be metal, plastic, or fiber and connect to the switchboards on the top of the cabinets or from under their bases. Figure 3.6 (a) shows common round electrical conduit containing insulated conductors, and Figure 3.6 (b) shows electrical conduit with rectangular cross sections (i.e. busway) connected to a switchboard.

| (a) Electrical Conduits | (b) Electrical Busway Enclosure |

Figure 3.6 Electrical Conduit and Busway Connected to Switchboard Cabinets

3.2.2.2   *Switchboard cabinets selected for the finite element models*

FE models of four different switchboard cabinets are generated, and their fundamental dynamic characteristics are evaluated. These four units (Wyle, 2008) have similar systems assembled with standardized modular steel frames and plates, but they have different width, depth, weight, and location of electrical devices as shown in Figure 3.7.

The structure of the cabinets is composed of steel frames and plates which are made of cold formed/rolled steel. The sections of the frames are similar to L-shape and C-shape steel, and they are used for the horizontal and vertical members respectively as shown in Figure 3.9 (a). For the finite element models, the local bucking problems of frame members are not considered, since the real horizontal and vertical members are slightly rolled and bent to prevent the local buckling problem. In addition, the shake table test results with cabinets also showed that the yield of screw or bolt connections is more vulnerable than the local buckling of frame members (Wyle, 2008). The sections of the elements and their dimensions are given in Figure 3.8.
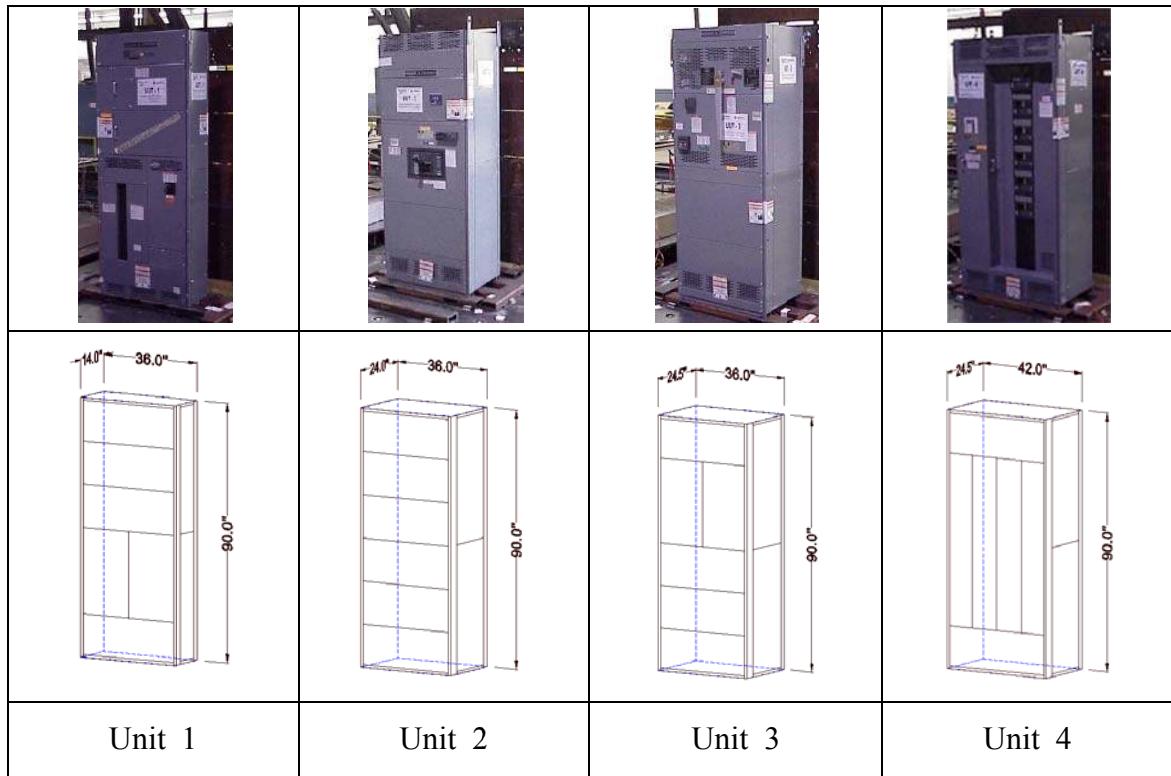
Figure 3.7 Dimensions of Switchboard Cabinets, Units 1-4.

The steel plates are affixed to the frame members to form the four exterior surfaces and the top surface as shown in Figure 3.9 (c). Some of the plates have a peripheral L-shaped bent edge to increase the stiffness of the edge. Two large plates form the sides and rear while a single plate forms the top (ceiling), and all plates are fastened to the frames with screws. On the front face, doors or drawers can be mounted with a lock or latch and hinge, and the other portions of the front face is covered by plates with screws similar to other sides as shown in Figure 3.7. This figure shows four switchboard cabinet configurations having different width, depth, weight and mass distributions, and for which simplified FE models are developed.
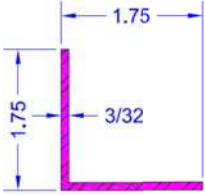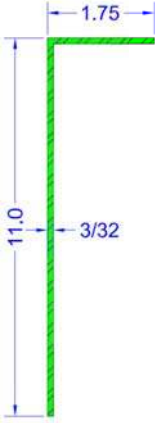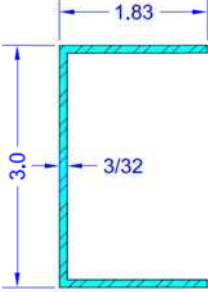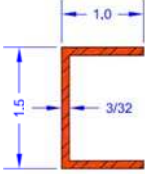
(unit: inch)			
Vertical Member (Rear Post)	Vertical Member (Front Post)	Horizontal member (Top and Bottom)	Horizontal member (Others)

Figure 3.8 Section of Frame Members

(a) Appearance	(b) Beam-Column Elements	(c) Plate (Shell) Elements
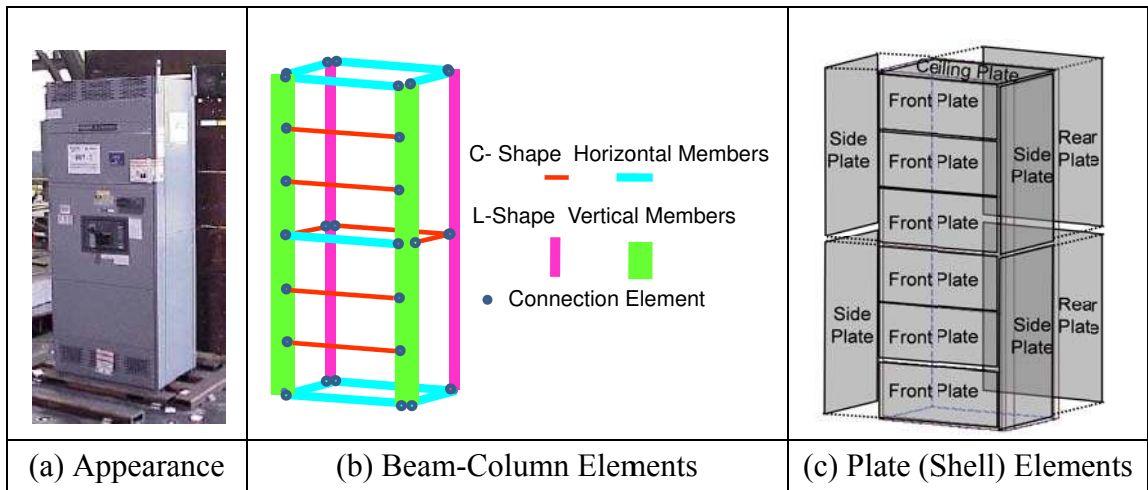
Figure 3.9 Structural Frames of Switchboard Cabinets

Table 3.1 describes the size and weight of the units where "Structural Frame Weight" means the weight of the enclosure including steel frames and plates, and "Devices and Conductors Weight" refers to the weight of the electrical devices/instruments and busbars or cables mounted within. "Total weight" includes the combined "Structural Frame Weight" and "Devices and Conductors Weight". Figure 3.10 shows the locations of the additional weights of the "Devices and Conductors Weight" which are modeled as lumped masses in the FE models. "Structural Frame Weight" is the self-weight of the structure and is considered as a distributed mass in the frame members. The ratio of the structural frame weight to the total weight is defined as α, and therefore (1- α) is the ratio of the additional weight due to devices and conductors to the total weight. Table 3.2 shows the material properties of structural members in cabinets as well as the size of the fasteners.

The vertical and horizontal members are modeled using elastic two-node beam-column elements, and the steel plates are modeled using four-node quadrilateral shell elements. For the boundary support conditions of the units, a total of four bolts (1/2"-13 Grade 5) per corner connect the base frame to the floor, as shown in Figure 3.11. The bolted connection is considered to be fixed at five degrees of freedom, and the sixth degree of freedom, which is the rotation about the bolt axis, is considered to be free. Screws connecting frames and plates are modeled using zero-length link elements. These connect each node from the frame and plate, and include the stiffness properties of bolts in the six-degree of freedom.

Table 3.1 Dimension and Weight of Units

Description			Unit 1	Unit 2	Unit 3	Unit 4
Size (inch)	Width		36	36	36	42
	Depth		14	24	24.5	24.5
	Height		90	91	91	91
Weight (lb)	Total Weight	WT	508	895	916	1176
	Structural Frame Weight	$\alpha \cdot$ WT	358	445	416	476
		α	0.70	0.50	0.45	0.57
	Devices and Conductors Weight	$(1-\alpha) \cdot$ WT	150	450	500	700
		$1-\alpha$	0.30	0.50	0.55	0.43

Table 3.2 Material Properties and Size of Fasteners

Steel Plate	Weight per unit Volume	0.2836 lb/in^3
	Modulus of Elasticity	29500 ksi
	Yield Stress	36 ksi
	Tensile Stress	58 ksi
Connection	Screws, Bolts	3/16", 1/4"
	Anchor Bolts	½'' Grade 5

| Unit 1 | Unit 2 | Unit 3 | Unit 4 |
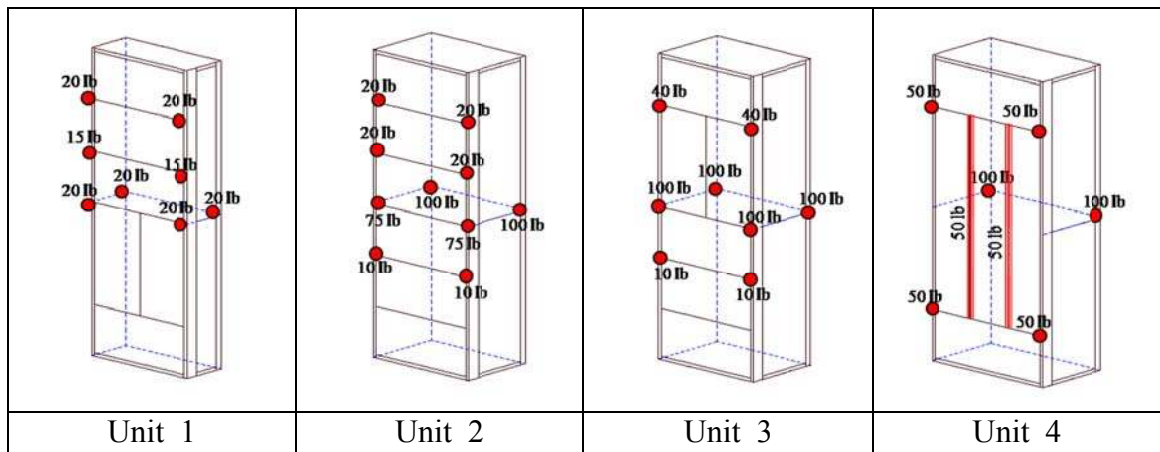
Figure 3.10 Devices and Conductors Weight
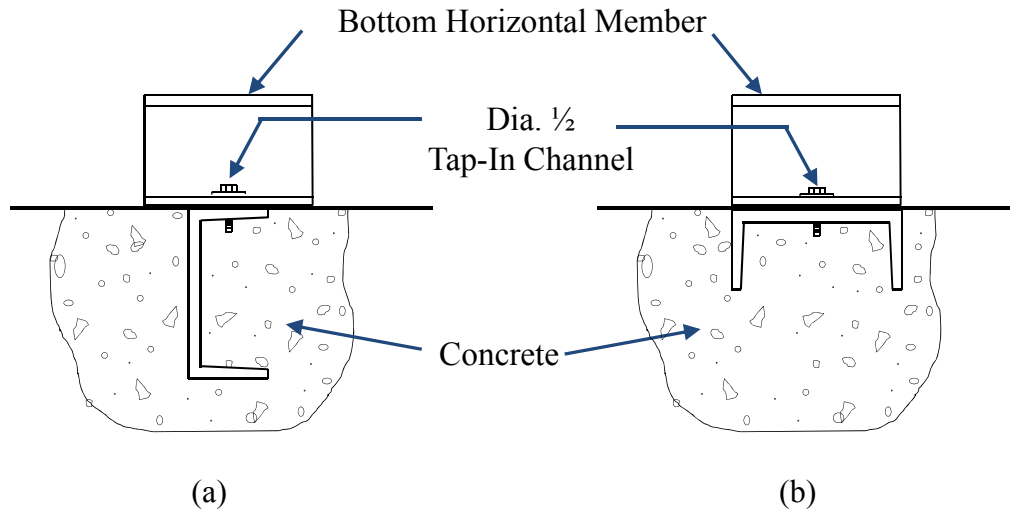
Figure 3.11 Details for anchor bolt

3.3   Dynamic Behavior of Switchboard Cabinets

The linear dynamic characteristics of the switchboard cabinets are evaluated using modal analyses of the constructed FE models in OpenSees (Open System for Earthquake Engineering Simulation, Version 2.2.2). Through the modal analyses, the fundamental frequencies and mode shapes are evaluated and compared to the experimental results from shake table tests by Wyle (2008). Section 3.3.1 discusses the influence of the steel plates on the dynamic behavior of switchboard cabinets. Section 3.3.2 details the significant frequencies and mode shapes of the switchboard cabinets considering local and global effects.

3.3.1   Box-Behavior Due to Steel Plates

In order to evaluate the influence of the plates, two sets of FE models with and without steel plates are generated. The first set explicitly accounts for the influence of steel plates in terms of mass and stiffness. As mentioned previously, steel plates are modeled with four node quadrilateral shell elements attached to the frames with zero-length link elements. The rear plates are divided into thirty six shell elements with six elements per edge, those at top and side plates are divided into twenty four shell elements with four and six elements per edge, and front plates are divided into twelve elements. The diagrams of the FE models and the location of link elements are illustrated in the Appendix. The link elements encapsulate the stiffness of the screws connecting the frames and plates, and their stiffnesses are explained in detail in 3.4.1. In the other set of models, the stiffness contribution of the steel plates is neglected, although the mass contribution from the self-weight of the steel plates is still accounted for by applying additional lumped masses to the frames. Both sets of FE models are generated using elastic beam-column elements with two nodes for the frame members in the cabinets.

Results of the modal analyses show that the FE models that account for the stiffness of the steel plates behave nearly rigidly and have fundamental frequencies higher than 10 Hz as shown in Table 3.3 (1). This is because the steel plates behave like diaphragms on the exterior surfaces and therefore increase the shear and torsional stiffness of the switchboard cabinet. The side plates control the displacement of the cabinet in the front-to-back direction, while the front and rear plates control the displacement of the cabinet in the side-to-side direction. These results indicate that the mode shapes and stiffnesses are close to the respective values of cantilevered boxes with fixed support condition.

On the other hand, the FE models neglecting the stiffness of steel plates and consisting only of frame members with L- and C-shaped steel members are relatively flexible as shown in Table 3.3 (2). The significant frequencies are less than 10 Hz in both front-to-back and side-to-side directions. This means that the frame has reduced flexural rigidity in comparison to the former case and behaves similar to a building frame system formed from a column and girder system.

Table 3.3 Comparison of Fundamental Frequencies

Unit	(1) Box Behavior (with Plates)		(2) Frame Behavior (without Plates)		(3) Resonance Search Test	
	Front-to-Back	Side-to-Side	Front-to-Back	Side-to-Side	Front-to-Back	Side-to-Side
Unit 1	15.6 Hz	26.5 Hz	6.3 Hz	7.6 Hz	8.3 Hz	17.0 Hz
Unit 2	15.5 Hz	22.0 Hz	5.0 Hz	5.8 Hz	7.3 Hz	8.0 Hz
Unit 3	15.7 Hz	21.4 Hz	4.8 Hz	5.7 Hz	6.0 Hz	7.3 Hz
Unit 4	10.9 Hz	15.0 Hz	4.8 Hz	5.8 Hz	7.0 Hz	9.0 Hz

Table 3.3 (3) shows the fundamental frequencies as determined experimentally from resonance search tests. (Wyle, 2008) A resonance search test is conducted to investigate the frequencies at which the switchboard develops significant response. It is one type of seismic qualification tests for electrical products that use shake table tests of cabinets at relatively low accelerations (<0.1g to minimize nonlinear response) over a broad range of frequencies. This table shows that the fundamental frequencies of the FE models (1) are higher than the fundamental frequencies of the real structure (3) as determined from testing on the shake table in both side-to-side and front-to-back directions. This is because the force-displacement behavior of the joint connection is overestimated in FE models since it is assumed that the frame connections are rigid for this comparison.

Therefore, the behavior of the frame connections should be modified considering the test results. This calibration procedure will be discussed in detail in Section 3.4.

Also noticeable in Table 3.3 is the influence of the steel plates on the frequency response of the switchboard cabinets. As expected, the inclusion of steel plates in the FE models significantly increases the fundamental frequency of the switchboards due to the additional stiffness imparted by their presence. Furthermore, the comparison to the shake table test results illustrates that the measured behavior of the cabinets falls between the extreme cases of box behavior and frame behavior in the elastic range.

3.3.2 Significant Mode Shapes of Switchboard Cabinets

The previous section explained how the combined behaviors of steel plates and frames affect the fundamental frequencies of switchboard cabinets. This section describes the fundamental mode shapes of switchboard cabinets considering the influence of the steel plates based on the results of a modal analysis for Unit 2 which is the most typical unit. In order to evaluate the fundamental frequencies and mode shapes of cabinets, the modified FE models for Unit 2 are generated considering the stiffnesses of the plates and frames and linear modal analyses are performed.

Figure 3.12 shows the steel plate behaviors in Unit 2, and Figure 3.13 illustrates significant frame behaviors in both directions. For the visualization of local mode shapes of plates and frames, they are separately plotted. The fine mesh shown in Figure 3.12 is used to highlight the mode shapes and does not represent individual finite elements. The mode shapes of switchboard cabinets are the combinations of steel plate behaviors in local modes and the frame behaviors in global modes as shown in Figure 3.14.
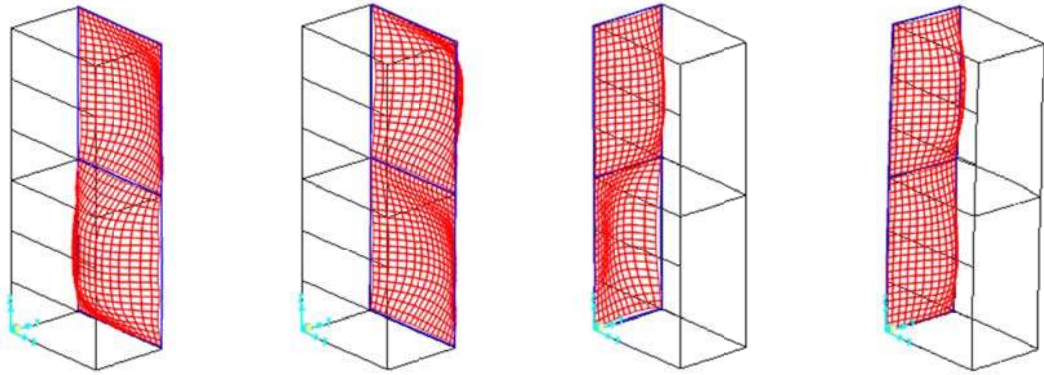
(a) Local Mode Shapes of Rear Plate   (a) Local Mode Shapes of Side Plate

Figure 3.12 The Local Mode Shapes of Steel Plates
(with fine meshes for the visualization of mode shapes of plates)
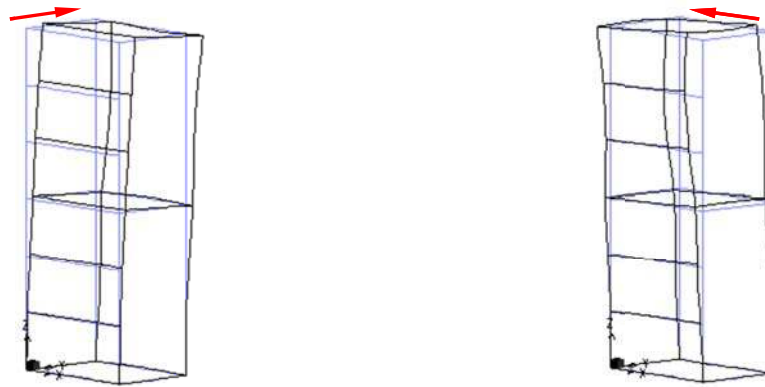
(a) Front to Back Direction   (b) Side to Side Direction

Figure 3.13 The Global Mode Shapes of the Frame

The effect of the local mode shapes of the steel plates is investigated by examining the modal participation mass ratios (MPMR) for the first several modes in the front-to-back direction shown in Figure 3.14 and Table 3.4. Figure 3.14 shows the fundamental mode shapes from the top view, 3D view, and of rear plates. The plots from the top view show that in the first mode, the cabinet is slightly displaced in the front-back direction and that in the second mode it displaces in the side-to-side direction combined with torsional rotation.   The third and fourth mode shapes show insignificant global

50

displacements in front-to-back, side-to-side and torsional directions, but the top views show that the local mode behavior of plates is significant. Table 3.4 lists the MPMR's and helps in understanding the effect of the local behavior of the plates in the third and fourth modes compared to the first two modes. The modal participation mass ratios (MPMR) for higher modes in the front-to-back and side-to-side directions are very small. Based on evaluation of the MPMR data, it is clear that the higher modes consist almost entirely of local mode response of the steel plates and that the higher cabinet bending modes are outside the range shown.

	(a) 1st Mode	(b) 2nd Mode	(c) 3rd Mode	(d) 4th Mode
Top View — Back ↕ Front				
3D View				
Rear Plates				
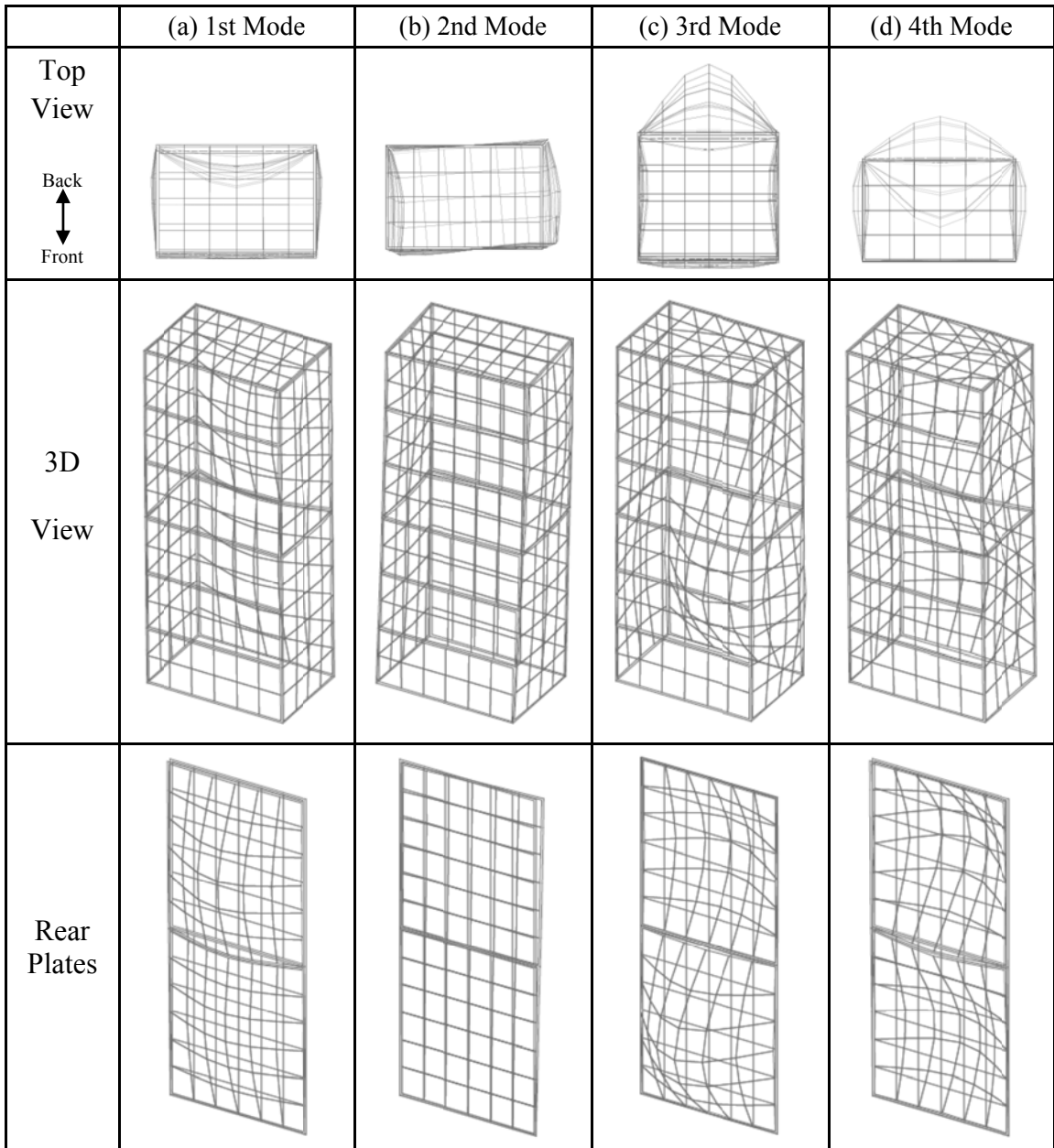
Figure 3.14 Fundamental Mode Shapes

The presented total mode shapes and MPMR explain the effect of frame behavior on the global mode shape of cabinets as well.   The first two modes show global displacement in the front-to-back and side-to-side direction respectively.   The mode shapes and MPMR values for the first two modes show the significance of the global behavior on the lower mode shapes of cabinets, while mode shapes and corresponding

MPMR values of higher modes show the negligible effect of the global behavior of the frame on the higher modes. In Table 3.4, UX and UY show MPMRs for each mode in side-to-side and front-to-back directions respectively, and the Sum UX and Sum UY are the accumulations of the MPMRs from the lower modes in each direction.

In addition, the frequency of the first mode (7.2 Hz) is considerably higher than that of the frame behavior (5 Hz) without plates as shown in Table 3.3 (3). Also, the frequency of the second mode (9.7 Hz) is higher than that of the frame behavior (5.8 Hz) without plates. The global behaviors are governed by a combined behavior of steel frames and plates similar to a steel box.

Table 3.4 Modal Mass Participation of Modified FE model for Unit 2

Mode	Frequency (Hz)	Side-to-Side (Dimensionless)		Front-to-Back (Dimensionless)	
		UX	Sum UX	UZ	Sum UZ
1	7.23	0.0000	0.0000	0.7244	0.7244
2	9.66	0.6742	0.6742	0.0001	0.7245
3	14.5	0.0000	0.6742	0.0096	0.7340
4	15.4	0.0000	0.6742	0.0011	0.7351
5	16.7	0.0324	0.7065	0.0000	0.7351
6	17.7	0.0000	0.7065	0.0030	0.7381
7	20.0	0.0000	0.7065	0.0360	0.7741
8	20.3	0.0191	0.7257	0.0000	0.7741
9	21.6	0.0002	0.7259	0.0000	0.7741
10	22.0	0.0000	0.7259	0.0054	0.7795

The local mode shapes such as the rear plate behavior govern higher mode shapes and frequencies of switchboard cabinets as shown in Table 3.4 and Figure 3.14. In order to better understand the relationship between the local mode shape of the plates and the

global mode shape of the structure, the fundamental frequencies and mode shapes of plates with different boundary conditions shown in Figure 3.15 are studied.

In case (a), the plate is fixed on all four edges, while in case (b) all the edges are simply supported. Case (c) more closely resembles the condition of the steel plate attached to the switchboard frames. The four edges of the rear plates of the switchboard cabinet are bent up, and therefore the boundary condition stiffens the edge to translational deformation (Δ_f) permitted. Precisely, this case represents the superposition of the global mode shape in the front-to-back direction characterized by the small deformation (Δ_f) and the steel plate local mode shape. For the comparison of three cases, the maximum displacement of each case is labeled δ_a, δ_b, and δ_c respectively. δ_c is equal to or larger than δ_a and can be larger than δ_b depending on the deformation of the edges (Δ_f).

| (a) 4 Edges Fixed | (b) 4 Edges Simply Supported | (c) Rear Plate of Cabinets |
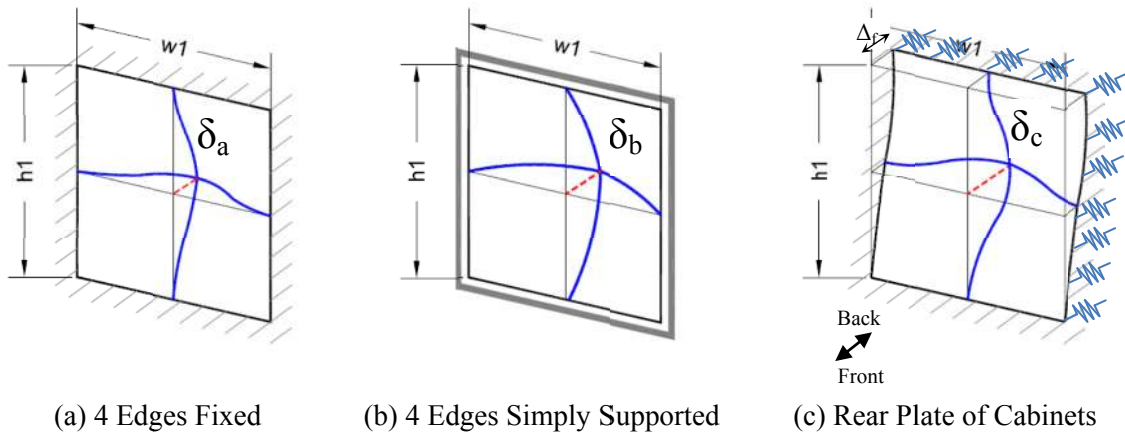
Figure 3.15 Fundamental Mode Shape of Three Plates

It is assumed that the dimensions of all three plates are the same as the rear plate of typical switchboard cabinets and that all plates have the same dimension and mass distribution. Their width (*w1*) is 36 inches; the height (*h1*) is 45 inches; the thickness of plates (*h*) is 3/32 inch; the steel mass density (*m*) is *7.345x10^{-7} kips/g/in^3*; elastic modulus

of steel (E) is 29000 ksi; Poisson's ratio of steel (v) is 0.3; the flexural rigidity is

$$D = \frac{Eh^3}{12(1-v^2)} \quad .$$

The natural frequency of Case (a), a rectangular plane with fixed four edges, can be estimated by Equation 3.1 (Szilard, 2004) where $w1$ and $h1$ are defined in Figure 3.15.

$$CASE(a): \omega = 4\sqrt{2\left(\frac{2^4}{w1^4} + \frac{2^8}{3^2 \times 7^2} \cdot \frac{2^4}{w1^2 h1^2} + \frac{2^4}{h1^4}\right) \cdot \sqrt{\frac{D}{m}}} \tag{3.1}$$

The natural frequency of Case (b), a rectangular plane with simply supported four edges, can be estimated by Equation 3.2 (Szilard, 2004)

$$CASE(b): \omega = \pi^2 \left[\frac{1}{w1^2} + \frac{1}{h1^2}\right] \cdot \sqrt{\frac{D}{m}} \tag{3.2}$$

The natural frequency for case (c) is obtained from the FE model. The natural frequencies of each plate are summarized in Table 3.5 below.

Table 3.5 Fundamental frequencies of rear plates with different boundary conditions

Case (a)	Case (b)	Case (c) FEA Result	Resonance Search Test
21.41 Hz	11.47 Hz	7.23 Hz (1st Mode)	7.3 ~ 8.3 Hz (Significant Modes)

The fundamental frequencies for Case (c) are determined using the FE model and modifying the connectivity to the frames for Unit 2 as given in Table 3.4. This comparison shows that the fundamental frequency of Case (c) is significantly affected by the stiffness of the frame (i.e., the global mode shape), since the fundamental frequency of Case (c) is lower than that of Cases (a) and (b).

3.4 Modified Finite Element Models of Switchboard Cabinets

Section 3.3.1 discussed the FE models with rigid connections between elements. The fundamental frequencies of these models are around 16~22 Hz (see Table 3.3 (1)) which are significantly higher than the frequencies from resonance search test results (see Table 3.3 (3)) implying that the FE models are too stiff. The steel plates are attached to the frames with screws, and the horizontal and vertical members of the frames are connected with bolts. As a result, these connections may not be fully rigid as assumed in Section 3.3.1. This section investigates the effect of these connections and compares the responses of the FE models with rigid connections and those with flexible connections.

3.4.1 Screw Connections between Frame and Plate

Figure 3.16 shows the details of the screw connection between the steel plates and frames. The screws are modeled with zero-length link elements with three degrees of freedom per node. Directions x, y, and z indicate the local axes of a screw, and these orientations are shown in Figure 3.16. The x-axis coincides with the screw's main axis which is oriented in the out-of-plane direction with respect to the steel plate, the y-axis is parallel to the edge of the plate, and the z-axis is perpendicular to the edge of the plate, both of these being in-plane of the steel plates. The link elements are defined by the axial and shear stiffnesses of the screw. The torsional stiffness about the axial axis of the bolt and bending stiffnesses about the transverse axes are neglected. In other words, the twist and flexural deformation of the frame and plate are independent.

Table 3.6 and Figure 3.18 show the assumed link stiffnesses along the three axes. Modal analysis is performed under the assumptions of linear force-displacement response,

and therefore the initial stiffness is important. The axial stiffness (K_a) and shear stiffness (K_s) are computed based on the section area of screw (A_s), thickness of plates (t_p), and the material properties of plates and screws. The determination of these values and failure modes are described in detail in Chapter 5. K_a is based on the force-deformation relationship for pull-out and pull-over/through failure in tension, and K_s is based on the initial stiffness of the pull-out failure due to tilting and bearing in shear. Although screws can elongate under axial force, their yield strength amounts to 100 ksi. Despite the preloaded tension which is around 1.8 kips (per a Number 10 screw which has a 3/16" diameter), the yield limit amounts to 2.8 kips. Therefore, it is assumed that the pull-over and pull-over/though failure govern the force-deformation function of a screw.
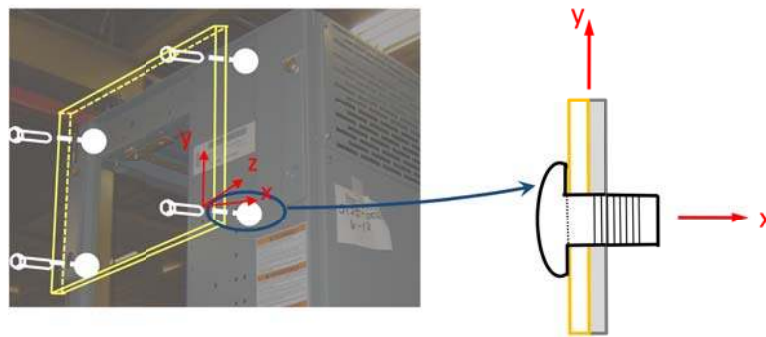
Figure 3.16 Link (Zero-Length) Element for Bolt Connection

(a) Axial Force   (b) Shear Force
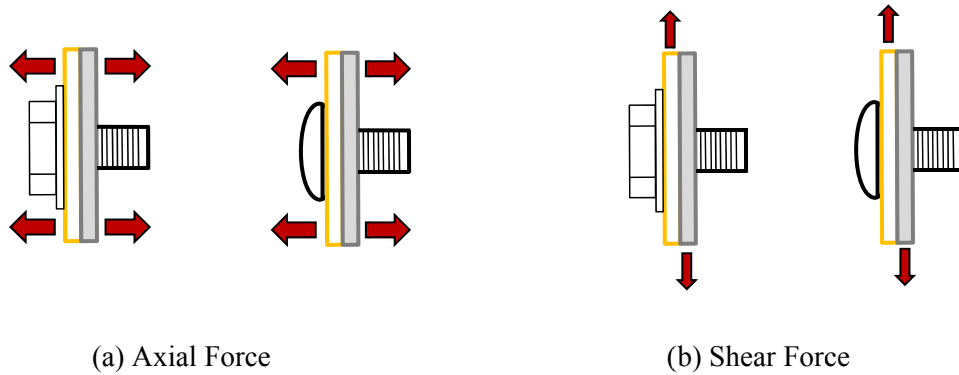
Figure 3.17 Acting Forces in Screws (Link Elements)

Table 3.6 Stiffness of Link Element for Screws

Fx	Fy	Fz	Mx	My	Mz
Pulling-out or Pulling-over/through In Tension	Tilting and Bearing in Shear	Tilting and Bearing in Shear	Free	Free	Free
K_a (kip/in)	K_s (kip/in)	K_s (kip/in)	-	-	-
7.60	24.1	24.1	-	-	-
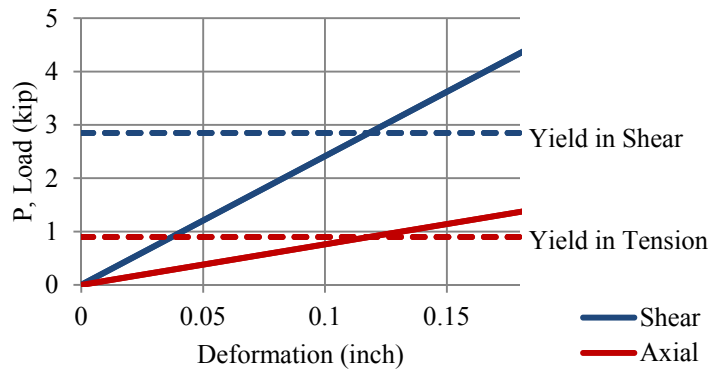
Figure 3.18 Stiffness in Link Elements for Number 10 Screws

3.4.2 Bolted Joint Connections

Bolted connections are used in the frame member connections, and the analysis in Section 3.3.1 treated situations where frame connections were rigid leading to higher fundamental frequencies in comparison to resonance search test results as shown in Table 3.3. In order to more accurately model the real behavior of the switchboard cabinets, it is therefore imperative to modify the beam bending and torsional stiffnesses of the frame connections in the FE models. Figure 3.18 shows the details of real connections of the frame members. Vertical members and horizontal members are connected with different

types of bolts, and the connections are not rigid, so it is a poor approximation to model these as rigid connections as if they were welded joints. Connections modeled with finite bending and torsional stiffnesses are more realistic, and therefore the bending and torsional moment capacities of the connections between horizontal and vertical members are reduced in the FE model with link elements of finite stiffness used for the linear modal analysis.

The connections shown in Figures 3.19 (a) and (c) are assumed to be partially-rigid, while the connections shown in Figure 3.19 (b) are assumed to be pinned and therefore cannot carry bending or torsional moments. The connections (a) and (c) transmit shear and axial forces as well as bending and torsional moments, while the connection (b) transmits shear and axial forces without any bending moments. In order to determine the force-deformation behavior of the partially-rigid connections, a detailed finite element model of the connection is generated in OpenSees, and the initial stiffness of the connection in each degree of freedom is evaluated and presented in Table 3.7. The detailed OpenSees models are described in Chapter 5. Effects of the characterized partial rigidity of the connection on the fundamental frequency of cabinet structures are studied in Appendix 1.3. The results for the cases of a cabinet with partially-rigid and rigid connections are presented in Table 3.8.

(a) Horizontal and Vertical Members at Top Front Side

(b) Horizontal and Vertical Members at Middle

(c) Horizontal and Vertical Members at Bottom
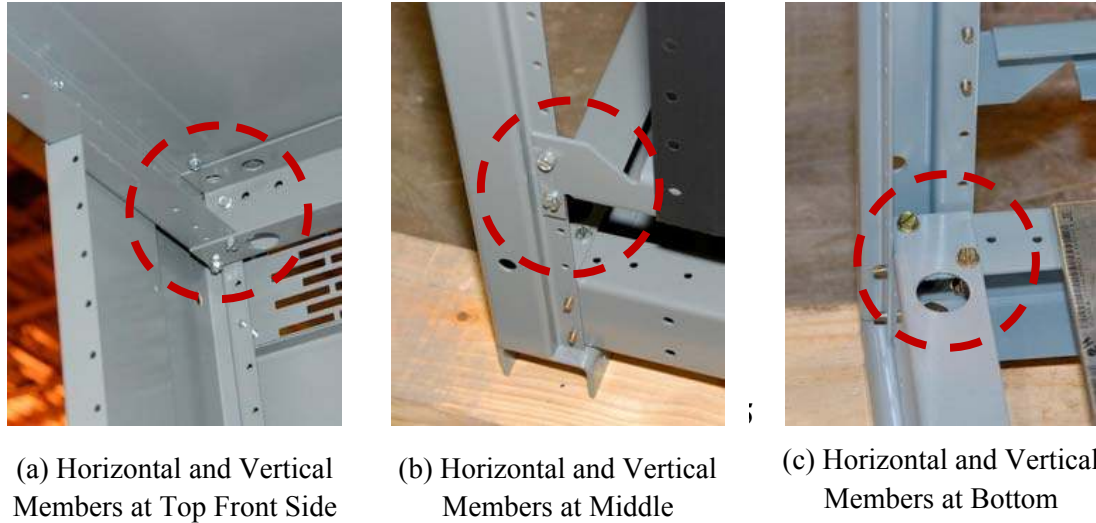
Figure 3.19 Joint Connections of Frames

For linear modal analysis performed on the FE model, the bending and torsional moment capabilities of beam-column elements at connections (a) and (c) are reduced from the rigid condition using link elements with finite stiffness properties. It is assumed that the beam deformations due to the shear and axial forces can be neglected, so that only the beam deformation due to bending is considered. In order to define the moment-rotation deformation relationships of these connections, more detailed FE models are formulated, and their initial stiffnesses in three directions are used for the FE models for the modal analysis.

Chapter 5 describes the specifications of the frame connection model considering both linear and nonlinear deformations.   In this chapter, only the computed initial stiffnesses are used in the zero-length elements in the OpenSees FE models for the modal analysis. Figure 3.20 shows a typical frame joint connection and the local coordinate for the left horizontal member shown in green. For the connection for the horizontal member, the deformations due to the axial (F_x) and shear (F_y and F_z) are neglected, and the rotational displacements due to moments (M_x, M_y, and M_z) are considered as shown in

Figure 3.21.   Each moment-rotation relationship has nonlinear behavior, but its initial stiffness is used for the linear modal analysis in this chapter.

(a) Typical Joint Connection   (b) Local Coordinate of Horizontal Beam
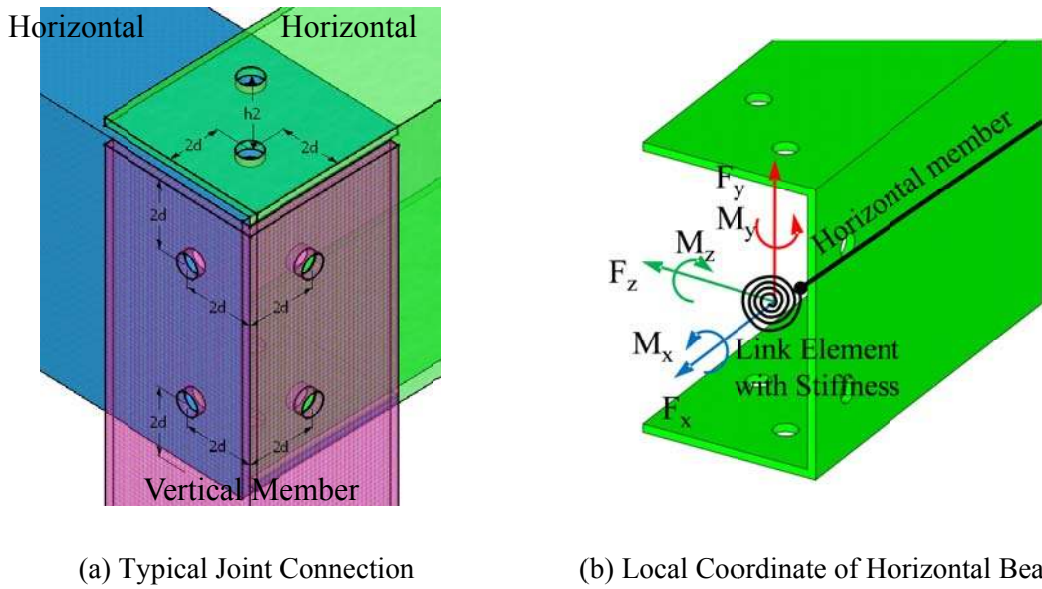
Figure 3.20 Local Coordinate of Horizontal Beam

(a) 1/4" Diameter Bolts   (b) 1/2" Diameter Bolts
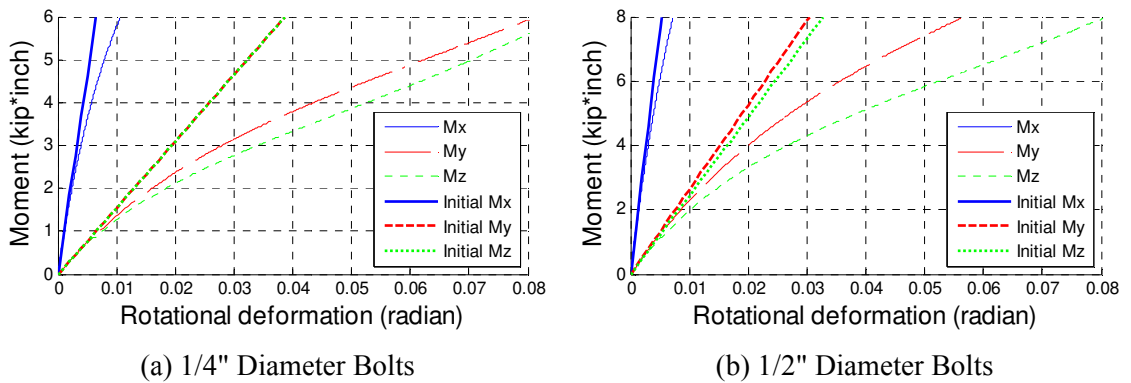
Figure 3.21 Stiffness in Link Elements for Bolted Connections

Table 3.7 Initial Stiffness in Link Elements for Bolted Connections

Fx	Fy	Fz	Mx	My	Mz
K_a (kip/in)	K_s (kip/in)	K_s (kip/in)	K_{Mx} (kip·inch/rad)	K_{My} (kip·inch/rad)	K_{Mz} (kip·inch/rad)
15.6	240	240	925	158	158

Table 3.8 shows a comparison of two FE models for Unit 2 with different connection conditions. Table 3.3 in a previous section showed the fundamental frequencies of all FE models with rigid connections, and Table 3.4 showed the fundamental frequencies of modified FE models with partially-rigid connections using link elements.

Table 3.8 Fundamental Frequencies of FE Models for Unit 2

Mode	Rigid Frame Connections (Hz)	Partially Rigid Frame Connections (Hz)
1	15.5	7.23
2	16.3	9.66
3	19.5	14.5
4	20.0	15.4
5	20.7	16.7

Depending on the stiffness of connections, the fundamental frequencies of cabinets varies. Appendix 1.3 includes tables for the variations of fundamental frequencies of cabinets with different stiffness of connections.

3.5   Closure

1. Versatile simplified Finite Element (FE) models are generated to evaluate the linear dynamic response characteristics of switchboard cabinets. The FE models are composed of the elastic quadrilateral shell, beam-column, and link elements that provide the ability to consider a wide range of frame and plate connection stiffnesses.

2. Through the linear modal analysis, the fundamental mode shapes and frequencies of switchboard cabinets and each modal mass participation factors are evaluated.

These results help in understanding the global mode shapes due to the frame behavior and local mode shapes of steel plates.

3. Two sets of FE models are generated to investigate the effect of steel plates on the dynamic behavior of switchboard cabinets. One set is generated considering the stiffnesses of frames and steel plates, and the other set is constructed accounting for only the stiffness of the frame without steel plates. Based on the modal analysis results of the two models, it is confirmed that the presence of the steel plates significantly increases the fundamental frequencies of the switchboards.

4. The local mode shapes and frequencies of rear plates are studied considering different boundary conditions. It is seen that the global behavior of the frame affect the local mode shapes and frequencies of rear plates at the lower modes. At the higher modes, on the other hand, the global behavior of the frame is negligible and the rear plate behaviors govern the mode shapes.

5. In order to capture realistic fundamental frequencies and mode shapes, the stiffnesses of the connections are considered in the FE models. Linear force-deformation relationships of bolted connections and screw connections are implemented in the FE models, and their modal analysis results are compared to those of the other FE models with rigid connections. The fundamental frequencies of the switchboard cabinets are sensitive to the stiffnesses of the bolted frame connections, as shown by modal sensitivity plots.

CHAPTER IV

NUMERICAL MODELS FOR NONLINEAR SUPPORT BOUNDARY CONDITION

4.1   Introduction

4.1.1   Numerical models of support boundary condition

The development of numerical models of switchboard cabinets using the finite element (FE) approach was discussed in Chapter 3. It was established that the dynamic characteristics of the model are very sensitive to the support boundary conditions. This is as expected because the switchboard cabinets themselves are relatively rigid structures.

In this chapter, the various types of motions of relatively rigid equipment acted on by ground excitation are explained and numerical models are presented for obtaining highly nonlinear behavior of cabinets resting on a plane surface. Damage from recent earthquakes (see photos in Chapter 2) shows that mechanical and electrical equipment in seismic zones should be anchored at the base. The support boundary conditions for switchboard cabinets examined by FEA in Chapter 3 were assumed fixed at the base. However, in many cases, heavy nonstructural components such as electrical and mechanical equipment are installed without complete base restraints, leading to sliding and rocking behavior during ground motion. The images in Figure 4.1 show examples of seismic damage to electrical cabinets due to the inadequate restraint conditions during the 2010 Haiti Earthquake. Figure 4.1 (a) shows the pull-out failure of anchor bolts and

spalling of concrete along the edge of the base pad. This suggests that the cabinets rocked back-and-forth during the earthquake. The anchor bolt embedment was not properly designed to resist the tensile force caused during seismic excitation. In Figure 4.1 (b), sliding of the electrical equipment led to another mode of failure. In both cases, the equipment is unlikely to remain operational after the earthquake. These failure modes show the importance of support boundary conditions to prevention of rocking and sliding failure modes.
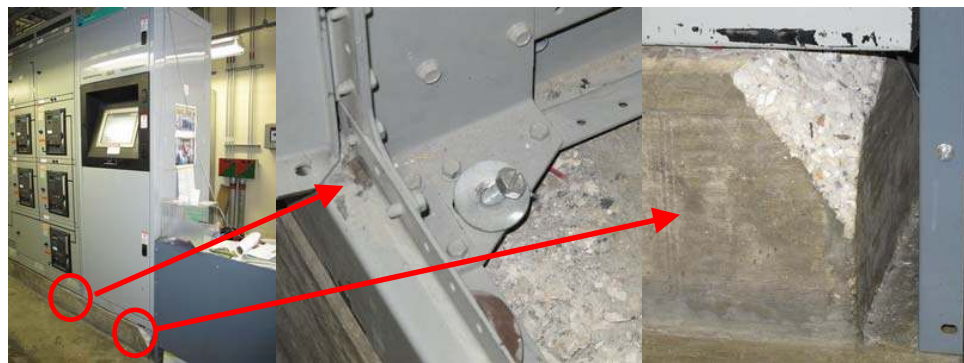
(a) Indoor Electrical Cabinets – Anchor Pull-Out

(b) Outdoor Electrical Cabinets – Sliding

Figure 4.1 Seismic Damage to Electrical Cabinets

Both rocking and sliding modes of failure can be established in experiments, such as shake table tests, for a limited range of cabinet configurations. However, numerical models provide a more efficient way to evaluate linear and nonlinear behavior of various types of equipment for a broad range of support motion input conditions. Numerical

models can then be used to conduct parametric studies to investigate the impact of total weight, geometry, type of fasteners, and different types and arrangements of internal contents on the performance of the cabinet under various earthquake ground motions.

Chapter 4 presents the development of numerical models for use in nonlinear response evaluation of electrical and mechanical equipment for a variety of support conditions. These FE models have the ability to capture various motion types associated with rigid blocks such as resting, sliding, rocking, and up-lift during seismic excitation as shown in Figure 4.2. The FE models are validated by comparison with analytical closed-form solutions. Section 4.2 presents a discussion of the nonlinear behavior of unrestrained rigid blocks is studied for different support boundary conditions. Unrestrained and restrained systems exhibit different response behaviors under seismic excitation. The nonlinearity in their responses depends on their geometry, total weight, conditions of the ground surface, type and properties of fasteners, and the characteristics of ground motions such as different peak ground acceleration or frequency content. Restrained equipment moves very little (if at all) under relatively weak excitations. However, as the magnitude of ground shaking increases, the fasteners may yield and the equipment may start to slide or rock. Eventually, the equipment behaves like a free-standing block after its fasteners have failed under the strong seismic excitation. This indicates that a multitude of dynamic response behaviors may be exhibited by relatively rigid nonstructural components mounted on the ground during seismic excitations. The detailed formulation of the finite element (FE) models to their dynamic response is presented in Section 4.3.

4.2   Analytical Models for Unrestrained Blocks

4.2.1   Previous Studies of Nonlinear Behavior of Rigid Blocks

For the study of dynamic behavior of nonstructural components, various types of motions of unrestrained rigid block have been studied. Shenton et al. (1996) classified the nonlinear behavior of unrestrained rigid blocks subjected to horizontal and vertical base excitation into five different types: resting, sliding, rocking, sliding-rocking, and free flight, as shown in Figure 4.2. This research also presented initiation conditions for each of the five motion types along with the governing equations. The governing equations included the effects of the slenderness ratio of rigid blocks, the coefficient of friction, and the peak horizontal acceleration, as shown in Figure 4.3. These equations have also been used by other researchers to develop analytical models which include sliding or rocking motions. Taniguchi (2002) suggested a more detailed classification of nonlinear behavior considering the commencement and termination conditions of each motion. The governing equations and conditions for each mode were also presented. These analytical solutions described different types of nonlinear behavior exhibited by

    (a) Resting   (b) Sliding   (c) Rocking   (d) Sliding-rocking   (e) Free Flight
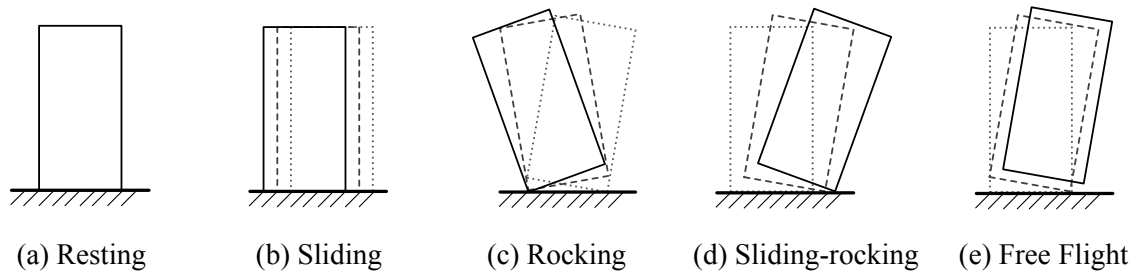
Figure 4.2 Motion Types of Free-Standing Rigid Block

rigid blocks under both vertical and horizontal seismic shakings, and each motion type has its own assumptions and conditions for the initiations.
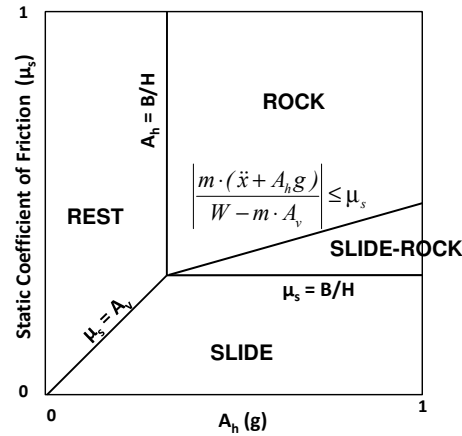
Figure 4.3 Motion Types Depending on Friction and Horizontal Acceleration
(Shenton, H et al., 1996)

Yim, et al. (1980) derived the governing equations of motion for the rocking behavior of unanchored blocks subjected to seismic shaking and presented their response sensitivity to the properties of ground motions. Aslam et al. (1980) studied the rocking motion of unrestrained and restrained rigid blocks using shake table tests, confirming that the experimental data under harmonic tests were repeatable and suitable for comparison with equivalent analytical results. However, similar tests using earthquake ground motion were not exactly repeatable and therefore could not be used for a precise comparison with analytical solutions. Makris and Zhang (2001) developed analytical models for rocking of anchored blocks under horizontal pulse-type motions and earthquake ground motions. They described how the ductility of anchor bolts affects nonlinear behavior of a rigid block in different frequency ranges and demonstrated rocking behavior under seismic excitation.

68

The analytical rocking models by Aslam et al. (1980) and Makris and Zhang (2001) cannot capture the extent of nonlinearity and true behavior, as a function of time, of rigid blocks under seismic excitation, although they provide information on the magnitude of the horizontal pulse required to cause the block to overturn. This can be attributed to the fact the their analytical models are characterized by rocking alone without capturing bouncing/pounding, as illustrated in Figure 4.4. Less slender blocks tend to bounce back (or pound the ground surface) instead of rocking after the block uplifts. In addition, analytical models which include pounding behavior fail to capture the force-displacement relationship of fasteners as well as the dynamic response of the blocks. Makris and Zhang (2002) and Taniguchi (2002) both considered the nonlinear dynamic behavior of restrained rigid blocks but ignored the pounding problem resulting from elastic impact of two rigid solid surfaces. This could lead to serious errors in the force and deformation results from time history analyses which include the rocking behavior of blocks. The rocking and pounding behaviors are explained at length in Section 4.3.3.

(a) Rocking   (b) Pounding
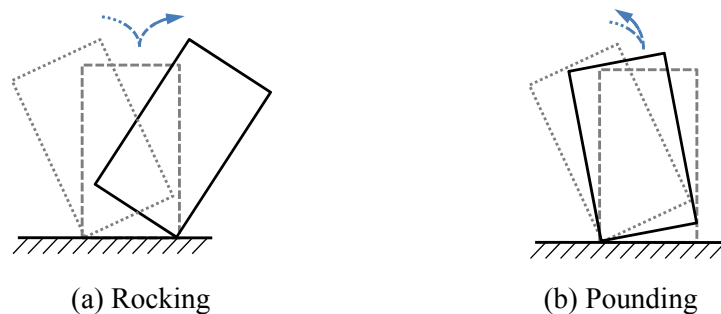
Figure 4.4. Rocking and Pounding

In contrast to the unrestrained block condition, a restrained rigid block does not move under seismic shaking until its fasteners yield or fracture. As the fasteners yield, the block starts to rock or slide. Lin et al. (1994) developed a sliding analytical model of a restrained block and considered the breaking limit of anchorage ties when the block was

subjected to horizontal and vertical base excitation. Garcia and Soong (2003) also considered the restraint breakage and sliding motion of blocks and developed seismic fragility curves of a restrained rigid block. Both of these studies used a Coulomb friction model to account for the friction force between the block and the underlying ground surface. The FE models were developed assuming that the rigid blocks were anchored by post-tensioned cables and were subjected to horizontal excitations (vertical acceleration effects were ignored). This means that the anchorages were assumed to resist only the vertical forces and not the relative lateral motion of two solid surfaces in contact. These models fail to capture the combined motion of rocking and sliding and further do not consider the force-displacement relationship of anchor bolts used for mechanical and electrical equipment which are vulnerable to vertical forces.

The existing literature does not offer much guidance on the application of such nonlinear models in practical situations. This is mostly due to the complexity of the response characterization of unrestrained and restrained rigid blocks under seismic excitation. The problem is compounded by the effect of support boundary conditions. The present study tries to address this gap and further the state-of-the-art by developing accurate FE models which could be used to better understand the vulnerability of these systems.

4.2.2 Sliding Analytical Model

4.2.2.1 *Analytical Background*

The sliding model represents pure sliding motion without any consideration of overturning or free-flight movement. Therefore, the supporting surface of the block

always remains in contact with the underside of the block. A free-standing rigid block of width b, height h, and mass m rests on a supporting surface and is subjected to horizontal and vertical base excitations of $\ddot{x}_g$ and $\ddot{y}_g$ respectively as shown in Figure 4.5. Several specific assumptions are needed in order to define the pure sliding model. Equation (4.1) below presents the required condition for the block not to jump but rather just slide laterally. If the vertical ground acceleration exceeds the acceleration due to gravity (g), the block jumps from the ground and enters free-flight motion illustrated in Figure 4.2 (e). The sliding model also assumes that the only resistance to horizontal inertia forces is the friction force. The friction force occurs at the block-ground surface interface, and the magnitude of the maximum friction force F is defined using a simple Coulomb-type friction model, as described in Eq. (4.2). The friction force, F, is proportional to the vertical force on the block, $m(g + \ddot{y}_g)$, and μ_s is the coefficient of static friction. When the horizontal inertia force, $m \cdot \ddot{x}_g$, surpasses the maximum friction force F, the block starts to slide. Equation (4.3) presents the condition for the commencement of sliding motion of the block.

$$\ddot{y}_g \leq g \tag{4.1}$$

$$F = \mu_s \cdot m(g + \ddot{y}_g) \tag{4.2}$$

$$\left| \ddot{x}_g \right| \geq \mu \cdot (g + \ddot{y}_g) \tag{4.3}$$

The condition that the sliding block should neither pivot nor rock is expressed in Eq. (4.4). If this condition is not satisfied, the block will pivot along the bottom edge, and the edge force is then equal to the total vertical force as shown in Figure 4.2 (c) and (d).

$$m\left|\ddot{x}_g\right|\frac{h}{2} \leq m(g + \ddot{y}_g)\frac{b}{2} \qquad (4.4)$$

Rearranging the above equation, we have,

$$\frac{b}{h} > \frac{\left|\ddot{x}_g\right|}{g + \ddot{y}_g} \qquad (4.5)$$

This equation shows that the geometry of the block (b and h), and in particular the slenderness ratio, b/h, as well as the magnitude of the base excitation determines if the block pivots or not, while the mass of the block does not play a role. The slenderness of the block may also be interpreted as the horizontal and vertical location of the center of the mass of a uniform block. For a complicated structure, the width-to-height ratio is computed from the center of the mass.

The equation of motion for the sliding model is expressed in Eq. (4.6). This equation shows that the mass of the block does not affect the sliding response under base excitations. The sign function, sgn($\bullet$), is defined in Eq. (4.7), and it characterizes the sign of the velocity. Coefficient μ is the coefficient of kinetic friction, which is assumed to remain constant during the entire excitation period.

$$\ddot{x}(t) + \mu \cdot [g + \ddot{y}_g(t)] \cdot sgn[\dot{x}(t)] = -\ddot{x}_g(t) \qquad (4.6)$$

$$sgn[\dot{x}(t)] = \begin{cases} 1, \dot{x}(t) > 0 \\ -1, \dot{x}(t) < 0 \end{cases} \qquad (4.7)$$

4.2.2.2 *Dynamic response of sliding analytical model*

As described by Eq. (4.6) in the previous section, the sliding response of a free-standing block is sensitive to both vertical and horizontal ground accelerations and also the coefficient of kinetic friction. For a more simplified equation, the vertical ground acceleration is assumed to be proportional to the horizontal ground acceleration, $k \cdot \ddot{y}_g(t) = \ddot{x}_g(t)$. Substituting this relation into Eq. (4.6), we have,

$$\ddot{x}(t) + \mu \cdot [g + k \cdot \ddot{x}_g(t)] \cdot sgn[\dot{x}(t)] = -\ddot{x}_g(t) \tag{4.8}$$

In Eq. (4.8), the sliding response is computed based on the horizontal ground acceleration, $\ddot{x}_g(t)$, the coefficient of kinetic friction, μ, and the ratio of horizontal-to-vertical ground acceleration, *k*. Interpretations of the value *k* were provided by Garcia and Soong (2003), who studied the sliding response of rigid blocks under El Centro ground motions. They showed that the response displacement of a sliding block decreases as the vertical ground acceleration increases. If the horizontal ground acceleration increases or μ decreases, the response displacement of a sliding block increases. In order to get the maximum sliding response as described in Eq. (4.8), the k-value (the ratio of vertical to horizontal ground acceleration) must be assumed to be zero.

Based on these ordinary differential equations, the displacement response *x(t)* is solved using the Bogachi-Shampine method (Shampine & Reichelt 1997) which is implemented in the function, *ode 23,* in MATLAB. It is a Runge–Kutta method of order three with four stages with the First Same As Last (FSAL) property, so that it uses approximately three function evaluations per step.

Figure 4.5(a) below presents unscaled ground accelerations recorded during the Northridge earthquake at the Rinaldi Station during January 17, 1994. Peak Ground Acceleration (PGA) as 0.84g. The plots in Figure 4.5(b) illustrate the displacement response *x(t)* of a rigid block subjected to the horizontal ground accelerations given in Figure 4.5 (a). They show the displacement response of the block as a function of the coefficient of friction, μ. The total residual displacement is not perfectly proportional to the magnitude of the coefficient of friction. The block with μ = 0.2 tends to fluctuate more on both sides of the dynamic equilibrium positions when compared to the block with μ = 0.4. Consequently the total residual displacement for μ = 0.4 is greater than
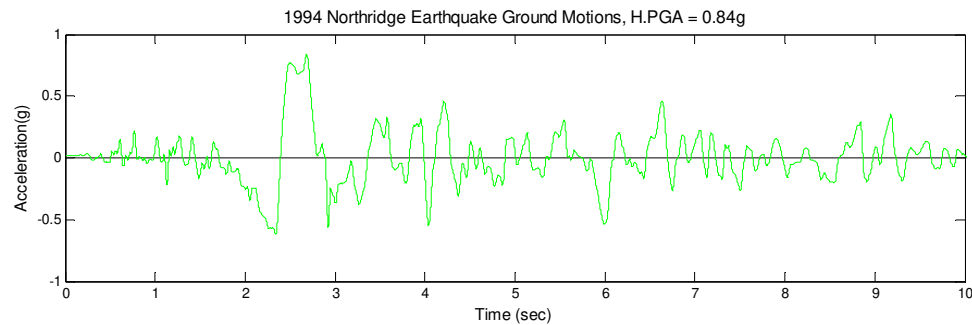
(a) Ground motion time history
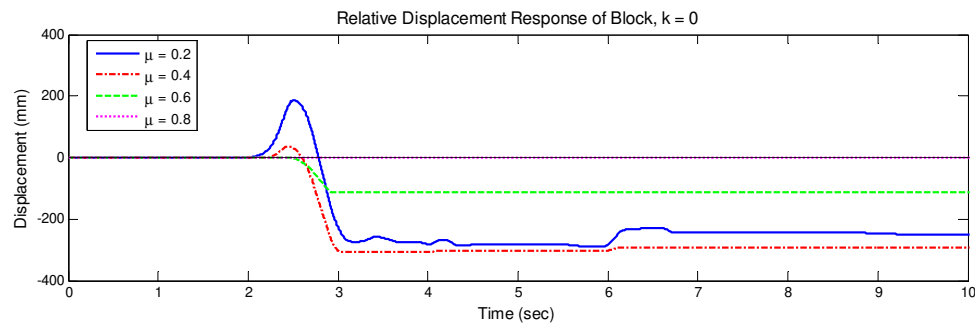
(b) Displacement response of rigid block

Figure 4.5. The effect of coefficient of kinetic friction, μ on the sliding response of rigid block for 1994 Northridge earthquake ground motions

that for μ = 0.2. This critical value of μ is dependent on the characteristics of the imposed ground motion.

Figures 4.6 and 4.7 show the effect of the magnitude of the horizontal peak ground acceleration on the displacement response of the block subjected to horizontal ground accelerations using the 1994 Northridge and 1940 El Centro earthquake time histories, respectively. The former is one of the strongest ground motion records with a PGA value of 0.84g, while the latter is characterized with broadband frequencies and a recorded PGA value of 0.35g. The two ground motions are scaled up and down with PGA values ranging from 0.3g to 0.9g, with the coefficient of friction set to 0.4, in order to determine the effect of the magnitude of the horizontal ground motions.
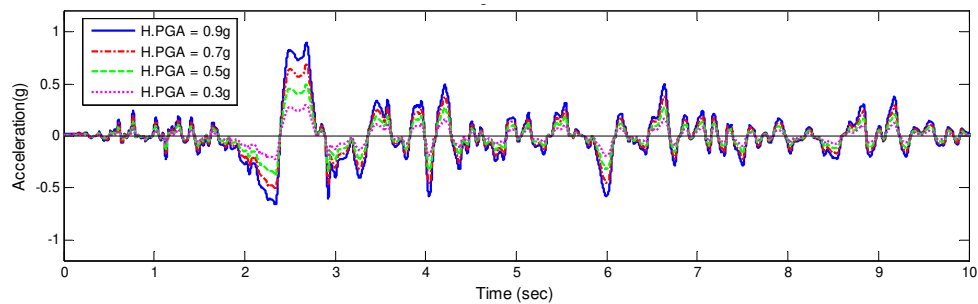
(a) The 1994 Northridge earthquake time histories scaled to different intensities
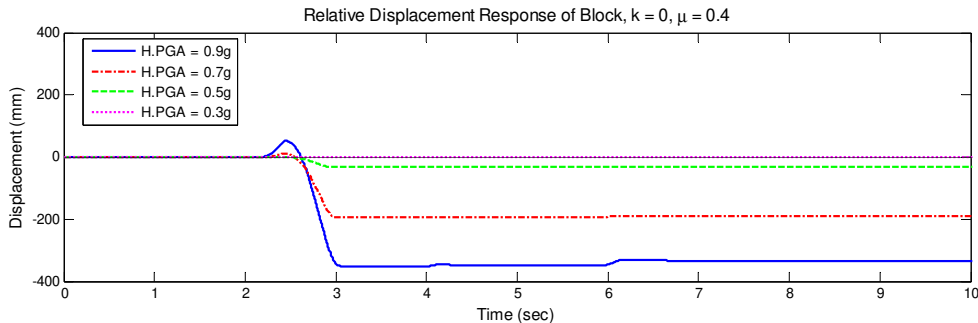
(b) Sliding response of rigid block

Figure 4.6. The effect of the horizontal peak ground accelerations from the 1994 Northridge earthquake on sliding response

The plots in Figure 4.8 show the maximum response displacement in both positive and negative directions as well as the residual displacement after ground shakings as a function of μ and PGA. These results are computed considering two sets of ground motions, with different PGA values ranging from 0.5g to 0.8g, and discrete coefficient of kinetic friction values ranging from 0.2 to 0.8. The Northridge and El Centro time histories are scaled up and down with the same PGA values, and the El Centro time history (30 sec) is three times longer than the Northridge time history (10 sec). However,
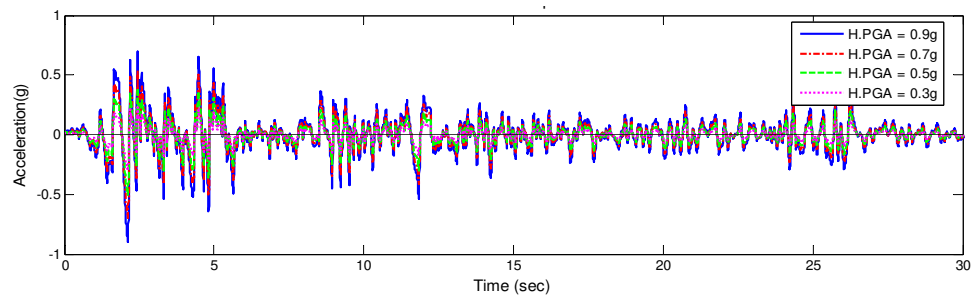
(a) The 1940 El Centro earthquake time history scaled to different intensities
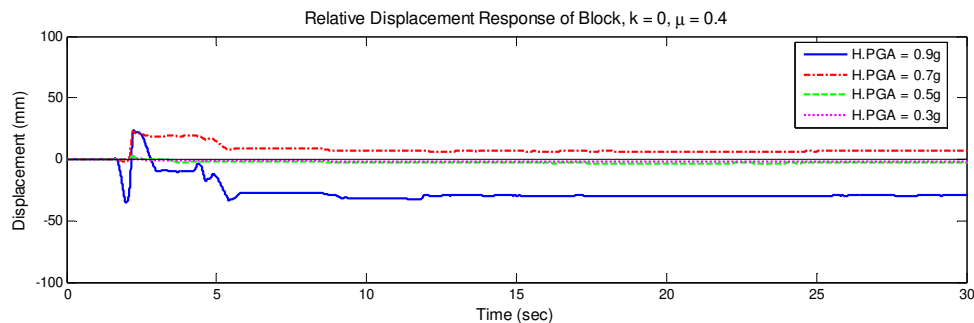
(b) Sliding response of rigid block

Figure 4.7. The effect of the horizontal peak ground accelerations from the 1940 El Centro earthquake on sliding response

both maximum response and residual displacements under the El Centro ground motion are much smaller than those under the Northridge ground motion. As the value of μ decreases, all response displacements tend to increase. However, some of the results under the same ground motions with same PGA show that they are not proportional to the

76

Scaled Northridge Ground Motions
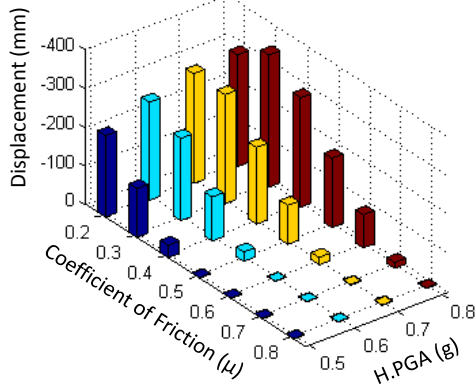
Scaled El Centro Ground Motions

(a) Maximum Displacement
in Negative Direction
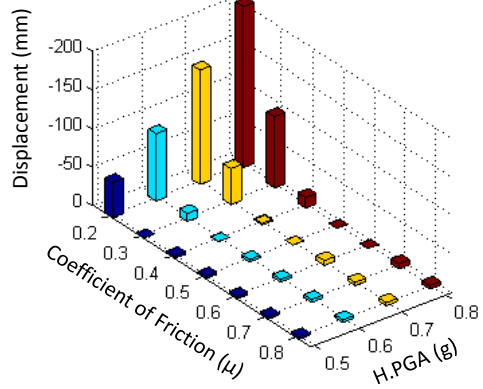
(b) Maximum Displacement
in Negative Direction
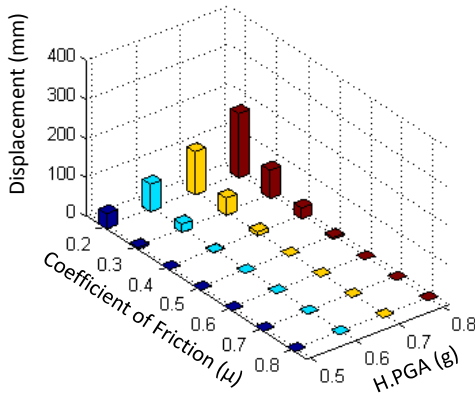
(c) Maximum Displacement
in Positive Direction
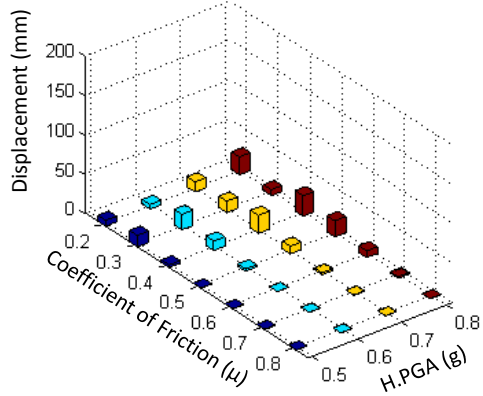
(d) Maximum Displacement
in Positive Direction
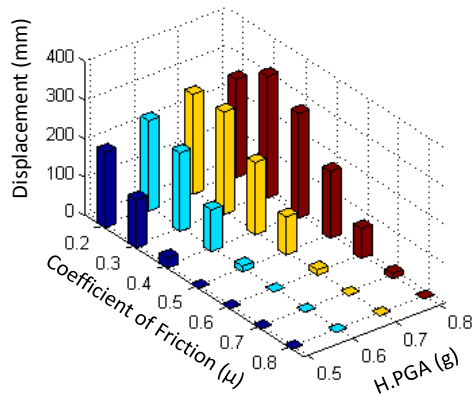
(e) Residual Displacement
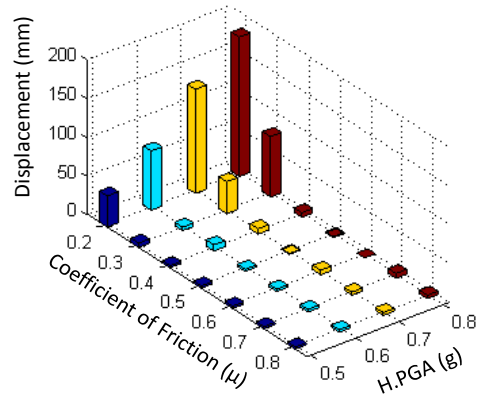
(f) Residual Displacement

Figure 4.8. Response displacement of analytical sliding models for two scaled ground motion sets

magnitude of the coefficient of friction, μ. Therefore, these results illustrate that the maximum response and residual displacements are dependent not only on the value of μ but also on the characteristics of the imposed ground motion.

4.2.3 Rocking Analytical Model

4.2.3.1 *Analytical background*

Unrestrained cabinet units can slide under seismic excitation, as illustrated in Figure 4.2 (b), while relatively slender restrained switchboard cabinet units tend to rock back and forth depending on their geometry and restraint types. Yim et al (1980) derived analytical solutions for the rocking motion of a free-standing rigid block. The ideal rigid block model used by Yim et al. is shown in Figure 4.9 (a). A free-standing rigid rectangular block is subjected to horizontal ground acceleration, $a_g{}^x$, and vertical ground acceleration, $a_g{}^y$. It is assumed that the geometric and mass centers are the same and that there is a sufficiently large friction force between the block and the ground surface that the block does not slide but rather rocks under horizontal ground excitations. The angular mass moment of inertia, I_o, about the center of rotation is assumed to be $\frac{4}{3}\frac{W}{g}R^2$ by considering that the total mass, $m = W/g$, where W is the weight of the block and g is the acceleration due to gravity, is uniformly distributed over the rectangular shaped base. The block oscillates about the centers of rotation O and O' as shown in Figure 4.9 (b). The angle, $\alpha = \tan^{-1}(B/H)$, is a measure of the slenderness of the block and represents a critical angle deciding the tipping point of the block. When the rotation, θ, of the block reaches the critical angle, α, the block approaches the bifurcation of stable and unstable

78

states. That is, when $|\theta| > \alpha$, the block falls over due to the overturning moment of the gravity load and then cannot return to the original position without an additional restoring force. However, the block experiences a rocking or oscillatory motion when $|\theta| < \alpha$.
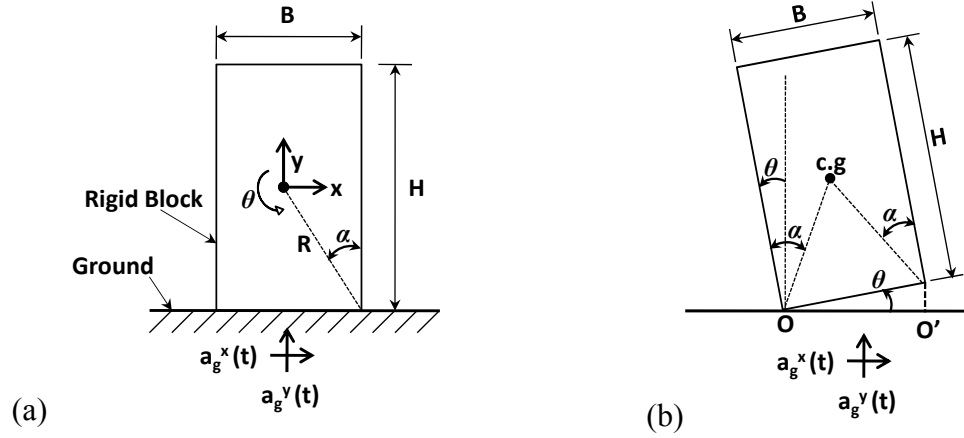
Figure 4.9. Schematic of Free-Standing Rocking Block

Equation 4.9 (a) describes the initial instant at the start of rocking motion of the block, when the overturning moment of the horizontal inertial force, $W \cdot a_g^x / g$, about the one of corners (O' or O) exceeds the restoring moment of the vertical inertia force due to the weight of the block, W, and vertical ground acceleration, $W \cdot a_g^y / g$.

$$\frac{W}{g} a_g^x \frac{H}{2} > \left(W - \frac{W}{g} a_g^y \right) \frac{B}{2} \qquad (4.9 \text{ a})$$

Rearranging the above equation, the limiting value for a_g^x is found to be

$$a_g^x > \frac{B}{H} g \left(1 - \frac{1}{g} a_g^y \right) \qquad (4.9 \text{ b})$$

Equations 4.10(a) and 4.10(b) show the equations of motion of the block in rocking motions about the centers of the rotation O or O' respectively. These equations are derived by considering the equilibrium of moments for the rotational angle θ response of the block.

79

$$I_o\ddot{\theta}(t) + W\left(1 - \frac{a_g^y(t)}{g}\right) \cdot R \cdot \sin(\alpha - \theta(t)) = -\frac{W}{g} \cdot R \cdot \cos(\alpha - \theta(t)) \cdot a_g^x(t) \qquad \text{(4.10 a)}$$

$$I_o\ddot{\theta}(t) + W\left(1 - \frac{a_g^y(t)}{g}\right) \cdot R \cdot \sin(\alpha + \theta(t)) = -\frac{W}{g} \cdot R \cdot \cos(\alpha + \theta(t)) \cdot a_g^x(t) \qquad \text{(4.10 b)}$$

where, R is $\frac{1}{2}\sqrt{B^2 + H^2}$ which is the distance between the center of the mass and the center of rotation.

4.2.3.2   *Dynamic Response of Rocking Analytical Model*

(1) The Effect of Block Weight (W)

Equation (4.11a) below results from substituting the expression for I_o in Eq. (4.10a). The weight of the block, *W*, is uniformly distributed over the rectangular shape of the block.

$$\left(\frac{4W}{3g}R^2\right) \cdot \ddot{\theta}(t) + W\left(1 - \frac{a_g^y(t)}{g}\right) \cdot R \cdot \sin(\alpha - \theta(t)) = -\frac{W}{g} \cdot R \cdot \cos(\alpha - \theta(t)) \cdot a_g^x(t) \qquad \text{(4.11 a)}$$

Equation (4.11b) is a simplified result of Eq. (4.11a) which is obtained by cancelling out W and R.

$$\frac{4R}{3g} \cdot \ddot{\theta}(t) + \left(1 - \frac{a_g^y(t)}{g}\right) \cdot \sin(\alpha - \theta(t)) = -\frac{1}{g} \cdot \cos(\alpha - \theta(t)) \cdot a_g^x(t) \qquad \text{(4.11 b)}$$

Equation (4.11c) below is given by defining $\omega_o^2 = \frac{3g}{4R}$ in Eq. (4.11b), where g is the gravitational acceleration, and R is the distance between the center of mass (i.e., geometric center for a rectangular shape) and the center of rotation O or O'.

$$\ddot{\theta}(t) + \omega_o^2 \cdot \left(1 - \frac{a_g^y(t)}{g}\right) \cdot \sin(\alpha - \theta(t)) = -\omega_o^2 \cdot \frac{1}{g} \cdot \cos(\alpha - \theta(t)) \cdot a_g^x(t) \qquad (4.11 \text{ c})$$

In this form, it is clear that, the rotational angle, θ, of a block is not related to the weight of the block, similar to the case of a simple pendulum. However, the radian fundamental frequency of this rigid block is not as simple as the pendulum. The radian fundamental frequency of a simple pendulum is $\sqrt{\frac{g}{L}}$, where g is the gravitational acceleration, and L is the length of the pendulum. On the other hand, the radian fundamental frequency of the rigid block is not constant, but it varies not only depending on $\omega_o = \sqrt{\frac{3g}{4R}}$ but also depending on the critical angle, α, as well as the vertical and horizontal ground accelerations, a_g^y and a_g^x.

These ordinary differential equations are solved for the rotational angle, θ, of ground motion time histories and blocks with various parameters using the *ode 23* function in MATLAB as used for the sliding motions.

(2) The Effect of Block Dimensions

The dimensions of blocks determine the critical angle, α, as well as the distance R from the center of the mass to the center of the rotation, and these two parameters are important to describe the dynamic characteristics of rocking blocks. As the ratio, *H/B,* increases, the block becomes more slender. A slender block has a smaller critical angle, and therefore it is more vulnerable to overturning and more prone to oscillate. Further the R value of the block is related to the period of oscillation. Their contributions to the dynamic characteristics of rocking motions are analyzed in this section.

81

Figure 4.10 (a) shows different shapes of blocks with the same distance, R, from the center of the mass to the center of the rotation. The slenderness ratio of blocks varies between 1.5 and 4, while distance R is constant. Figure 4.10 (b) shows the same slenderness ratio of blocks with variable of R values. The R values of blocks with the same critical angle are proportional to the height and width of block. Figure 4.10 (c) shows different R values and slenderness ratios of blocks having the same width. The slenderness ratios are identical to Figure 4.10 (a) but the dimensions of blocks are different.

Same $\frac{1}{2}\sqrt{B^2+H^2}$	Different $\frac{1}{2}\sqrt{B^2+H^2}$	Different $\frac{1}{2}\sqrt{B^2+H^2}$
Different H/B	Same H/B	Different H/B
		Same Width
(a)	(b)	(c)
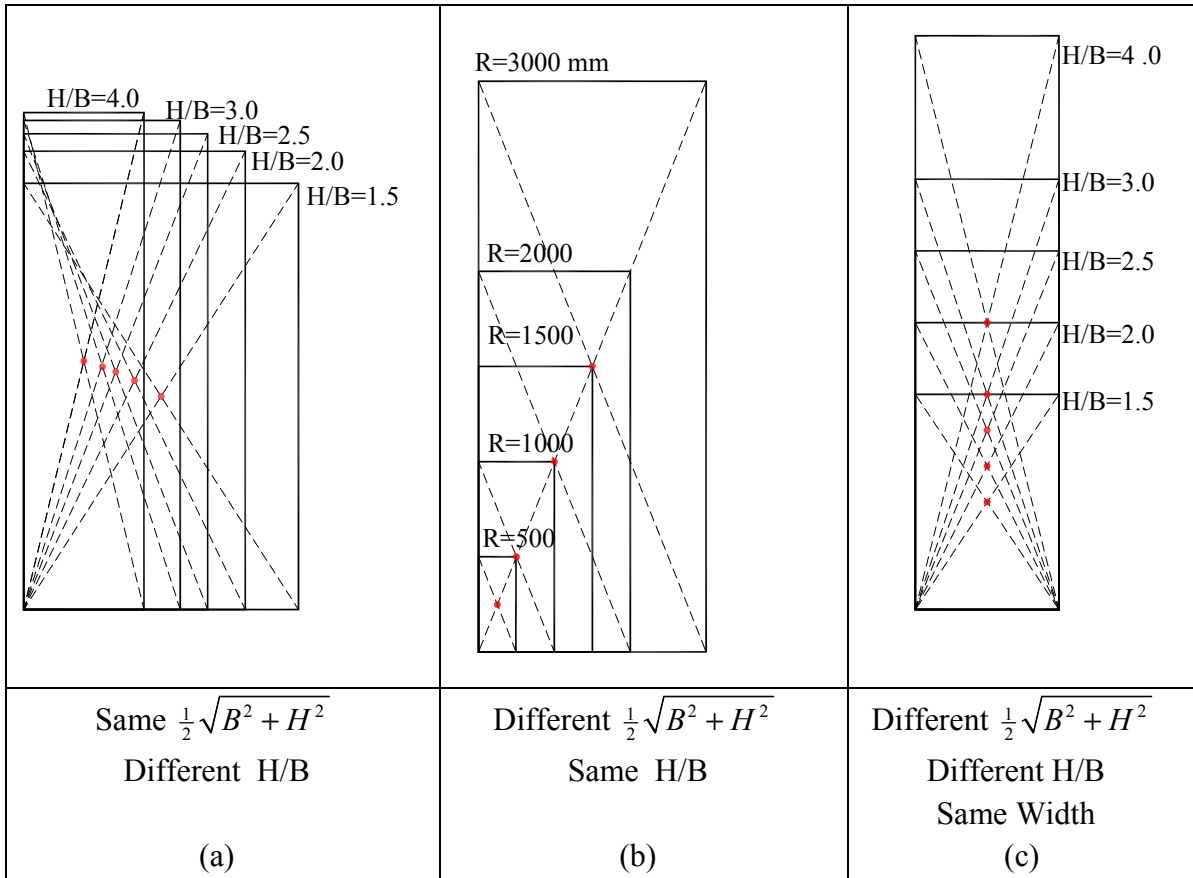
Figure 4.10. The Effect of geometry of blocks on rocking response

Figure 4.11 (a) shows the unscaled Northridge Earthquake ground acceleration histories record at Rinaldi in Jan. 14, 1994 which was illustrated in Figure 4.6 (a) (scaled to different intensities) and was used for horizontal excitation. Using this ground motion, the rotational response, θ, of a rocking block is computed from the differential equations, Eqs. (4.10 a, b) for each time step. Figures 4.10 (b), (c), and (d) illustrate the rocking behavior of blocks for conditions described in Figures 4.10 (a), (b), and (c), respectively. For these analyses, the effect of vertical ground acceleration is ignored. It is also assumed that blocks do not slide and are characterized by a rocking motion alone, as explained in Section 4.2.2.1. In each case, the vertical axis is the ratio of rotational response to the critical angle, θ/α. When this ratio reaches 1 or -1, the block topples over and cannot return to the original position.

Figure 4.11 (b) shows the rotational response of blocks with different slenderness ratios but the same R value under the 1994 Northridge Earthquake ground motion. Less slender blocks (H/B=1.5 and H/B=2) tend not to topple over, although for H/B=2 the block tends to oscillate about the dynamic equilibrium position. On the other hand, blocks with H/B values of 2.5 and larger toppled over at approximately 3 sec.

Figure 4.11 (c) shows the rocking response of blocks with same slenderness ratio (H/B=2.5) but different R values. Blocks with greater R values such as 3000 mm oscillate about the dynamic equilibrium position, while smaller blocks with R values of 1500 mm and below overturned at approximately 3 sec. This is attributed to the fact that the fundamental frequencies of blocks are switched depending on the R values and also the response period changes depending on the ground motion.
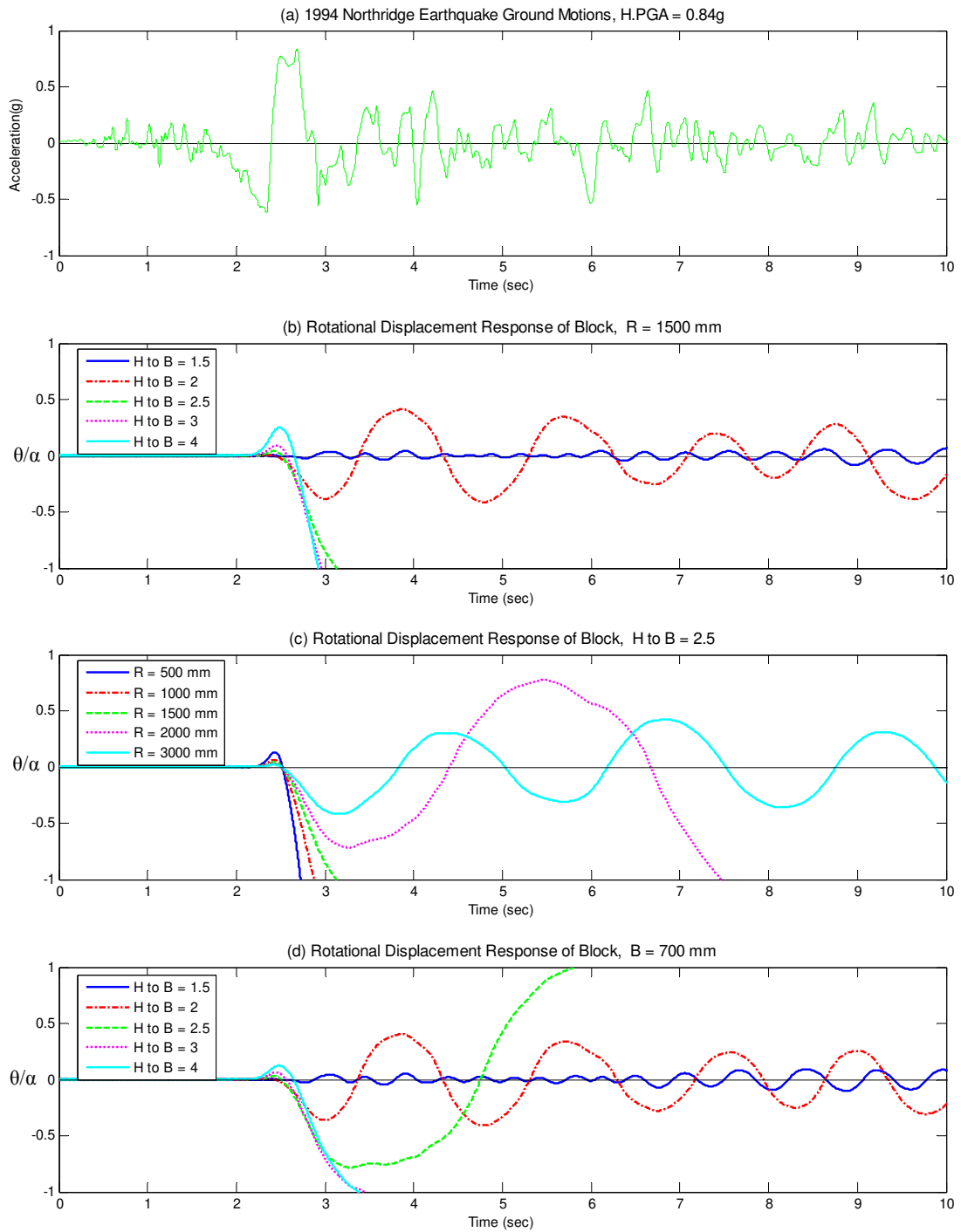
Figure 4.11. The effect of dimensions of blocks on rocking response

Figure 4.11 (d) shows the rocking response of blocks with constant width but different *R* values and slenderness ratios, and should be compared to the plots in Figure 4.11 (b), as the slenderness ratios are the same but the dimensions are different. Some interesting inferences can be drawn based on inspection of Figure 4.10 (d). For example, it can be seen that for the same value of slenderness ratio, *H/B* = 1.5 the response amplitude for a block with *R*=1500 mm shown in Figure 4.11(b) is smaller than that of a block with *B*=700 mm and *H/B* = 1.5, which is *R*=631 mm, shown in Figure 4.11(d). Moreover, the response amplitude of a block for *H/B*=2.5 and *R*=1500 mm in Figure 4.11(b) is greater than that of a block for *H/B*=2.5 and *R*=1885 mm in Figure 4.11(d). In other words, greater *R* values are associated with smaller amplitudes of rocking response of blocks as shown in Figure 4.11(c) for this ground motion.

(3) The Effect of Mass Distribution

The previous sections on rocking response are based on the assumption that the mass of the block is uniformly distributed, and therefore rotational mass is $I_o = \frac{1}{3} m \cdot (B^2 + H^2)$ about the center of rocking motion as shown in Figure 4.12 (b). However, the mass distribution of the electrical equipment such as switchboard cabinets need not be uniformly distributed, depending on the location of devices inside and their overall configuration. Therefore, blocks with the same total weight and dimensions can have different mass distributions, and consequently their rotational mass could be quite different. Figure 4.12 shows extreme cases of concentrated mass and uniformly distributed mass. The rotational mass for each case is computed on the assumption that the dimensions and center of mass are identical for each case. The rotational mass of a block with uniformly distributed mass is 4/3 times greater than the case with concentrated

mass. In Figure 4.12, f denotes the mass distribution factor which is zero for case (a) and one for the uniformly distributed mass as in case (b).
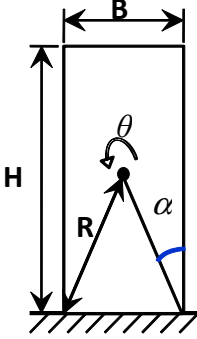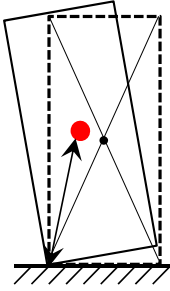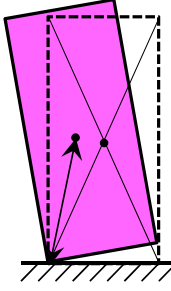
Description	(a) Concentrated Mass	(b) Uniformly Distributed Mass
f = Mass Distribution Factor	$f = 0$	$f = 1$
Rotational Mass $I_o = m \cdot R^2 + \dfrac{m}{12} \cdot (B^2 + H^2) \cdot f$ $R^2 = \dfrac{1}{4}(B^2 + H^2)$	$I_o = \dfrac{1}{4} \cdot m \cdot (B^2 + H^2)$	$I_o = \dfrac{1}{3} \cdot m \cdot (B^2 + H^2)$

Figure 4.12 Mass Distribution of Block

Figure 4.13 illustrates the rotational response of blocks with different mass distributions. Four different cases (f = 0, 1/3, 2/3, 1) are considered to capture the effect of mass distribution, f, on the rocking response of rigid blocks. Figures 4.13 (a) through (d) show the response of blocks for H/B=3 and R=9367 mm subjected to scaled Northridge earthquake ground motion (see Figure 4.6), while Figures 4.13(e) though (h) show the response for blocks with H/B=4 and R=1031 mm for the same ground motions.

Based on an inspection of all the figures, it is clear that mass distribution significantly affects the rotational response of the blocks. The rocking response of blocks with different mass distributions shows different trends during ground shaking. As the horizontal PGA of ground motions increases, the blocks with more concentrated mass

topple over earlier for this ground motion. Slender blocks oscillate about their dynamic equilibrium position without overturning under the higher PGA values. However, the maximum response amplitude of the blocks is not a function of the mass distribution. As shown in Figures 4.13 (a), (b), and (g), the response amplitude for blocks with less distributed mass (i.e., $f < 1$) is higher than that for $f = 1$ which is the response of a block
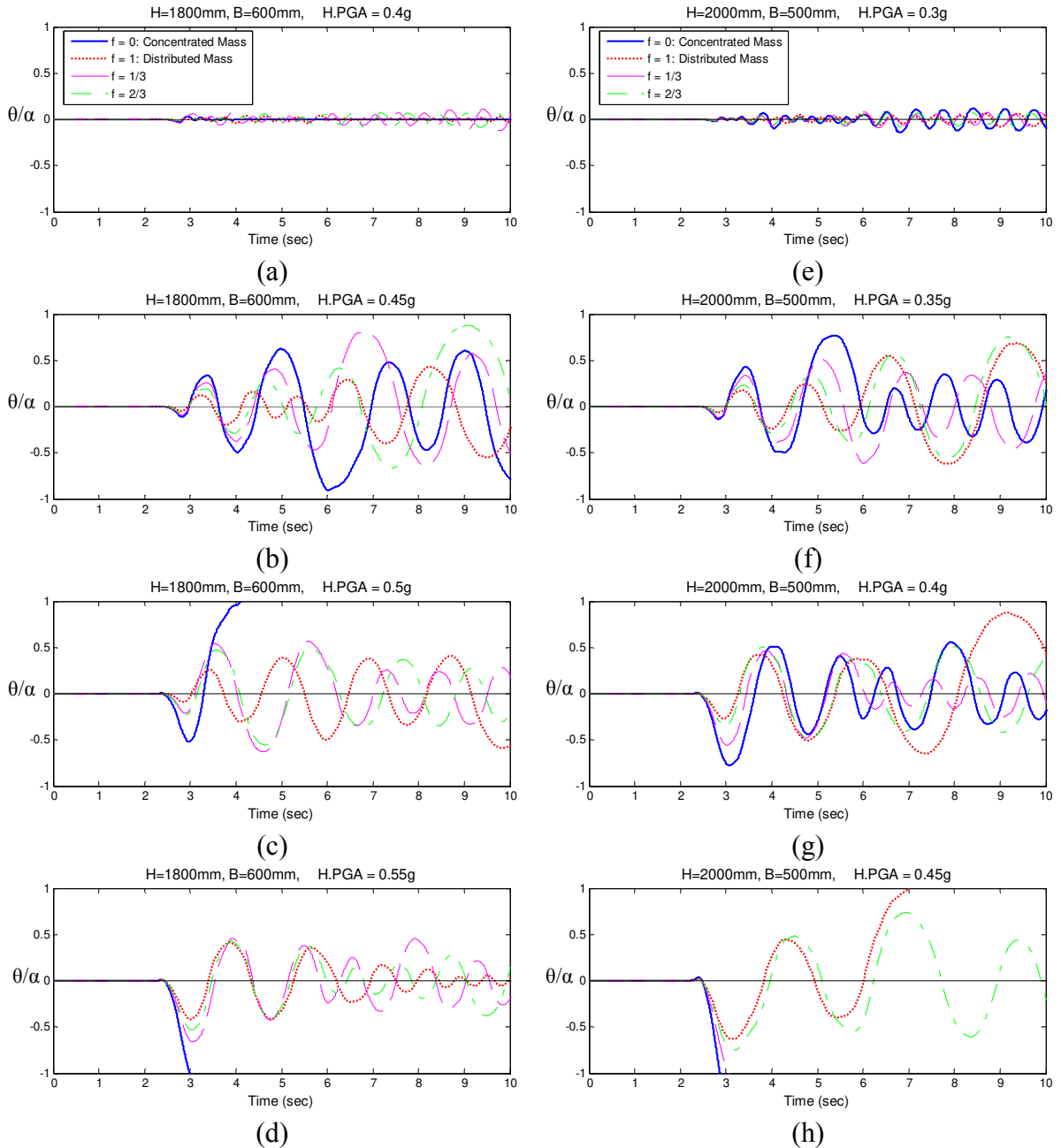
Figure 4.13 The Effect of Mass Distribution on Angular Displacement Response

with fully uniformly distributed mass for relatively small horizontal PGA values. These results show that the mass distribution of blocks influences the rotational amplitude as well as the frequency response of rigid blocks in rocking motion. However, its effect does not correlate in a simple manner with the angular displacement response. It interacts with the slenderness ratio and the characteristics of ground motions, and these factors together affect the rocking behavior of blocks.

(4) The Effect of Ground Motions

The characteristics of ground motions are typically prescribed using intensity measures such as peak ground response measures (acceleration, velocity and displacement), frequency, and duration. These characteristics directly affect the dynamic response of building structures and also affect the response of unrestrained nonstructural components resting on a plane surface. The dynamic response of unrestrained nonstructural components such as electrical equipment is highly nonlinear compared to that of building structures due to the high rigidity and unique boundary conditions, which results in their fundamental frequencies easily switched during ground shakings.

In this section, two different ground motions are used to evaluate the rocking response of blocks - the 1994 Northridge earthquake time history record at Rinaldi and 1940 El Centro time history. The two motions are scaled to the same horizontal PGA value to facilitate this response comparison.

Figures 4.14(a) and 4.15(a) show the Northridge and El Centro time histories scaled to PGA values of 0.3g, 0.45g, 0.6g and 0.75g respectively. Figures 4.14(b) and 4.15(b) illustrate the rocking response of blocks subjected to these ground motions. The

dimensions of the blocks are assumed to be close to typical switchboard cabinet units, which were introduced in Chapter 3. For both ground motions with scaled horizontal PGA value of 0.3g, the block does not oscillate. The block falls over when subjected to scaled Northridge earthquake with PGA value of 0.6g, but does not overturn when subjected to the scaled El Centro time history with the same PGA value. For both ground motions with scaled horizontal PGA value of 0.75g, the block topples over. However, as shown in Figures 4.14 (b) and 4.15 (b), the response due to the two ground motions is very different despite being characterized by same horizontal PGA values. This indicates that peak ground acceleration is not an effective intensity measure to explain the maximum dynamic response of these blocks and this warrants further investigation.
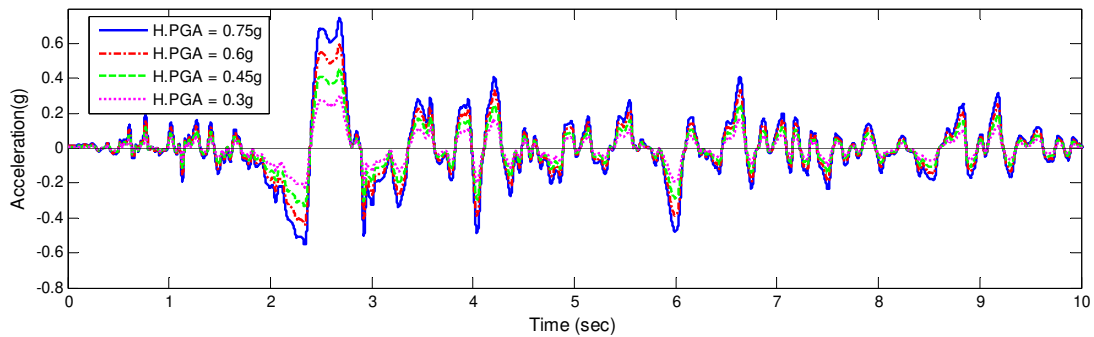
(a) Scaled 1994 Northridge Earthquake Ground Motions
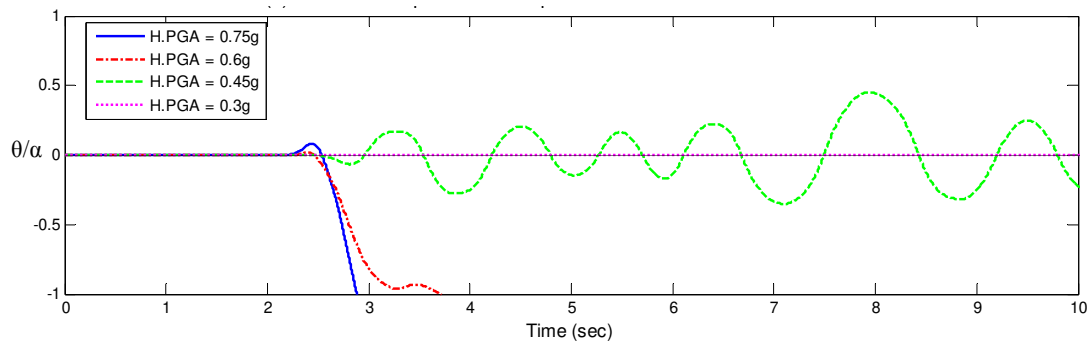
(b) Rotational Displacement Response of Block, H=2100mm, B=700mm

Figure 4.14 The effect of horizontal peak ground acceleration on the rocking response of rigid blocks using scaled 1994 Northridge Earthquake Ground Motions
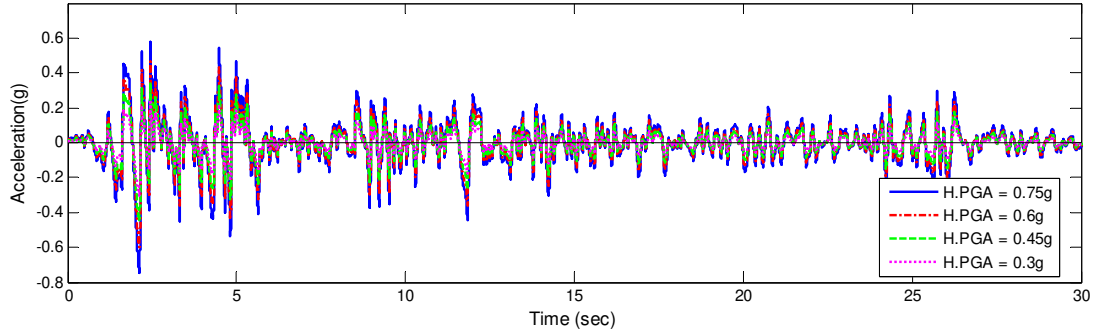
(a) Scaled 1940 El Centro Earthquake Ground Motions
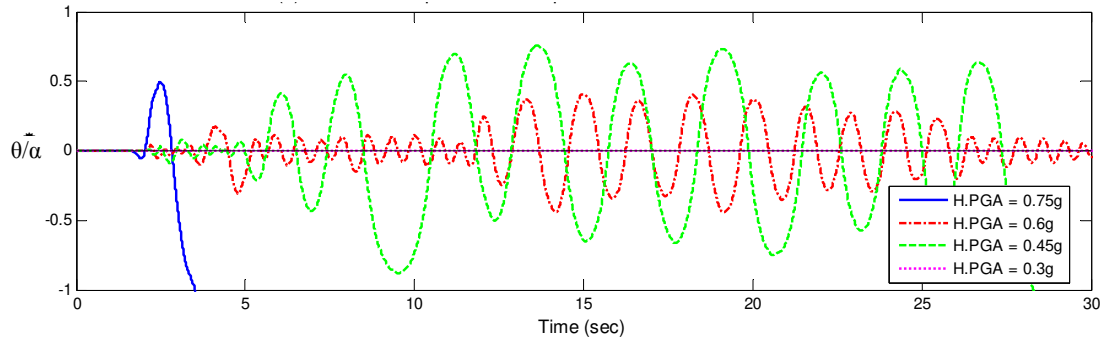
(b) Rotational Displacement Response of Block, H=2100mm, B=700mm

Figure 4.15 The effect of horizontal peak ground acceleration on the rocking response of rigid blocks using scaled 1940 El Centro Earthquake Ground Motions

4.2.4   Limitations of Analytical Models

Through the analytical models described in previous sections, the dynamic response of rigid block and their seismic behaviors are analyzed for different time histories of ground motions.   However, there are a number of limitations in capturing the real response of blocks as described in below:

• Sliding analytical models are limited to analyzing seismic response of various types of equipment under seismic shakings.   Relatively slender equipment can slide and rock simultaneously depending on vertical and horizontal ground motions.   Moreover,

90

any shape of rigid block resting on a rugged surface may not slide under seismic shakings.

- Analytical models are too simplified to apply to asymmetric or complicated equipment with multiple degrees of freedom. For rocking analytical models, it is assumed that the center of the mass and geometric mass are located at the same location and that the distances from the center of mass (c.g.) to the centers of rotations (O and O') are the same.

- As noted in Section 4.2.3.1, rocking analytical models do not capture the pounding behavior of blocks, and therefore the load-displacement relation of the anchorage for restrained blocks may not be evaluated with sufficient accuracy for performance assessment through the analytical models.

- Using the analytical solutions, it is difficult to realistically capture various types of motions of blocks such as the response acceleration and displacement of blocks, and load-displacement of restraint. These response motions are important to estimate the seismic damage of nonstructural components such as electrical cabinets. However, for various types of nonlinear motions of rigid equipment, the equations for the analytical models should include more degrees of freedom in order to capture all types of motions.

- Based on the above limitations, numerical models are necessary to analyze the seismic response of rigid equipment with varying configurations, irregular shapes, mass distributions, and different boundary conditions.

4.3   Numerical Models of a Free-Standing Block

Numerical models of unrestrained rigid blocks are formulated in this section using the finite element (FE) method.   Using these numerical models, the nonlinear dynamic behavior of unrestrained blocks is investigated in more detail and the results are compared to those obtained from analytical solutions explained in previous section.   The FE models are generated using the Open System for Earthquake Engineering Simulation (OpenSees, Ver.2.2.2), and rigid beam elements and various zero-length elements are applied to construct FE models.   For the complex and different support boundary conditions, the nonlinear force-deformation of each condition is determined and named as Type 1-3.   In order to compare results to the analytical solutions presented above, numerical models for pure sliding and rocking motions are generated and analyzed separately.

4.3.1   Numerical Models for Sliding Motion of Blocks with Low Aspect Ratios

The finite element models for sliding behavior are shown in Figure 4.16 (a). For the rigid block with width B and height H, three nodes and three rigid bars are generated. Numbers in parentheses denote nodes of the finite elements. Node (3) is at the center of the geometry as well as the center of the mass (c.m.) of the block, and nodes (1) and (2) are at the lower corners of the block, which are connected to the nodes (4) and (5) with zero-length elements of Type 1.   Zero-length elements have no physical length but contain the nonlinear force-deformation relationship between the block and the plane surface on which the block is mounted. Therefore, the nodal coordinates for (1) and (2)

are the same as those for nodes (4) and (5), respectively, and the constraint boundary

conditions are assigned to nodes (4) and (5). Figure 4.16 (b) shows the sliding behavior

of a block, in which (1'), (2'), and (3') are the displaced nodes from the original location

of nodes (1), (2), and (3). As the displacement of nodes (4) and (5) is constrained, they

remain at their original positions.

(a) Numerical Model for sliding behavior   (b) Sliding behavior
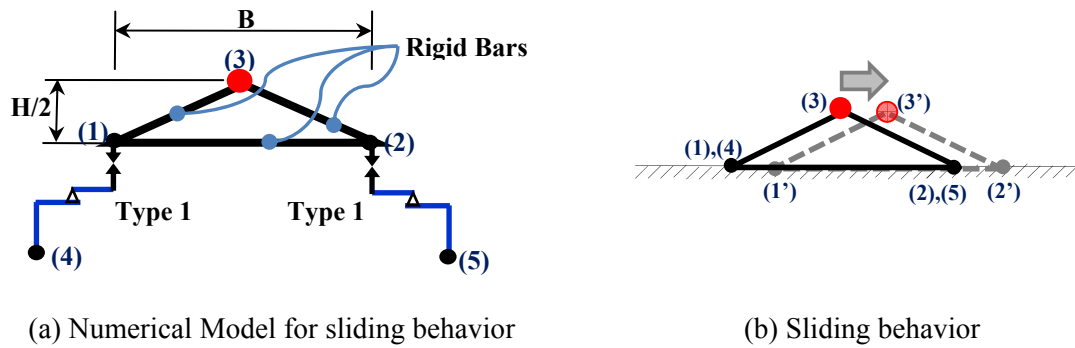
Figure 4.16. Schematic of a finite element model for sliding motions

The force-displacement property for horizontal sliding behavior is assigned as Type 1,

which is composed of zero-length elements connecting nodes (4) and (5) to nodes (1) and

(2) respectively. In order to capture the sliding motion of the rigid block, Type 1 is

assumed to be a flat slider with a friction model. The flat slider deforms laterally in both

left and right directions, but once the force reaches the critical force, i.e., $F_X = \mu \cdot N$, where

μ is the coefficient of kinetic friction between the surface and the block and N is the

vertical reaction, it slides in both the left and right directions. The sliding model works

only under vertical compressive forces and does not engage if the vertical force F_Z is

tensile. In order to capture this behavior, the Type 1 element is composed of two springs

working in orthogonal directions. The vertical behavior of the flat slider is modeled using

93

a no-tension element with rigid behavior in the compression zone. The horizontal behavior of the element is modeled using a Coulomb friction model in OpenSees. The configuration of Type 1 element and the force-deformation behavior of its constitutive components are shown in Figures 4.17 (a) and (b) respectively. In the FE analysis described in this section, vertical ground acceleration histories are not applied in order to compare the numerical results with analytical solutions in section 4.2.

(a) Type 1: Friction Model   (b) Force-Deformation of the Components in Type 1
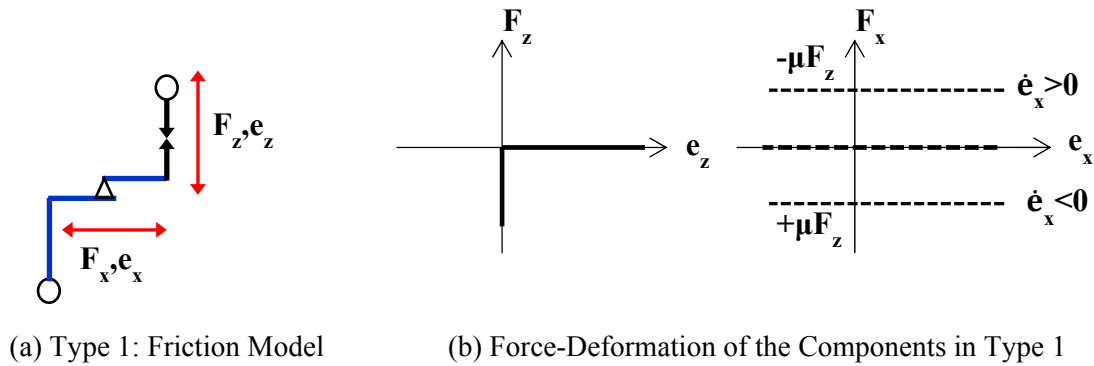
Figure 4.17. Friction model and its force-deformation property

The dynamic response of the FE models is computed using nonlinear time history analysis. For the time history, scaled 1994 Northridge earthquake ground motions at Ranaldi with various values of horizontal PGA are used, and the value of μ is assumed to vary from 0.2 to 0.8. Figures 4.18 and 4.19 show nonlinear sliding responses of a rigid block subjected to the horizontal ground motions. Figure 4.18 shows the displacement response from the analytical model in Eq. 4.2 as well as those from numerical models with two different friction models which are provided by OpenSees. "Numerical Model (1)" uses the Coulomb friction model, and "Numerical Model (2)" uses the velocity dependent friction model. The Coulomb friction model uses the same value of μ=0.4 as the analytical model, while the velocity dependent friction model considers static and kinetic coefficients of friction, μ_s and μ_k. Two coefficients of friction are combined with

94

the velocity at each time step, and the modified coefficient of velocity dependent friction (μ) is defined as follows:

$$\mu = \mu_k - (\mu_k - \mu_s) \cdot e^{-r \cdot v} \tag{4.12}$$

where r is the transition rate from low to high velocity and v is the resultant velocity of sliding (Constantinou et al., 1999).

As shown in Figure 4.18, the results of the analytical models are in very good agreement with those of the numerical models for four different horizontal PGA (H.PGA) values. The results of the velocity dependent friction model (Numerical model(2)) are in better agreement with those of analytical models for all values of H.PGA, while the results of the Coulomb friction model are close to the results of the analytical models for large values of H.PGA. As shown in Figure 4.18 (d), the maximum as well as residual displacements from the three models are in very good agreement. As a result, the velocity-dependent friction model is used following the following in studies which use the sliding numerical models.
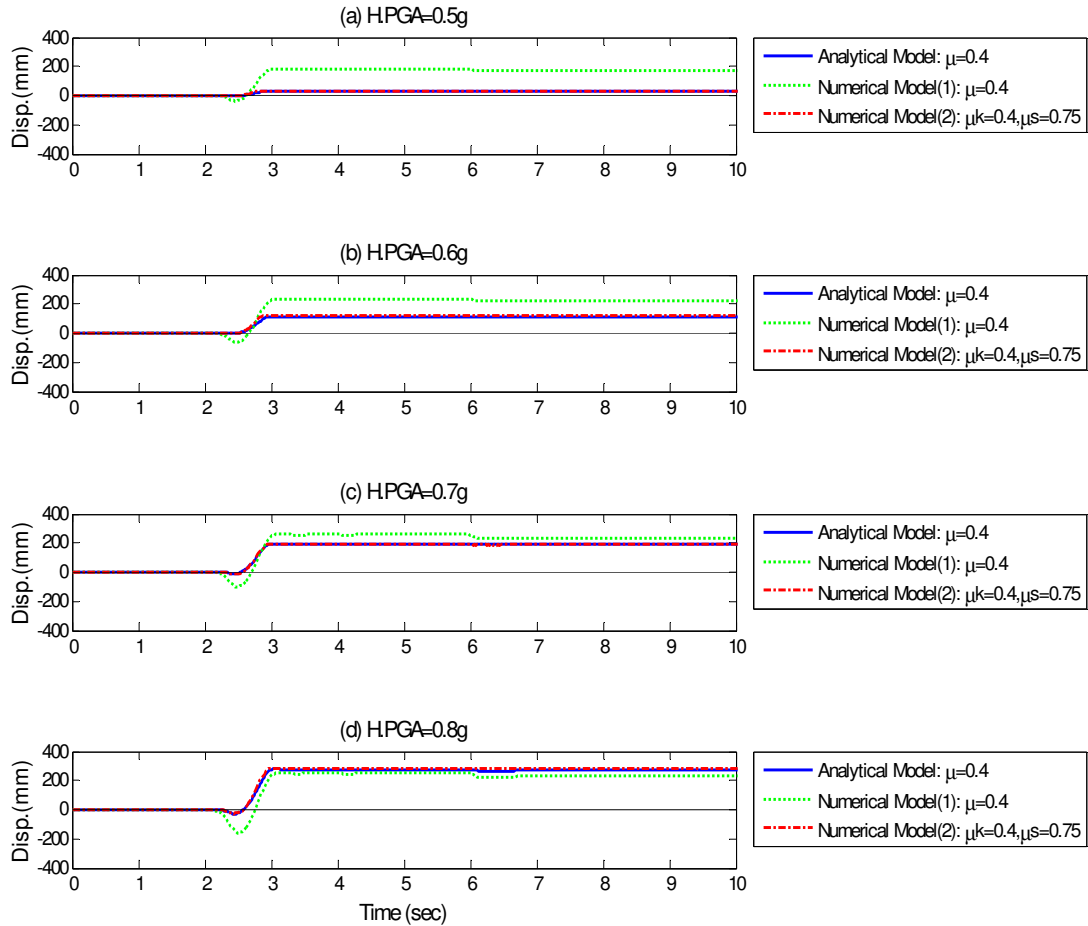
Figure 4.18. Sliding responses from analytical and numerical models
under the scaled 1994 Northridge earthquake time history

Figure 4.19 illustrates the response displacement of analytical and numerical models with different values of coefficients of friction ranging from 0.2 to 0.8. For these analyses, unscaled Northridge earthquake ground motions with H.PGA=0.84g are applied, and the velocity dependent models are used. Figure 4.19 clearly shows that the sliding responses of numerical models are close to those of analytical models for the selected values of μ.
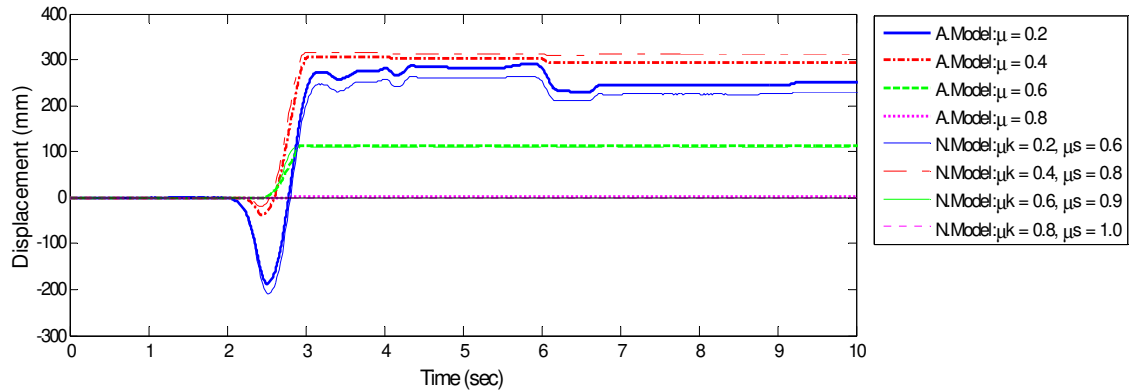
Figure 4.19. Sliding responses from analytical (AM) and numerical (NM) models
under the 1994 Northridge earthquake time history (H.PGA=0.84g)

4.3.2 Numerical Models for Rocking Motion of Relatively Slender Blocks

The finite element models for rocking behavior are illustrated in Figure 4.20 (a). For a rigid block with width *B* and height *H*, the same numbers of nodes and same types of rigid elements are generated as previously described for sliding models. However, different types of zero-length elements are used for the unique boundary conditions in the study of rocking motion. Section 4.2.2 explains that the rocking analytical model does not slide but instead uplifts around one of the bottom corners of the block while the other bottom corner works as a pivot hinge, as shown in Figure 4.20 (b). For this rocking motion, no-tension zero-length elements are used to control the vertical and horizontal displacement between nodes (1)-(4) and nodes (2)-(5). As for the sliding FE model, the locations of nodes (1) and (2) are initially the same as nodes (4) and (5), and the node pairs are connected with two different types of zero-length elements.

(a) Numerical model for rocking motion   (b) Rocking motion
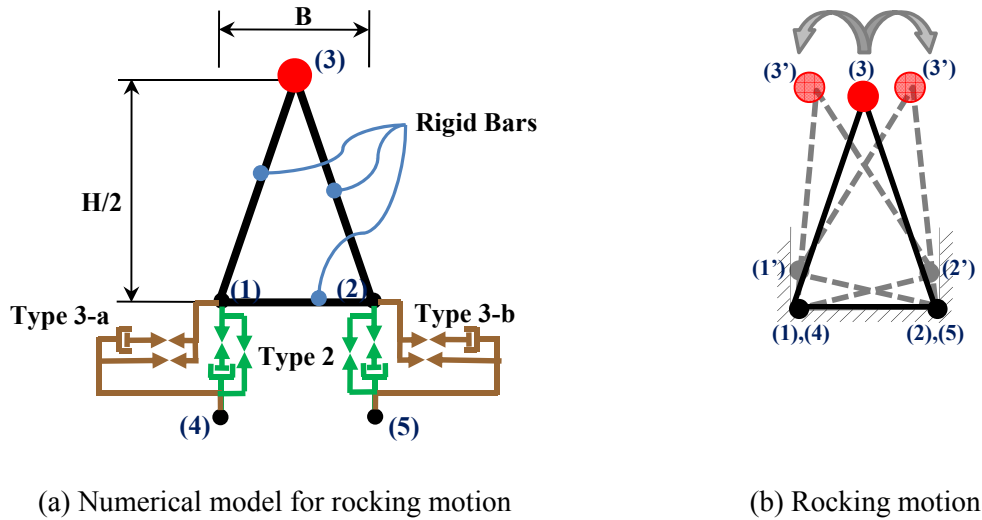
Figure 4.20. Schematic of a finite element model in rocking motions

In Figure 4.20 (a), the nonlinear property of Type 2 is generated with a no-tension element and viscous damping element for the vertical displacement. Figures 4.21 (a) and (b) show that this element does not deform under compressive force ($-F_z$). However, the stiffness for the tension side is zero as shown in Fig 4.21 (b)-(i), and therefore it will drastically deform under the tensile force (F_z). Only if the block is anchored with bolts with tensile yield force of f_t will the element deform linearly until it reaches u_t as shown in Figure 4.21 (b)-(ii). Type 3-a and Type 3-b are also no-tension elements similar to Type 2, but they control the horizontal displacement. Type 3-a is located at the left corner of the block, and Type 3-b is located at the right corner of the block. The left corner does not allow the leftward displacement of Node (1), and the right corner does not allow the rightward displacement of Node (2). That is, each element at Nodes (1)-(4) and Nodes (2)-(5) does not resist a tensile force but rather resists the compressive force as shown in Figures 4.21 (d) and (f).
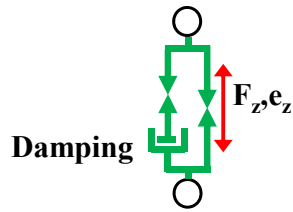
(a) Type 2: No-tension element (b) Force-Deformation of Type 2
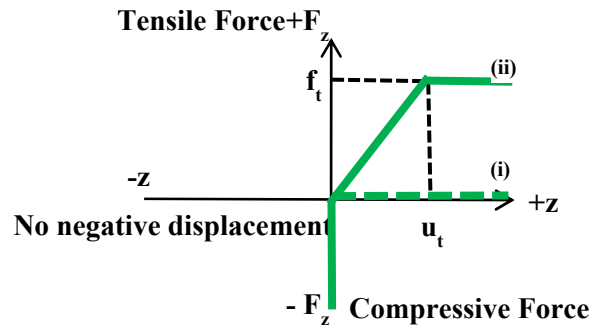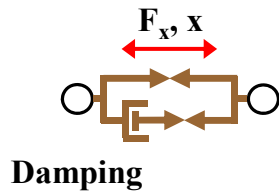
(c) Type 3-a: No-tension element (d) Force-Deformation of Type 3-a
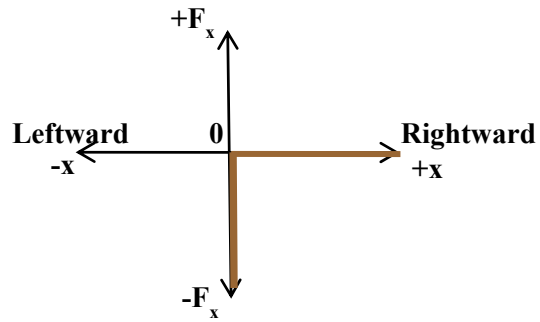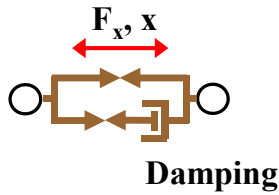
(e) Type 3-b: No-tension element (f) Force-Deformation of Type 3-b
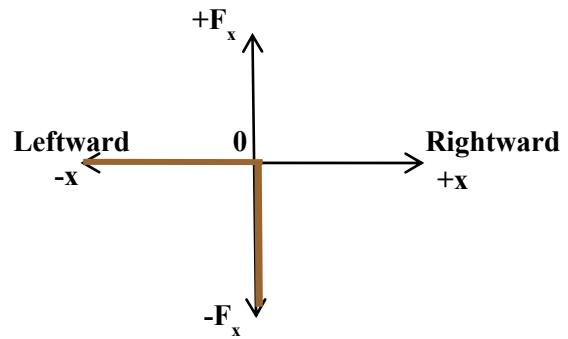
Figure 4.21. No-tension elements and their force-deformation property

For the comparison between analytical and numerical models, two models with different values of slenderness ratio, H/B, are generated. One model is for H/B=10, where H=10000mm and B=1000mm, and the other is for H/B=3, where H= 3000mm and

B=1000mm. Two models are analyzed under the unscaled 1994 Northridge earthquake ground motion recorded at Ranaldi with H.PGA=0.84g.

Figure 4.22 shows the rotational response of a slender block by analytical and numerical models. The ratio *H/B* of the block is 10, and the damping ratio, ζ, equals 0.01 in order to reduce the impact energy once a lifted block falls down. As seen in this plot, two results have a very good agreement along the whole time history. The maximum responses at 2.6 sec and 8.2 sec are also match very well.
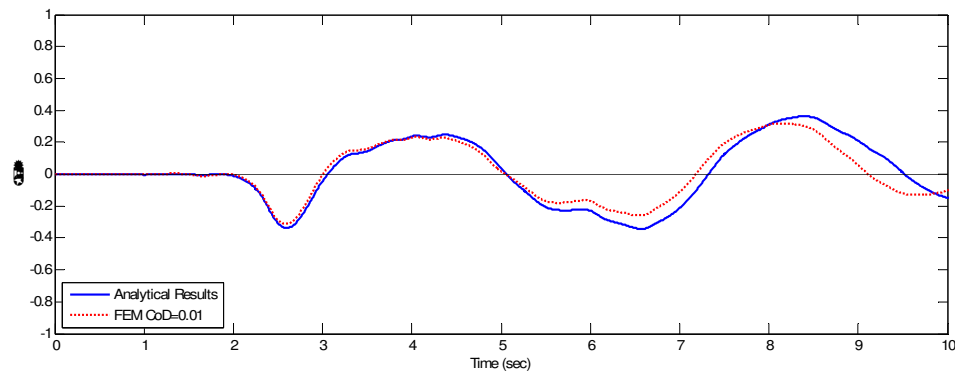
Figure 4.22. Rocking responses from analytical and numerical models with *H/B*=10 under the 1994 Northridge earthquake time history recorded at Ranaldi (H.PGA=0.84g)

In contrast, Figure 4.23 shows the rotational response of a less slender block with *H/B*=3 obtained from one analytical model and several sets of numerical models with different values of damping ratio, ζ, ranging from 0.01 to 0.20. It can be seen that the response of the numerical models is not close to that of analytical model. Despite the damping effect, the numerical models do not rock smoothly but uplift and then fall down in the same direction. Since the analytical model given in Eq. (4.11) assumes that blocks show pure rocking motions, the response by the analytical model cannot capture the

pounding motion in the numerical models. This shows the critical difference between analytical and numerical rocking models, which is explained at length in the next section.
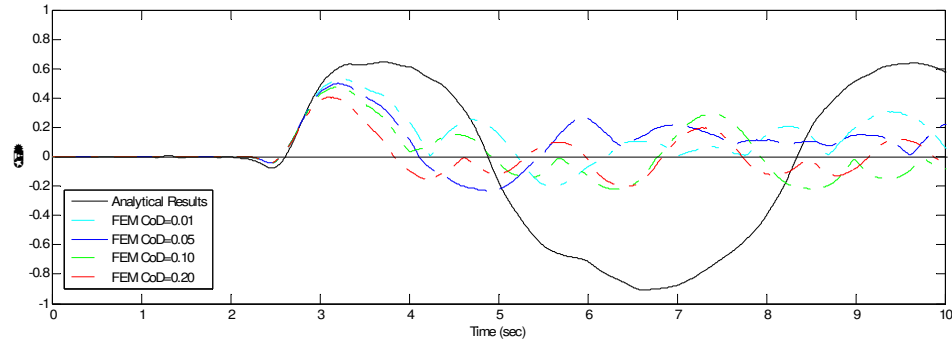
Figure 4.23. Rocking responses by analytical and numerical models with H/B=3 under the 1994 Northridge earthquake time history (H.PGA=0.84g)

4.3.3 Rocking and Pounding/Bouncing

Section 4.3.2 shows that the rocking responses of less slender blocks with *H/B*=3 predicted using analytical analysis are different from those predicted by numerical analysis. This is caused by the pounding motion of less slender blocks due to the impact occurring when one corner of blocks falls down after uplift. Equations (4.13) – (4.15) below explain the difference between pounding and rocking motions. Equation (4.13) expresses the conservation of momentum before and after impact between a ground surface and a rocking block. The left side of the equation is the momentum before impact, and the right side is the momentum after impact, where $\dot{\theta}_1$ and $\dot{\theta}_2$ are the angular velocities before and after impact respectively. Equation (4.14) presents the ratio of kinetic energy quantities after and before impact. The ratio $(\dot{\theta}_2/\dot{\theta}_1)$ of before to after angular velocities is denoted by *e* which is the coefficient of restitution (COR) as shown in Eq. (4.15). When the COR reaches unity, the block is elastically bouncing, and therefore its angular velocity after impact is close to the angular velocity before impact.

101

On the other hand, when the COR is 0, the block does not pound or rock but stops as soon as one of its corners hits the ground.

$$I_o\dot{\theta}_1 - \frac{W}{g} \cdot R \cdot B \cdot \dot{\theta}_1 \cdot \sin\alpha = I_o\dot{\theta}_2 \tag{4.13}$$

$$r = \tfrac{1}{2} \cdot I_o\dot{\theta}_2^{\,2} \Big/ \tfrac{1}{2} \cdot I_o\dot{\theta}_1^{\,2} = \dot{\theta}_2^{\,2} \Big/ \dot{\theta}_1^{\,2} \tag{4.14}$$

$$e = \dot{\theta}_2 \big/ \dot{\theta}_1 \tag{4.15}$$

Equation (4.16) expresses the ratio of kinetic energy quantities derived using Eqs. (4.13) and (4.14), with ratio r also expressing the potential energy stored in the system when the angle of rotation is zero.

$$r = \left[1 - \frac{W}{g}\frac{R^2}{I_o}(1 - \cos 2\alpha)\right]^2 = e^2 \tag{4.16}$$

Equation (4.16) is plotted in Figure 4.24 (a) which shows the idealized value of COR for rocking blocks versus the slenderness ratios of blocks and illustrates that slenderer blocks contain higher value of COR, while less slender blocks have low values of COR. In other words, more slender blocks hold less stored energy under the conservation of momentum principle, and therefore easily rock without any energy change from before to after impact. On the other hand, less slender blocks need to decrease their kinetic energy in order to rock smoothly. As shown in Figure 4.24 (a), for H/B =10, the value of COR is close to 1, and therefore the block can rock without any energy loss. For H/B=3, however, the value of COR is close to 0.85, and therefore the block needs to lose some kinetic energy in order to rock as shown in Figure 4.24 (b). It means that less slender blocks can pivot at one corner only if they partially lose their kinetic energy in any forms

of energy such as the kinetic energy ($\frac{1}{2} \cdot I_o \dot{\theta}^2$) is transferred into internal, strain or other forms of energy.

(a)   (b)
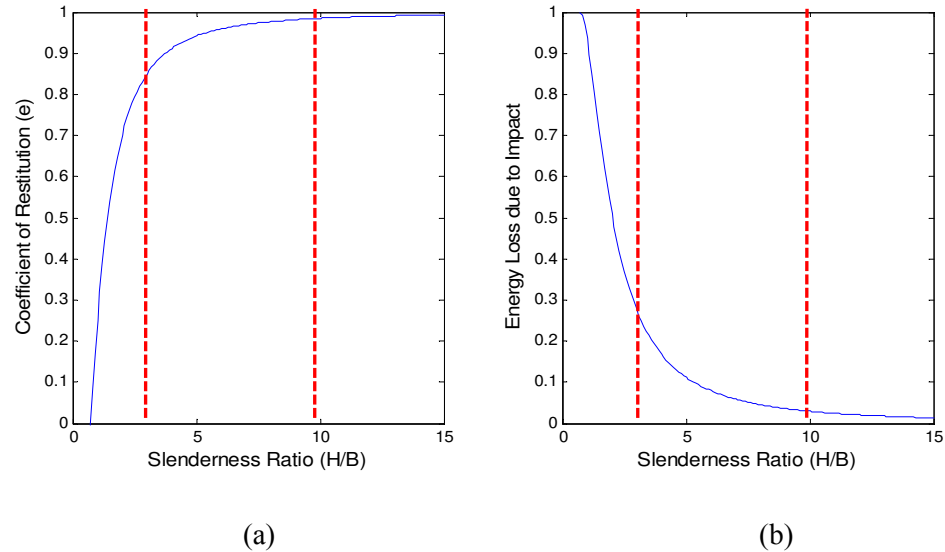
Figure 4.24. Coefficient of Restitution and Required Energy Loss not to Bounce

In the analytical rocking model of Eq. (4.11), it is assumed that the blocks rock perfectly and do not pound as shown in Figures 4.4 (a) and (b), and the angular momentum must be conserved as given in Eq. (4.13) by the principle of conservation of momentum. That is, blocks are not re-bouncing into the same falling back direction, and their rotational angle smoothly moves from the positive direction to zero and to the negative direction or vice versa. However, this assumption means that the analytical rocking models have fictitious values of the COR according to their slenderness ratio. As their slenderness ratio varies, their COR should be changed for this assumption. However, the COR is determined by the material properties of the block and surface, not by the slenderness ratio of blocks, and the kinetic energy loss depends on the value of COR rather than the slenderness of blocks. Hence, less slender blocks tend to pound, as

103

shown in the plots for numerical models, since their kinetic energy exceeds the required amount for rocking smoothly. Unlike analytical models, numerical models can capture this pounding action, and are more suitable for evaluating the seismic response of equipment as well as the linear and nonlinear force-deformation of anchor bolts of equipment.

4.4   Closure

1. Previous chapters describe the dynamic behavior of nonstructural components such as electrical and mechanical equipment and showed that this behavior is very sensitive to support boundary conditions in that they are relatively rigid structures compared to the building structures. Therefore, it is necessary to develop and validate the numerical models for general support boundary conditions which have an effect on dynamic response of unrestrained equipment subjected to earthquakes.

2. This chapter explains the nonlinear behavior of unrestrained rigid blocks mounted on a plane surface include resting, sliding, rocking, pounding, and free-flight. These motions are described using analytical models, and their limitations as well as the advantage of numerical models are explored.

3. The numerical models of rigid blocks with special boundary conditions are generated using the finite element approach, and their results are compared to the analytical results.

4. Using the time history analysis of analytical and numerical models, the dynamic response of rigid blocks is evaluated, and various parameters are characterized for each motion.

5. The numerical models for the general support boundary conditions in this chapter are extended for unrestrained and anchored FE models of switchboard cabinets, and the dynamic response of rigid blocks in this chapter is compared to that of switchboard cabinets under the same seismic excitations.

CHAPTER V

SEISMIC RESPONSE OF SWITCHBOARD CABINETS USING NONLINEAR
NUMERICAL MODELS

5.1 Introduction

The numerical models in Chapter 3 were generated using a finite element approach in OpenSees software (the Open System for Earthquake Engineering Simulation). These initial finite element models were restricted to linear force-deformation behavior, and their support boundary conditions were assumed to be fixed in all base level degrees of freedom. In Chapter 4, the effect of support boundary conditions was considered in the computation of nonlinear dynamic behavior of electrical equipment. In order to focus on the support boundary conditions, the cabinet itself was assumed to be a rigid body. Finite element models for unrestrained rigid bodies were generated using zero-length elements with different properties. These models are able to capture the various dynamic motions of free-standing rigid bodies on a ground floor subjected to seismic shakings and provided the initial results needed to now develop the numerical models of anchored equipment with nonlinear behavior.

The numerical models described in this chapter will build upon this previous work and will consider the total nonlinear behavior of the cabinets. For the evaluation of their nonlinear behavior under seismic effects, these numerical models are generated in OpenSees building upon the linear numerical models in Chapter 3. The numerical models presented here are generated considering the inelastic material properties, various force-

deformation relationships of joint connections, and three different types of support boundary conditions. Nonlinear Time History Analysis (NTHA) is carried out to find the dynamic behavior of switchboard cabinets under seismic ground motions. The nonlinear response of connections between frame members as well as between plates and frame members is now included in the model. Finally, the effect of various support boundary condition cases including the fully restrained, nonlinearly anchored, and unrestrained conditions is investigated.

The basic properties of the linear and nonlinear models considered in Chapters 3 and 4, as well as the full nonlinear model to be presented in this chapter, are summarized in Fig. 5.1.
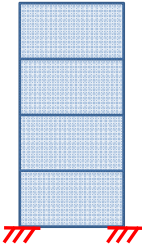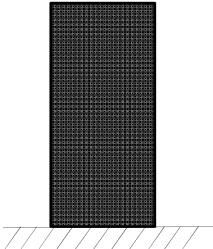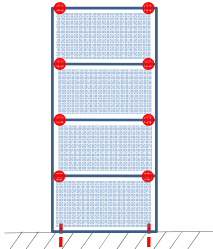
(a) Models in Chapter 3	(b) Models in Chapter 4	(c) Models in Chapter 5
• Linear model • Cabinet is modeled using steel frame and plate elements • Fixed boundary conditions at base	• Nonlinear model • Cabinet is represented as a rigid block • Unrestrained support boundary conditions to capture various motions (rocking and sliding) • Nonlinear behavior compared to analytical solutions	• Nonlinear models • Inelastic material properties of steel frame and plates • Various types of support boundary condition • Nonlinear force-deformation relationship of frame connections and anchor bolts

Figure 5.1 Numerical models with different properties and support conditions

5.2 3D-Nonlinear Models of Switchboard Cabinets

5.2.1 Material properties of steel frame and plates

It is assumed that the steel cabinets are designed according to AISI Specifications (2007) and the AISC steel manual (2005). The material properties of the steel are assumed to follow the stress-strain curves shown in Figure 5.2. Fasteners have high strength, and their yield strength (f_y) is assumed to be 100 ksi. The yield strength of steel plates and frames is set at 50 ksi. In order to define the nonlinear material behavior of the steel in OpenSees, material *steel01* was assumed for the fasteners. Material *steel01* is a uniaxial bilinear steel material model with kinematic hardening and optional isotropic hardening described by a nonlinear evolution equation. Material *steel02* was assumed for the steel plates and frame members, which is a uniaxial Giuffre-Menegotto-Pinto steel material model with isotropic strain hardening. As shown in Fig. 5.2, the material type *steel01* for fasteners assumes bilinear behavior but does not include the hardening range, while *steel02* for steel plates and frames includes both yielding and a hardening curve.
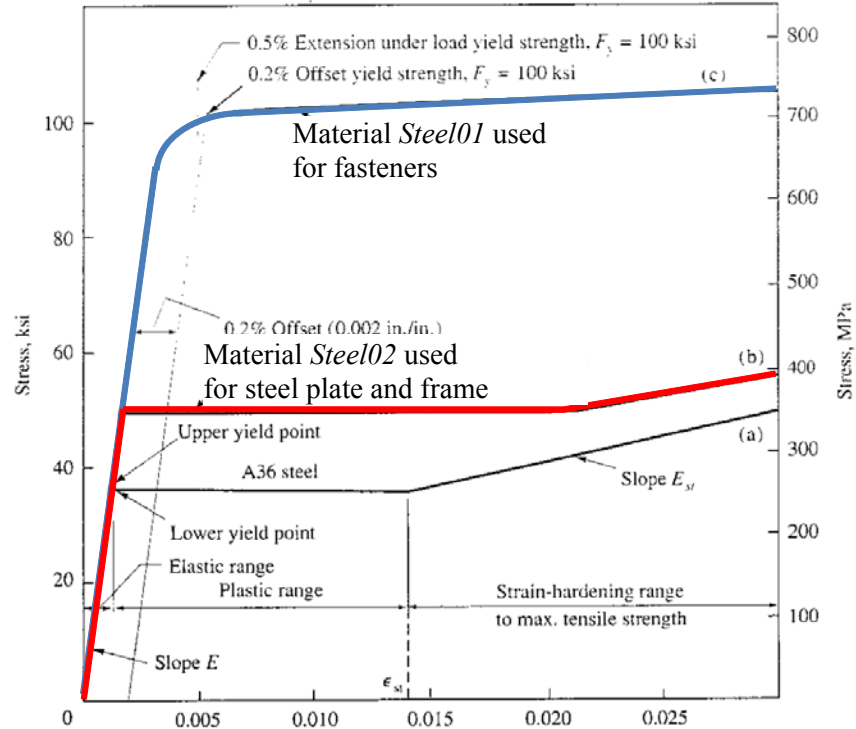
Figure 5.2 Typical Stress-Strain Curves for Steel Cabinet Plate and Frame Elements
(Salmon and Johnson, 2009)

5.2.2 Force-deformation of plate to frame connection

Various types and different sizes of fasteners are used in a switchboard cabinet. In the numerical models, it is assumed that the steel plates are fastened to the frames with screws without washers and nuts. The diameter (d) of screws is 4.8 mm. As shown in Figure 5.3, screw connections can fail under shear, in tension, or in a combination of modes such as screw pull-out with bearing and tearing of plates. These failure modes depend on the strength and thickness of plates as well as the hole size, spacing, and edge distance of fasteners. It is assumed that all connections conform to the AISC Steel Construction Manual (2005) and AISI North American Cold-Formed Steel Specification

(2007). The minimum distance between the centers of fasteners is 3d, and the minimum edge and end distances from the center of a fastener to the edge of any part are 1.5 d.

Of the failure modes presented in Figure 5.3, the failure modes involving one fastener between plates and frames, such as pull-out or pull-over, are the most common failure modes of electrical cabinet structures under earthquake loads based on the shaking table test (Wyle, 2008). Therefore, it is assumed that these failure modes occur before shear failure of a screw or yielding or rupture due to insufficient edge or end distance. The failure of fasteners depends on the thickness and tensile stress of the sheets and the diameter of a screw. Fig. 5.3 (a) presents the failure mode under shear force, which is limited by tilting and bearing with local compressive yielding, and finally may cause a fastener to pull out; Fig. 5.3 (b) shows pull-out of a screw under tensile force without tilting or bearing of a sheet; Fig. 5.3 (c) illustrates the pull-over/through mode, which involves tearing and distortion of a upper sheet around the head of fastener, and disconnects the upper plate completely from the fastener.

In-plane	Out-of-Plane
(a) Tilting and Bearing in Shear	(b) Pulling-out in Tension (c) Pulling-over/through in Tension
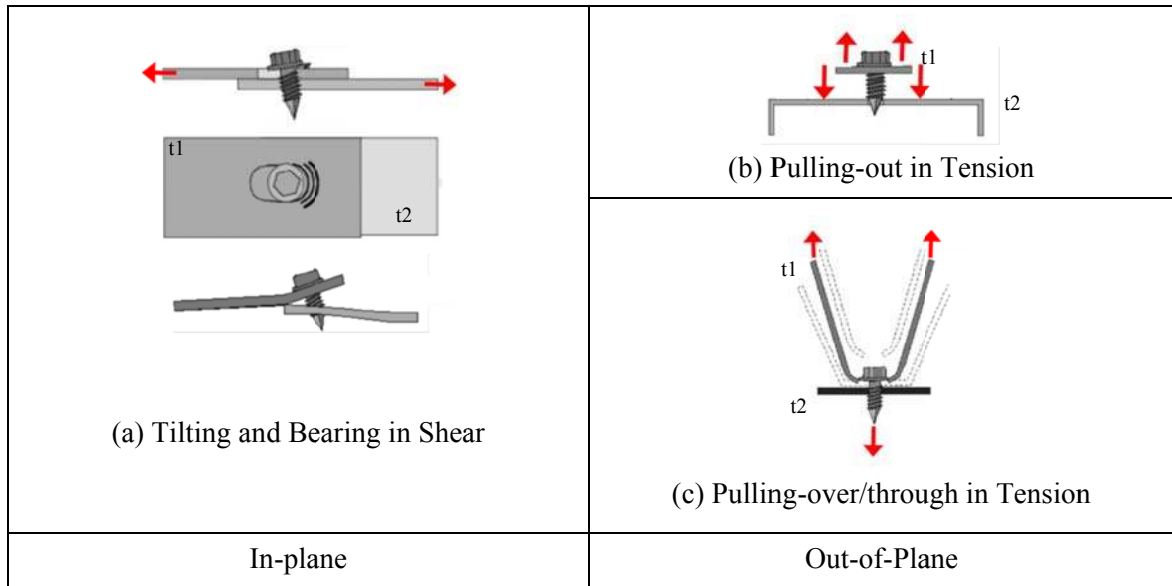
Figure 5.3 Failure Modes of Screw Connections
(Source: ECCS TC7 TWG 7.10 Connections in Cold-formed Steel Structures, 2009)

The European Convention for Constructional Steelwork (ECCS, 2009) describes tests to determine the failure modes of screw connections in cold-formed steel structures subjected to two different force actions, shear and tension. For the tests, ECCS sets the ultimate resistance of the fastener as the maximum load recorded during the test, and recommended defining the failure load as the peak load in the deformation of 3 mm. Figures 5.4 (a) and (b) show the two likely cases for the force-deformation behavior of connections in cold-formed steel structures. As illustrated in these figures, the maximum load within the first 3mm deformation is defined as the failure load.

Figure 5.4 Failure limits for test
(Source: ECCS TC7 TWG 7.10 Connections in Cold-formed Steel Structures, 2009)

111

In the FE models of switchboard cabinets, the shear and axial force-deformation behavior of screw connections are defined using the equations from Chapter 9 of *"Cold-Formed Steel Structures to the AISI Specification"* (2007), and the tensile strength (F_u) of steel plates and frames is taken as 65ksi. For the FE models, it is assumed that a screw connection has three degrees of freedom, including one in an axial direction and two in each transverse direction. In addition, it is assumed that the in-plane failure in shear controls the pull-out mode due to tilting and bearing, and that the out-of-plane failure in tension controls the pull-out or pull-over/through mode illustrated in Fig. 5.3. Therefore, the shear force-deformation relationship of a screw is based on its in-plane behavior, and the axial force-deformation relationship of a screw is based on its out-of-plane behavior.

(1) Shear force and deformation

Screw connections loaded in shear can reach the failure by screw shear, edge tearing, tilting and subsequent pullout of the screw, or bearing failure of the parent plates. In order to prevent these failures, the AISI Specification specifies the minimum distance between screws and the screw to edge and end distances to be 1.5d or greater. With these distances, AISI states that the nominal shear strength per screw (P_{ns}) can be evaluated as the smallest of Eqs. 5.1 (a), (b), and (c):

$$P_{ns} = 4.2 \cdot \sqrt{t_2^{3} \cdot d} \cdot F_{u2} \tag{5.1 a}$$

$$P_{ns} = 2.7 \cdot t_1 \cdot d \cdot F_{u1} \tag{5.1 b}$$

$$P_{ns} = 2.7 \cdot t_2 \cdot d \cdot F_{u2} \tag{5.1 c}$$

where d is the nominal diameter of a screw, F_{u1} is the tensile strength of a steel plate in contact with screw head or washer, and F_{u2} is the tensile strength of a frame member not in contact with screw head or washer. Likewise, variables t_1 and t_2 are the thicknesses of those members in and not in contact with screw head or washer, respectively as shown in Fig. 5.3. It is assumed that F_{u1} and F_{u2} are identical, as plates and frames are also assumed to be the same cold-formed steel.

(2) Tensile force and deformation

Screw connections loaded by tensile force can reach failure by a screw pulling out of the plate, by the sheeting pulling over a screw head and washer, or by tensile failure of a screw. Based on the performance test data (Wyle, 2008), it is assumed that the failure due to pulling out or pulling over occurs before tensile failure of a screw. Therefore, the nominal shear strength per screw (P_{ns}) is assumed as the smallest of Eqs. 5.2 (a) and (b):

$$P_{not} = 0.85 \cdot t_c d F_{u2} \tag{5.2 a}$$

$$P_{nov} = 1.5 \cdot t_1 d_w' F_{u1} \tag{5.2 b}$$

which are the nominal pullout capacity (P_{not}) and pullover capacity (P_{nov}) respectively, where t_c is the lesser value of thicknesses t_1 and t_2, and d_w' is the effective pull-over resistance diameter related to the size of washer. Based on these equations and the limit

state of deformation, the force-deformation relationship for a screw connection is represented in Figure 5.5 and Table 5.1.
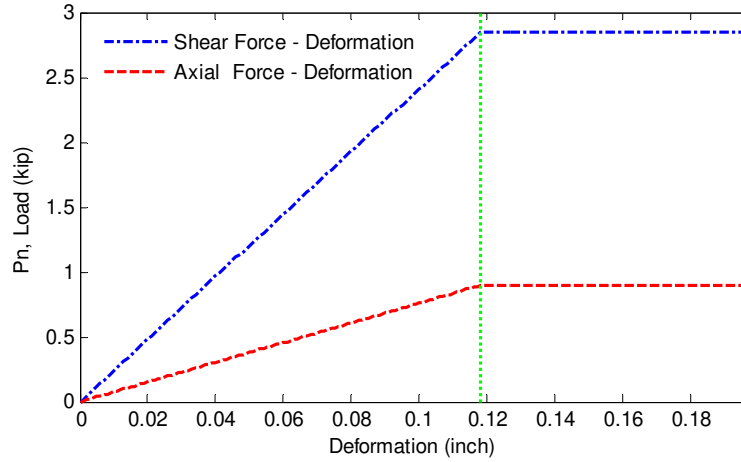
Figure 5.5 Force-Deformation of One Screw Connection (Dia. 3/16")

Table 5.1 Force-deformation of screw connection

Forces	Diameter (φ) (inch)	Initial Stiffness (kip/inch)	Yield Force (kip)	Limit Deformation (inch/mm)
Shear	3/16	24.1	2.8	0.12/3
Axial	3/16	7.60	0.9	0.12/3

In order to define the nonlinear behavior of a screw connection in the FE models, the zero-length elements with bilinear properties are used. These elements connect the frame members and plates. In order to model the bilinear property, material steel02 specified in OpenSees is used, which provides the yielding and hardening curves as shown in Fig.5.5.

5.2.3 Force-deformation of frame to frame connections

The details of the joint connections between frames determine the stiffness of cabinets as well as their fundamental frequencies and mode shapes as discussed in Chapter 3. Based on observations during inspections after seismic events, the joint connections usually deform into the nonlinear range, and these deformations contribute to various dynamic behaviors of cabinets. Chapter 3 described the initial stiffness of the FE models; this chapter describes the post-linear force-deformation relationships of joint connections in cabinets for nonlinear FE models.

As shown in Figure 5.6, the main joints between horizontal and vertical members are fastened with two sets of bolts at each face. For the numerical models of cabinets, it is assumed that the main connections with horizontal and vertical members at the top and bottom of cabinets transfer the axial force, shear forces, and moments from a horizontal member to vertical member as shown in Figs. 5-6 (a) and (b). The joints connecting small horizontal members to vertical members are as shown in Fig. 5-6 (c). These connections are assumed to be pinned connections which transmit axial and shear forces but do not carry any moment.

Inelastic Moment Connection		Pinned connection
(a) Horizontal and Vertical Members at Top	(b) Horizontal and Vertical Members at Bottom	(c) Horizontal and Vertical Members at Middle
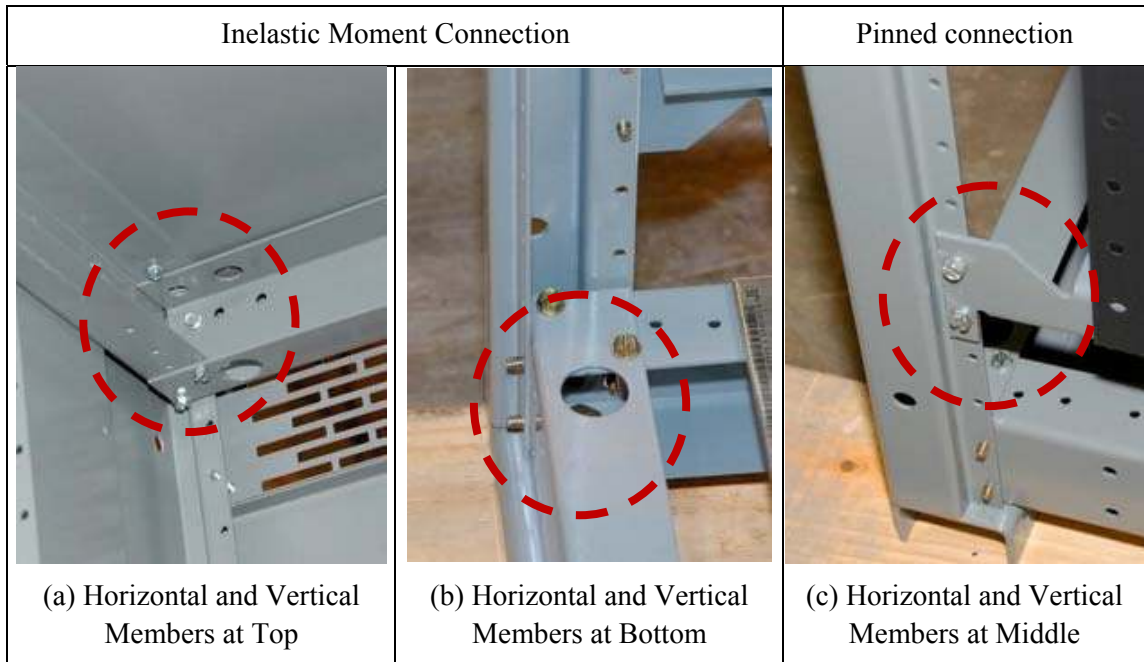
Figure 5.6 Frame to Frame Bolt Connection

Fig. 5-7 (a) illustrates the main connections between two horizontal members and one vertical member. The connection from a horizontal member to the vertical member has six degrees of freedom and transfers the internal forces and moments. The force-deformation relationship in each degree of freedom direction is derived using detailed FE models of the connection as shown in Figs. 5.7 (a) and (b). The FE models are generated in OpenSees, and two C-shape horizontal members and an L-shape vertical member are generated using shell elements. Fig. 5.7 (b) shows the connection model used to represent the force-deformation of a horizontal member (right side member shown in green color). It is assumed that the vertical member is continuous, that its end is fully constrained in all directions (Constraint 1), and that the other horizontal member (left side member shown in blue color) is also continuous (Constraint 2). Therefore, there is

neither angular nor transverse deformation at Constraints 1 and 2. The force-deformation relationship is measured at the centroid of the horizontal member (C.G.).

(a) Edge distance   (b) Local axes of horizontal member
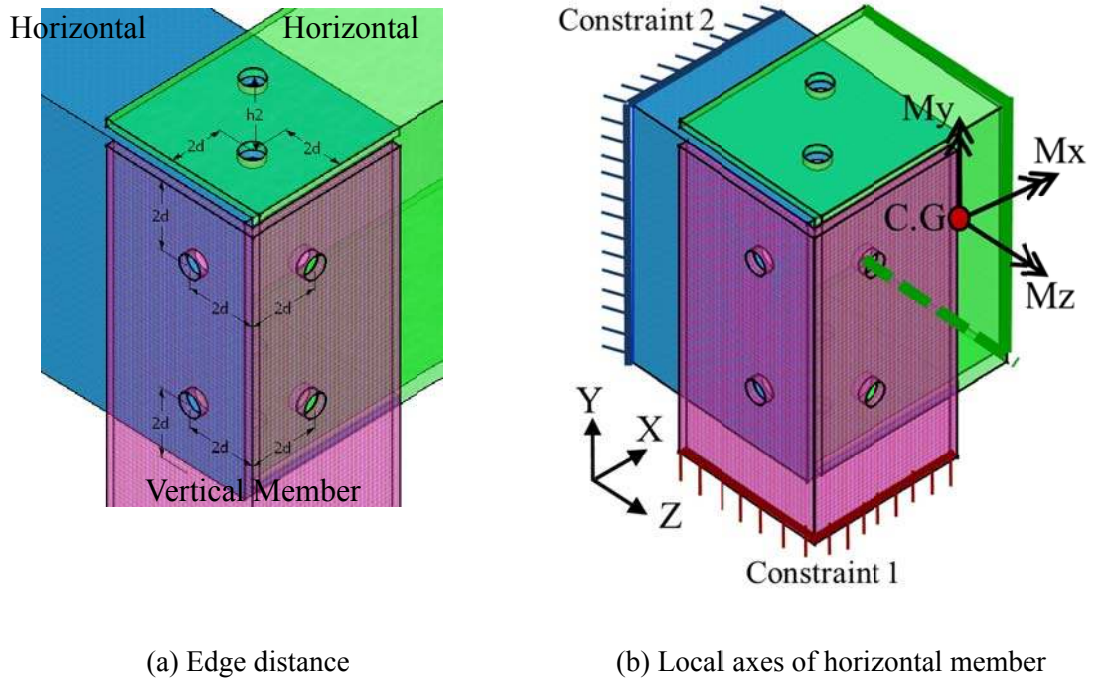
Figure 5.7 Connections for horizontal and vertical members

Zero-length elements with nonlinear properties are used to represent the bolt connections between two members. It is assumed that the nonlinear properties in the elements include the slip/bearing deformation due to shear forces in transverse directions as well as the pull over failure due to moments in a bolt's axial direction. The work by Uang et. al. (2010), which involved cyclic tests conducted on bolted moment frame connections of cold-formed steel, showed that the slip-bearing deformation at the bolted connection controls the total deformation at joint connections subjected to bending moments and that the cyclic behavior of bolted connections was characterized by a linear response, a slip range, and a significant hardening response due to bearing at bolt holes. In addition, the inelastic action through the bolt slip and bearing in the connection

117

occurred earlier than the local bucking of C-shape steel members, and its deformation governed the localized deformation of the beam and column.

The force and slip-bearing deformation relationship of connections can be characterized using various parameters such as the size and thickness of the member, the size of the bolt and washer, the pre-tension in the bolts, and the distance and location of bolts. This characterization can be applied to the nonlinear FE models of switchboard cabinets. For the slip-bearing model, Rex and Easterling (2003)'s work was used to characterize the behavior of both the slip and bearing deformations of single bolt connections. Their approximate analytical model is represented by Equation 5.3, which describes the force-deformation behavior for a bolt bearing on a single plate:

$$\frac{P_{bearing}}{R_{n,bearing}} = \frac{1.74\overline{\Delta}}{(1+\overline{\Delta}^{0.5})^2} - 0.009\overline{\Delta} \tag{5.3}$$

Where P = plate load

R_n = nominal plate strength ($R_n = L_e t_e F_u \leq 2.4 d_b t_p F_u$)

$\overline{\Delta}$ = normalized deformation due to bearing force $= \Delta \beta K_i / R_n$

Δ = hole elongation

β = steel correction factor considering the material properties of steel

$$\left(\beta = \frac{30\%}{\%Elongation}\right)$$

K_i = initial bearing stiffness.

Equation 5.3 was derived from test results, which is the data of failures including bearing of bolts, and tearing out or splitting of the plates by the maximum load. Figure

5.9 shows the force-deformation behavior of a bolted connection from experiment and the analytical relationship provided in Equation 5.3 by Rex and Easterling (2003). As shown in this figure, the analytical model does not include the apparent boundary between the initial stiffness and the slip range which is shown in the cyclic test result by Uang et. al. (2010). The % elongation is taken as 30% for typical steel which yields a steel correction factor of unity. The initial bearing stiffness K_i was given by Rex and Easterling (2003) as follows:

$$K_{i,bearing} = \frac{1}{\dfrac{1}{K_{br}} + \dfrac{1}{K_{b}} + \dfrac{1}{K_{v}}} \tag{5.4}$$

K_{br} = bearing stiffness, $K_{br} = 120 t_p F_y d_b^{0.8}$

K_b = bending stiffness, $K_b = 32 E t_p (L_e / d_b - 1/2)^3$

K_v = shearing stiffness, $K_v = 6.67 G t_p (L_e / d_b - 1/2)$

From Eqs. 5.3 and 5.4, the bearing stiffness model and bending and shear stiffness models are estimated. Figure 5.8 (a) and (b) illustrate the terms in Eqs. 5.3 and 5.4, and they show that the size of the bolt hole, the edge/end distance of bolts, and the thickness and yield strength of plates are related to the bending and shear stiffness of the models, as well as the bearing stiffness. Figure 5.9 shows one of the validations of the suggested bearing stiffness model by Rex and Easterling; the analytical model has a very good agreement with the test result.
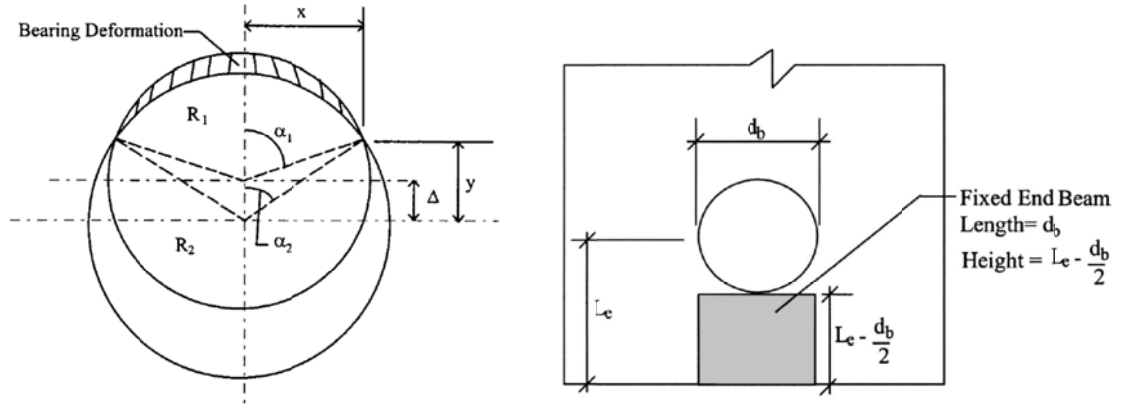
(a) Bearing stiffness model   (b) Bending and shear stiffness model

Figure 5.8 Stiffness Models

(by Rex and Easterling, 2003)
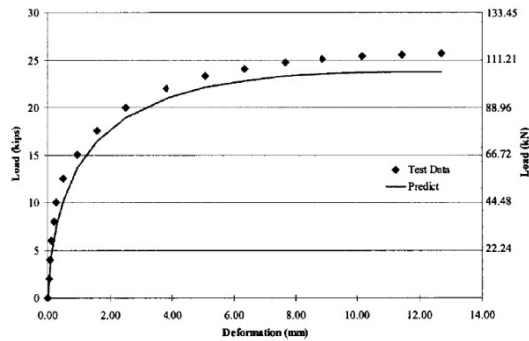
Figure 5.9 Test versus normalized load-deformation prediction for test 41

(by Rex and Easterling, 2003)

Based on the previous slip-bearing model, the shear force and deformation relationship of a bolt connection are estimated considering two different bolt sizes as shown in Table 5.2 and Fig. 5.10. These properties are implemented in the FE models of this study.

Table 5.2 One-way shear force-deformation of a bolt connection

Bolt		Initial Stiffness	Yield Shear Force	Limit displacement
Diameter (φ)	Set	(kip/inch)	(kip)	(inch/mm)
1/4	1 ea	120	2.0	0.12/3
	2 ea	240	4.0	0.12/3
1/2	1 ea	230	4.0	0.12/3
	2 ea	460	8.0	0.12/3
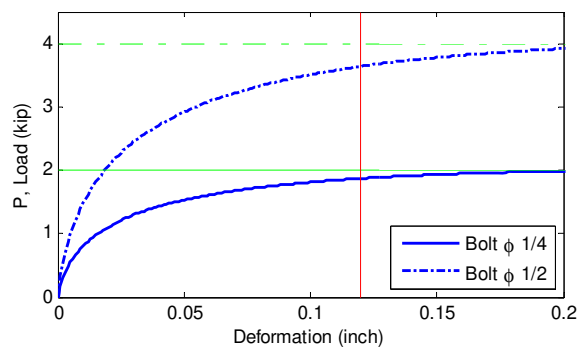
Figure 5.10 Slip-bearing Force-Deformation of a Bolt

The axial force and deformation relationship of a bolted connection is estimated by Eq. 5.2 considering Pull-over/through failure as shown in Fig. 5.11 (a). Under axial forces between two plates connected by a bolt, there is no deformation due to compressive force. On the other hand, there can be nonlinear deformation (Δ) between two plates due to tensile force. It is assumed that, under tensile force as shown in Fig. 5.11 (a), the pull-over/through failure occurs before the tensile force of a bolt reaches yield. Although tightened bolts hold preloads which are tensile forces due to the torque, the bolts themselves have the high yield strength (100 ksi), and the pull-over/through failure governs under axial forces.

Table 5.3 and Fig. 5.11 (b) show the estimated maximum tensile forces and deformations depending on the size of bolts; these properties are implemented in the FE models.

| (a) Pull-Over with Washer | (b) Force-Deformation |
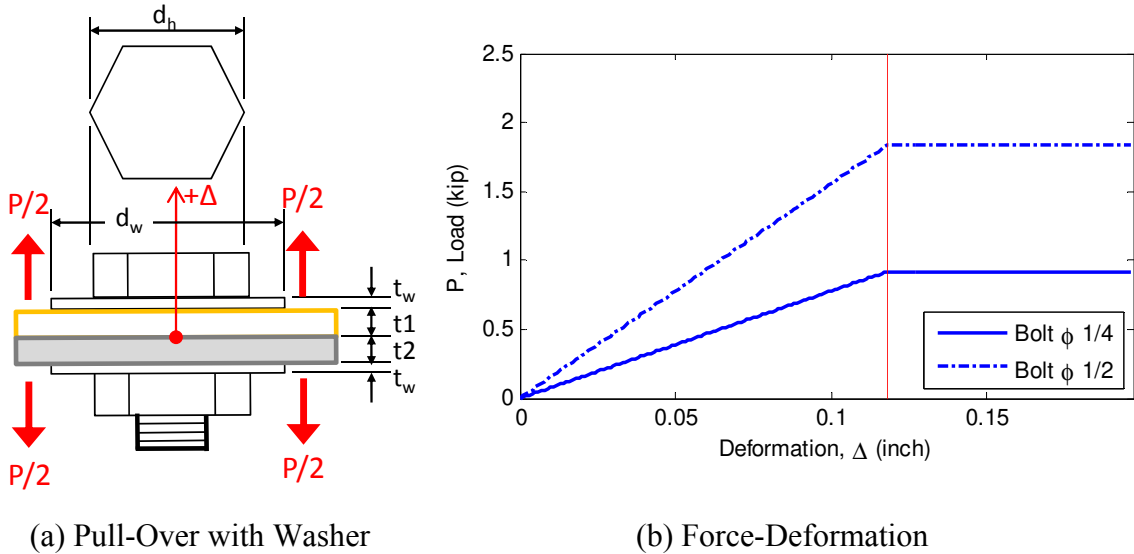
Figure 5.11 Axial Force-Pullover Deformation of a Bolt

Table 5.3 Axial force vs Pull-over/through deformation of a bolt connection

Bolt Diameter (inch)	Washer Diameter (d_w) (inch)	Initial Stiffness (kip/inch)	Yield Axial Force (kip)	Limit displacement (inch/mm)
1/4	0.48 ~ 0.734	7.8	0.92	0.12/3
1/2	0.96 ~ 1.25	15.6	1.84	0.12/3

Figures 5.12 show the deformation of detailed FE connection models due to moments in three axes, and Fig. 5.13 presents the hysteretic behavior of the connection in each

direction. As shown in Fig. 5.12, the angular deformation due to Mx, which is the torsional moment applied to the horizontal member (right side) shown in green color, is much smaller than the corresponding quantities in the two other directions implying that the torsional stiffness is much higher than the other stiffnesses.

| (a) Mx-Direction | (b) My-Direction | (C) Mz-Direction |
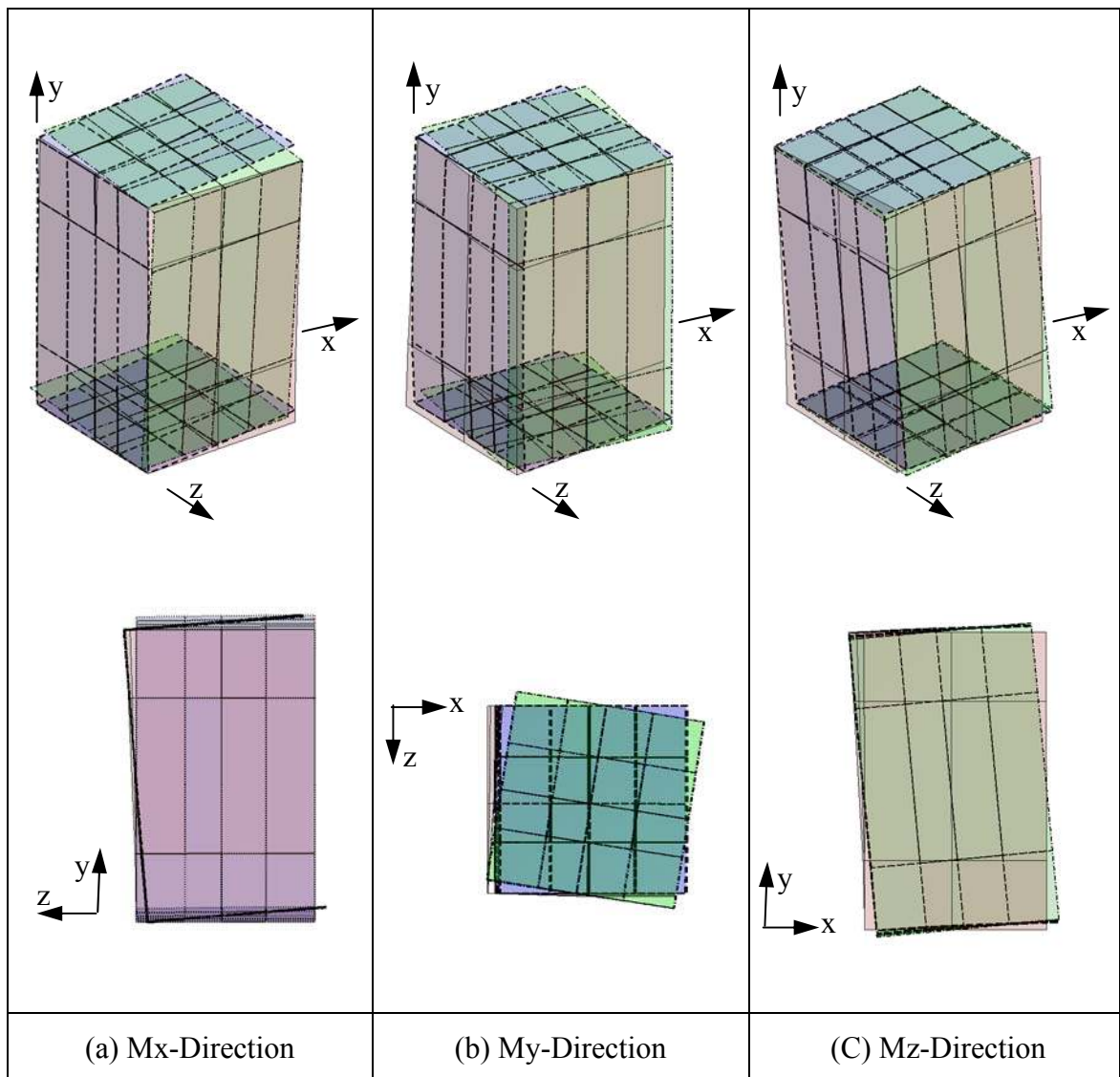
Figure 5.12 Force-Deformation of Bolted Connections
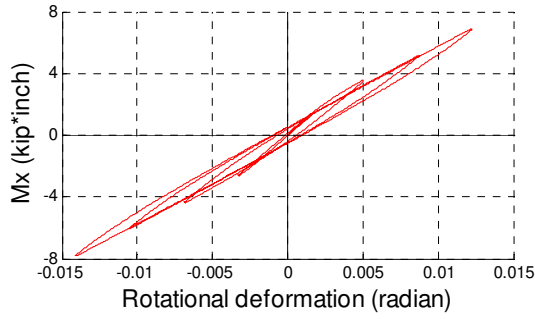
(a) Mx-Dir of Dia. ¼"
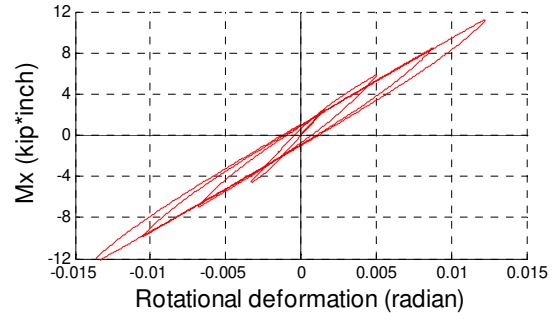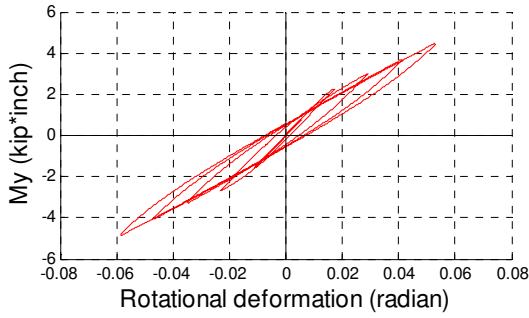
(d) Mx-Dir of Dia. ½"
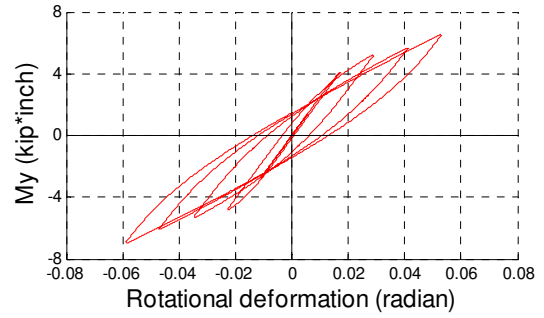
(b) My-Dir of Dia. ¼"
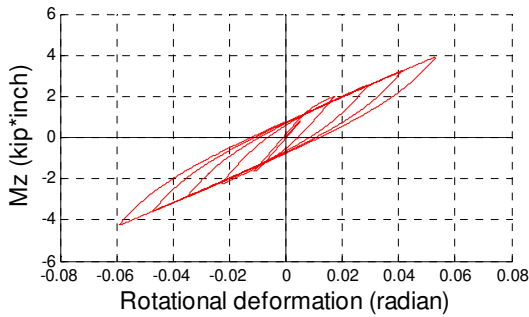
(e) My-Dir of Dia. ½"
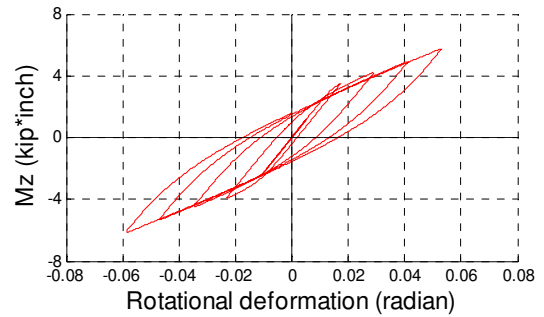
(c) Mz-Dir of Dia. ¼"

(f) Mz-Dir of Dia. ½"

Figure 5.13 Moment-Angular Displacement at the C.G of a Horizontal Member

5.2.4 Support boundary conditions

Previous studies have not included the nonlinear behavior at the support boundary conditions of switchboard cabinets under earthquake ground motion, as the cabinet support boundary conditions have been assumed to be fully fixed. As noted in Chapters 2 and 4, however, the seismic damage at supports can and can lead to physical and operational failure of the equipment.

Fig. 5.14 presents schematics of three different support boundary conditions: restrained, anchored, and unrestrained support conditions. In Fig. 5.14 (a), the restrained condition represents the case in which there is no vertical, horizontal, and angular displacement between the cabinets and the support boundary under any loadings. In Fig. 5.14 (b), the anchored condition presents the most common support boundary conditions for switchboard cabinets in practice, which allows inelastic deformation between the switchboard cabinets and the support boundary under strong ground motions. This deformation is related to the size and length of anchor bolt and washer, their spacing and details, and thickness of plates. Depending on these parameters, the nonlinear properties of this condition can be determined. In Fig. 5.14 (c), the unrestrained condition shows a free-standing case on a plane support. As mentioned in Chapter 4, nonstructural components with this condition can be vulnerable to horizontal and vertical ground motions. Depending on their size, weight, slenderness ratio, and mass distribution, their dynamic behavior drastically changes under seismic shakings.
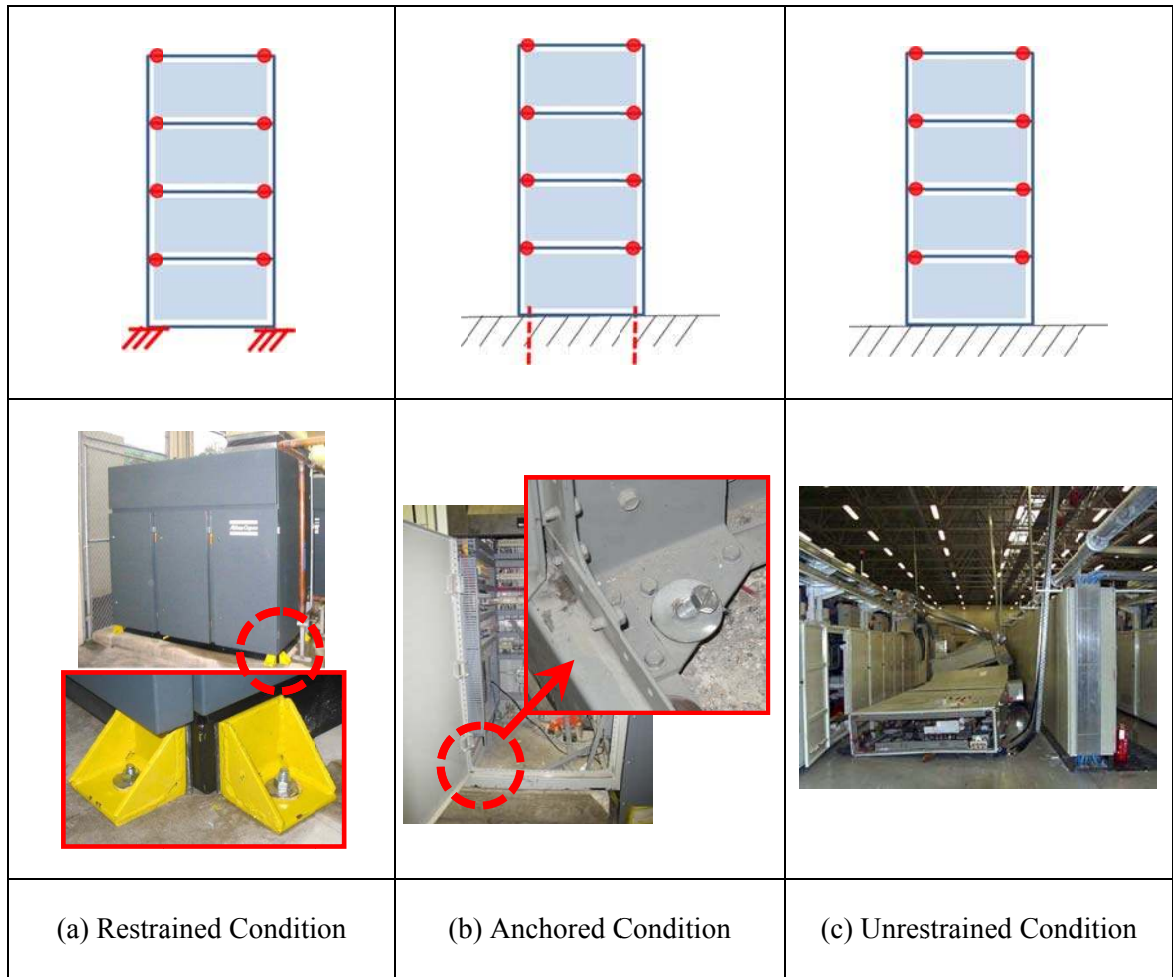
Figure 5.14 Structural Frames of Switchboard Cabinets

(a) Restrained Condition	(b) Anchored Condition	(c) Unrestrained Condition

For the unrestrained condition, the numerical models were constructed based on the numerical models in Chapter 4, which can capture all types of boundary motions of blocks resting on a plane surface under seismic shakings. The unrestrained model is generated using FE elements as shown in Fig. 5.15 (a). This FE model is also composed of three rigid bars and zero-length elements, and behaves under seismic shakings as shown in Fig. 5.15 (b). The support boundary conditions are like those on a plane surface with friction between the block and surface. This model can handle multi-motions,

including sliding, rocking, and pounding depending on the geometry of blocks, properties of the constraint, and characteristics of ground motions.

For the support boundary condition, the Type 1 element controls the horizontal displacement and sliding motions, and the Type 2 element controls the vertical displacement and uplift motions, as mentioned in Chapter 4. These elements are included in the FE models using *flatSliderBearing* elements and zero-length elements in OpenSees respectively between two nodes in parallel. As shown in Fig. 5.15 (b), the nodes (1)-(3) can deform to locations (1')-(3') based on the acceleration content of the ground motions.
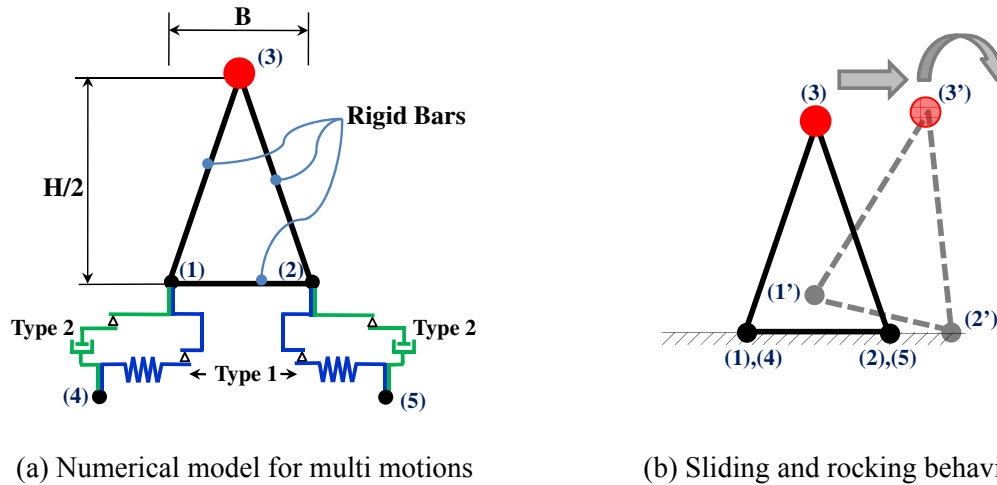
(a) Numerical model for multi motions   (b) Sliding and rocking behavior

Figure 5.15. Schematic of a finite element model with unrestrained support condition

As shown in Fig. 5.16, element Type 1 and element Type 2 are in parallel. When force F_z is a tensile force $(+F_z)$, the vertical displacement increases as element Type 2 deforms. When force F_z is a compressive force, the horizontal stiffness of element Type 1 resists the horizontal force due to ground motions with the friction model.
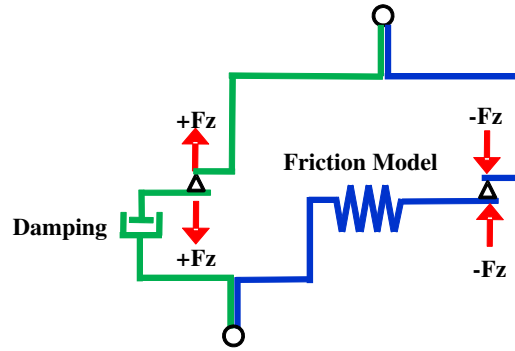
Figure 5.16 Combined no-tension element and friction model

5.3 Analysis results

The nonlinear numerical models with three different support boundary conditions are analyzed using the NTHA method. The *restrained model* refers to the numerical models with nonlinear properties except for the support boundary conditions, in which there is no vertical or lateral deformation at the support. The *anchored model* is the nonlinear numerical model which includes the nonlinear behavior of the anchor bolts at the cabinet base. It is assumed that two bolts with ½"-diameters (Grade 5) are anchored at four corners for support. The *unrestrained model* is the nonlinear numerical model that is free-standing on rigid ground with the coefficient of kinetic friction of 0.4 (μ=0.4). These three different models were analyzed to determine the nonlinear effect of boundary conditions on the dynamic response of a switchboard cabinet.

For the earthquake ground motions, one strong ground motion is applied, which is the fault-normal component of the ground acceleration histories of the January 17, 1994, Northridge, Calif., earthquake recorded at the Rinaldi station. The ground motion is

scaled up and down for the analysis. A larger number of ground motions are considered in the next chapter.

Figures 5.18 – 5.20 illustrate the seismic responses at the top of the switchboard cabinet through the NTHA with the scaled Northridge earthquake ground motions (PGA=0.5g). The scaled ground motions are applied to the horizontal front-to-back direction in Z-axis as shown in Figure 5.17.
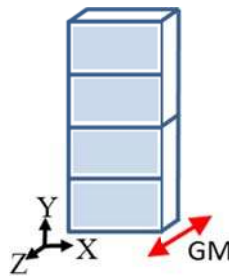
Figure 5.17 Global coordinates and the direction of applied GM

Figs. 5.18 (a)-(c) show the response acceleration in three directions, respectively, at the top of the switchboard cabinets under the Z-dir. excitation (front-to-back direction, see Fig. 5-17). Figs. 5.19 (a)-(c) show the response displacement in three directions respectively at the same location as in Figs. 5.18 (a)-(c). Under the Z-dir excitation, the response accelerations in the side-to-side (X) direction are barely affected, as shown in Fig. 5.19 (a), and the response displacements in the same direction are also unaffected (Fig. 5.19 (a)). On the other hand, in the vertical (Y) direction, the response acceleration of the anchored model is drastically increased, although the vertical response displacement amounts to only 2 mm. In the front-to-back (Z) direction, the response accelerations of all three models are affected as ground motion (GM) varies in Fig. 5.18 (c). It is observed that the maximum accelerations of three models are very close to each

other, but the response time histories of three models are different. Furthermore, it is seen that the response displacement of the unrestrained model in Fig. 5.19 (c) is much larger than in the other models, but as shown in Fig. 5.20 the response drift of anchored model is much larger than in the other models. Rocking behavior is more pronounced in the anchored model than in the two other models, and therefore the vertical response displacement in Fig. 5.18 (b) and the response drift in Fig. 5.20 are larger than the others.

(a)

(b)

(c)
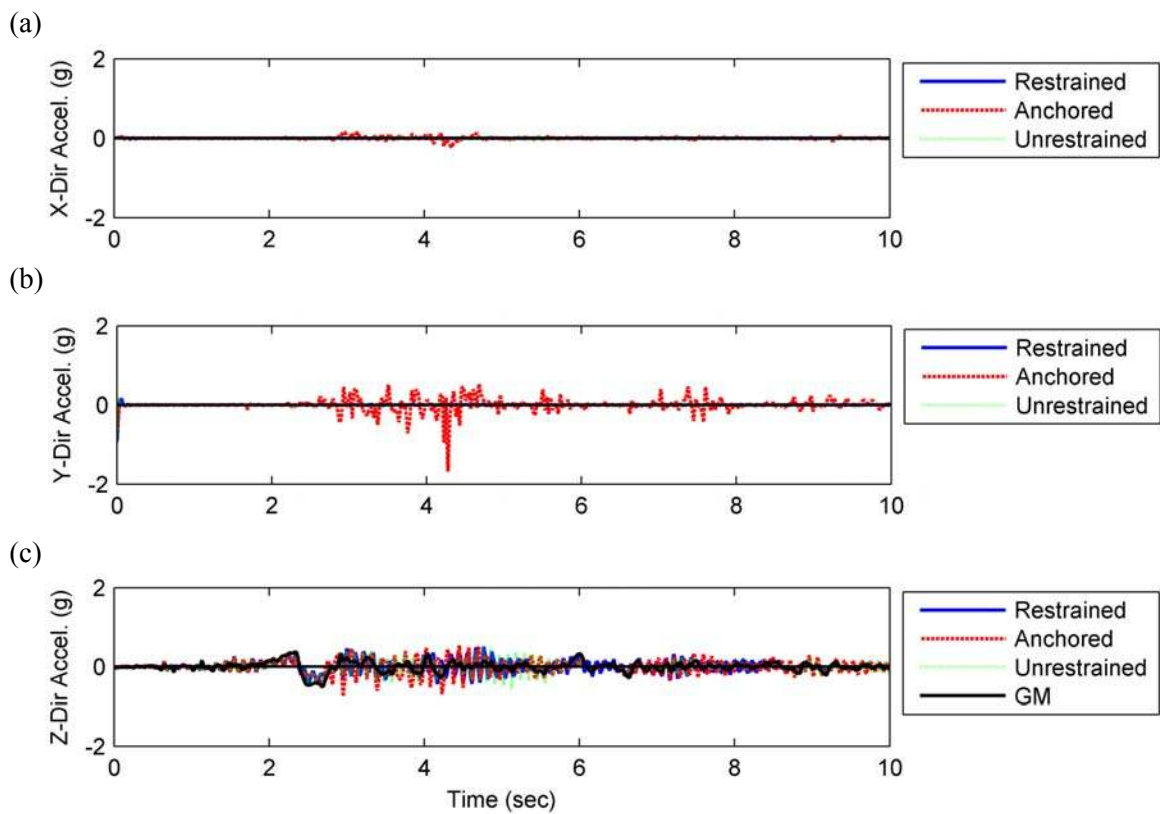
Figure 5.18 Response acceleration at top of three models with different support conditions
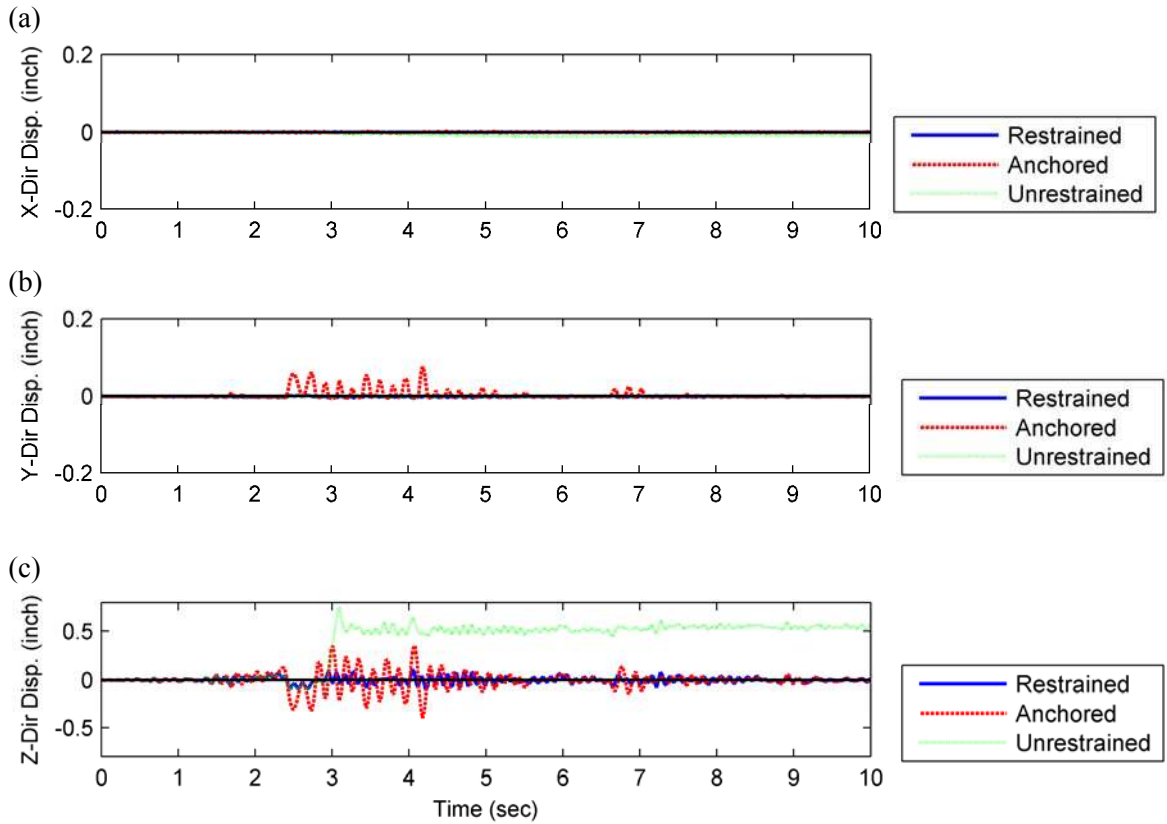
Figure 5.19 Response displacement at top of three models with different support conditions
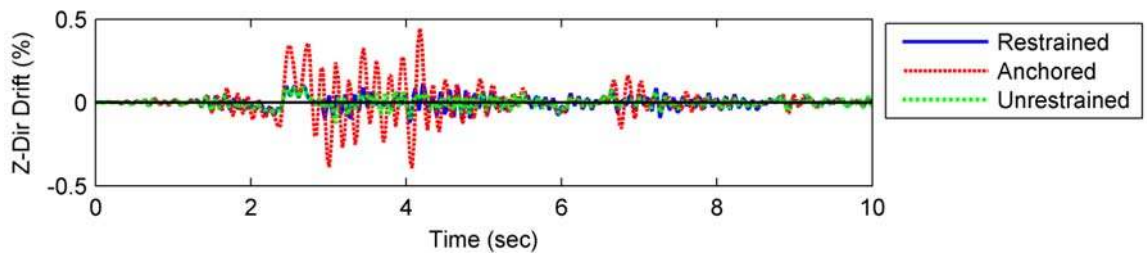
Figure 5.20 Response drift of three models with different support conditions

These results show, for one ground motion only, that the dynamic behavior of anchored and unrestrained switchboard cabinets is drastically changed once they undergo nonlinear force-deformation behavior. The anchored model is capable of exceeding the

131

response acceleration in three directions despite a small deformation. Most of the electrical devices mounted on the switchboard cabinets are sensitive to the acceleration, and the amplitude of response acceleration varies depending on ground motions.

5.4 Closure

This chapter presented the development of the nonlinear numerical models of switchboard cabinets for use in investigating their dynamic behavior during seismic events. The numerical models were constructed using a finite element approach, and the nonlinear properties at the joint connections in cabinets as well as three different support boundary conditions were included in the models and then considered in the nonlinear time history analyses. It was observed that as the amplitude of horizontal excitations increase, seismic response enters the nonlinear range and overall behavior of the cabinet structure changes significantly. The following results were observed:

1. The anchored models appear to have larger responses than the unrestrained models in terms of lateral drift as well as vertical and lateral acceleration responses.

2. The total lateral displacement of the cabinets in the unrestrained models is significantly larger than the corresponding response in the anchored models primarily due to the contribution of the sliding response in the unrestrained models.

3. The perfectly constrained models, fixed at the base, appear to have smaller responses than the other two models in all displacement and acceleration response measures.

4. The FE modeling approach presented in this chapter yields additional insights into cabinet responses during earthquakes. This is achieved by properly capturing the nonlinear behavior of the cabinet as well as the boundary conditions at the base.

CHAPTER VI

PROBABILISTIC SEISMIC DEMAND MODELING AND A METHODOLOGY FOR SEISMIC VULNERABILITY OF SWITCHBOARD CABINETS

6.1   Introduction

The seismic vulnerability evaluation of electrical equipment such as switchboard cabinets is quite complex. Switchboard cabinets are complicated as well as diverse in type, making it difficult to predict their operational and physical damage under seismic effects. A single unit of a switchboard contains hundreds of components that can experience different types of physical damage and operational failure.

In addition, an evaluation of the seismic vulnerability of electrical equipment requires characterization of earthquake ground motions as well. Earthquakes are characterized by their amplitude, frequency content, duration, and their return period, each of which are described using probabilistic models. For instance, Los Angeles, California is exposed to seismic risk from different types of earthquake ground motions. Figure 6.1 shows the response spectra of ground motions in Los Angeles suggested by the SAC Project (1997), and the spectra collectively represent an earthquake with 2% probability of exceedance in 50 years. Clearly, earthquake ground motions in a single location can have varied amplitudes and frequency content. The duration of the earthquakes can vary significantly

from a few seconds to several minutes. These characteristics directly influence the dynamic behavior of electrical equipment resulting in various types of damage. Due to the inevitable uncertainty present in earthquakes, these acceleration histories are selected using probabilistic models.
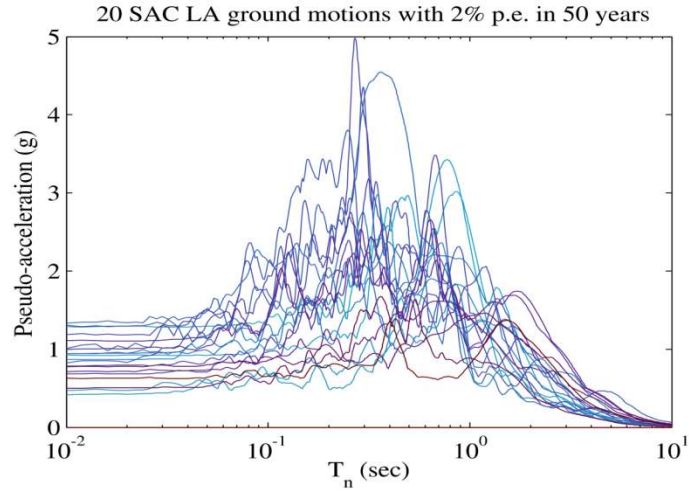
Figure 6.1 Earthquake Ground Motions with 2% Probability of Exceedance in 50 Years

A seismic fragility function describes vulnerability as the probability that a specified limit state is equaled or exceeded, conditioned on a level of demand from the specified seismic hazard and this is expressed in Eq. (6.1) (Wen et al. 2004):

$$Fragility = P[LS<D|IM] = 1 - \Phi\left(\frac{\lambda_{LS}-\lambda_{D|IM}}{\sqrt{\beta_{D|IM}^2+\beta_M^2+\beta_{LS}^2}}\right) \tag{6.1}$$

where LS is the limit state or damage level of the electrical equipment; IM is the earthquake intensity measure such as peak ground acceleration or spectral acceleration at characteristic periods; $\Phi(\cdot)$ is the cumulative distribution function of a standard normal variant; λ_{LS} and $\lambda_{D|IM}$ are the median limit states and the corresponding median demand of specific interest for a given IM, respectively; $\beta_{D|IM}$ and β_{LS} represent the uncertainty

associated with demand representative models and limit states; and β_M is the epistemic uncertainty in modeling the system.

Figure 6.2 shows hypothetical fragility curves based on the formulation presented in Eq. (6.1). The vertical axis denotes the probability of exceeding particular damage states, and the horizontal axis presents the IM of choice. It is seen that, as the level of IM increases, the probability of meeting or exceeding limit states also increases. The other component in Eq. (6.1) is the uncertainty term, $\sqrt{\beta_{D|IM}^2 + \beta_M^2 + \beta_{LS}^2}$, which is related to the dispersion of these functions. A higher dispersion value indicates a greater variability of the fragility function, and therefore the dispersion changes the slope of the function. As shown in Figure 6.2, the fragility curve becomes flatter as the dispersion increases.
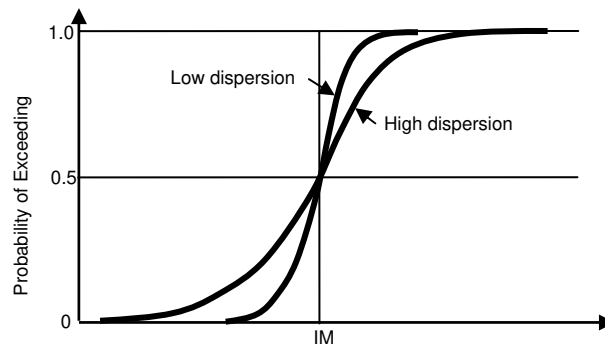
Figure 6.2 Illustration showing the effect of dispersion on fragility functions

According to Eq. (6.1), the evaluation of the seismic vulnerability of switchboard cabinets requires the development of probabilistic seismic demand models (PSDMs) for components in cabinets. In order to develop seismic demand models in this chapter, the critical components in cabinets are identified, and seismic responses are computed using

several ground motion time histories with the finite element based nonlinear time history analysis models developed in Chapter 5.

6.2   Ground Motions Selection

In order to generate PSDMs for critical response measures of switchboard cabinets, the selection of ground motions is important since they are the inputs for nonlinear time-history analysis. Choice of ground motions plays a significant role in the seismic response prediction and characterization. The ground motions should be representative of the anticipated earthquake scenarios at a site.   For the evaluation of the seismic performance of switchboard cabinets, a suite of ground motions pertinent to Los Angeles, California, developed as a part of the SAC Phase 2 Steel Project (1997) is chosen. The acceleration time histories were selected based on the joint magnitude-distance probabilistic models. The suite consists of 60 pairs of time histories at three intensity levels; 2%, 10% and 50% probabilities of exceedance in 50 years. They were derived from historical recordings or from physical simulations and have been altered so that their mean response spectrum matches the 1997 NEHRP design spectrum. In addition, their associated soil type was S_B-S_C to soil type S_D, and their hazard levels were specified by the 1997 USGS maps. A summary of the characteristics of these selected ground motions is shown in Table 6.1 and Figs 6.3 and 6.4.

As seen in Figure 6.3, the peak ground accelerations (PGAs) range from 0.11 to 1.33g. Further, a wide variation is seen in the pseudo spectral accelerations from 0.1to 1 sec, which is the period range of interest for switchboard cabinets.

Table 6.1 Characteristics of selected acceleration time histories

Ground Motion characteristics	2 % | 50 years (min - max)	10 % | 50 years (min - max)	50 % | 50 years (min - max)
Earthquake Magnitude (M)	6.7 - 7.4	6 - 7.3	5.7 - 7.7
Distance from Fault (km)	1.2 - 17.5	1.2 - 36	1 - 107
Duration (sec)	14.9 - 59.98	14.9 - 79.98	26.14 - 79.98
PGA (g)	0.42 - 1.33	0.23 - 1.02	0.11 - 0.79
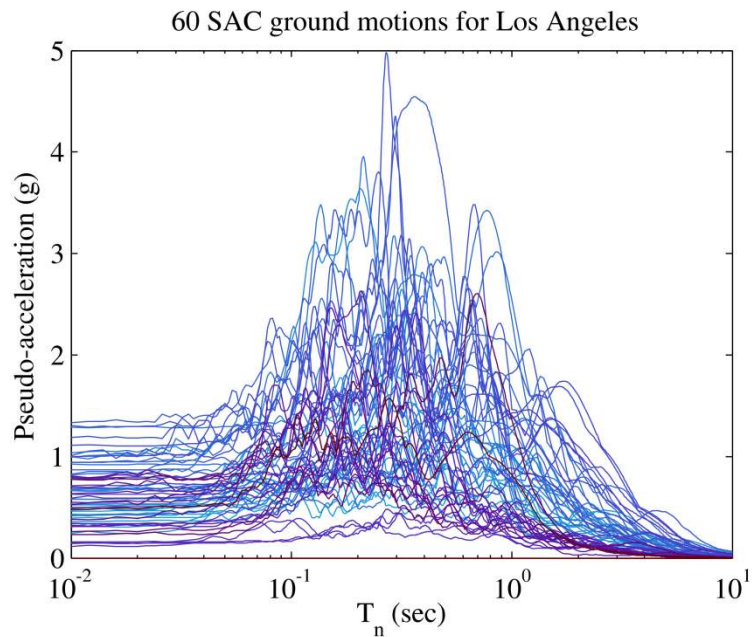
Figure 6.3 Response Spectra of 60 sets of ground motions for Los Angeles

Figure 6.4 shows the hypocentral distance (R) from the fault and three acceleration measures versus moment magnitude (M) of the 60 acceleration histories. Figure 6.4 (a) presents pairs of M and R for earthquakes with different hazard levels that are generated using the deaggregation of the probabilistic seismic hazard at this site. It is observed that the moment magnitude of the earthquakes ranges from 5.5 to 8.0, and distance to the fault varies between 1.0 and 107.0 km. Figure 6.4 (b) shows the distribution of the PGA of ground motions versus M. It is observed that PGAs are well-distributed with respect to

M and range from 0.11 to 1.33g. As expected, ground motions with larger return periods (with 2% in 50 years) have larger PGA. Figures 6.4 (c) and (d) show the average pseudo spectral acceleration (PSA_{Avg}) between the periods of 0.0625-0.25sec (frequencies of 4-16Hz) and the pseudo spectral acceleration (PSA_{Tn}) at the period of 0.1sec (the frequency of 10Hz) respectively. The PSA_{Avg} and PSA_{Tn} also are well distributed. These IMs are explained later in this chapter, and will be shown to provide good correlation with the structural responses of switchboard cabinets.
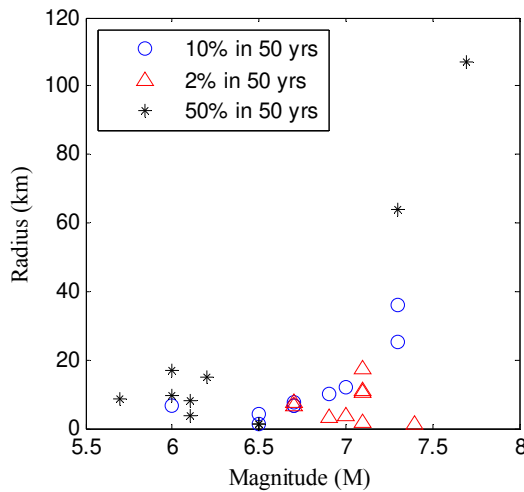
(a) Hypocentral distance (R)
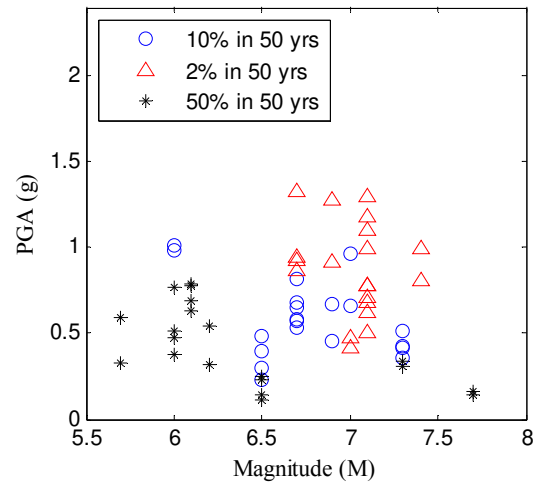
(b) Peak Ground Acceleration (PGA)
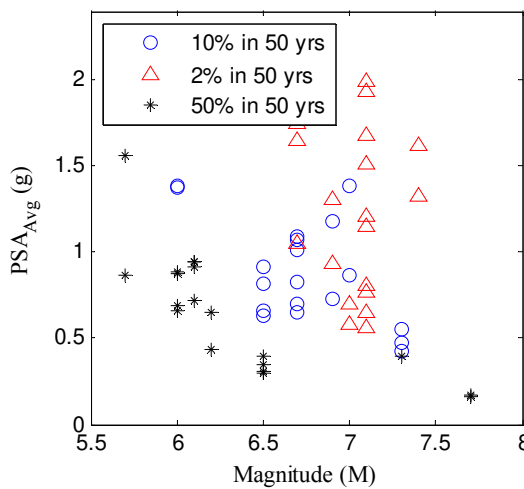
(c) Average Spectral Acceleration
(PSA_{Avg})
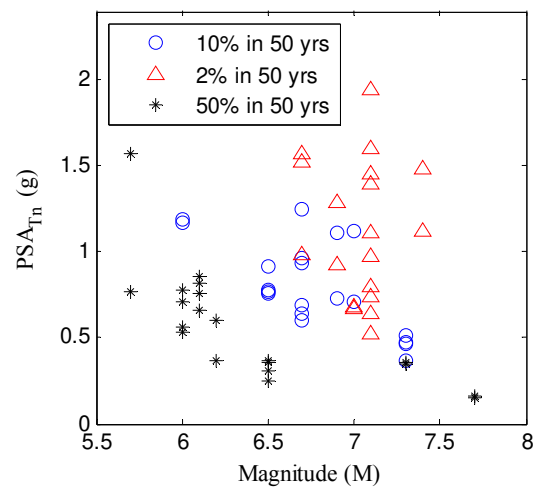
(d) Spectral Acceleration at T_n=0.1 sec
(PSA_{Tn})

Figure 6.4 Characteristics of Selected Ground Motions

6.3 Methodology for Probabilistic Seismic Demand Models of Switchboard Cabinets

6.3.1 Probabilistic Seismic Demand Model (PSDM) Formulation

One of the essential components of the fragility (conditional probability of failure) in Eq. (6.1) is the demand model for which a probabilistic analysis is required to determine the parameters $\lambda_{D|IM}$ and $\beta_{D|IM}$. For the response measures of interest of individual components of the system, Cornell et al. (2002) suggested a candidate seismic demand model using a power function as given in Eq. 6.2:

$$D(IM) = a \cdot IM^b \cdot \varepsilon \qquad (6.2)$$

In Eq. (6.2), ε is a unit-median lognormal random variable with logarithmic standard deviation (dispersion) of $\beta_{D|IM}$ describing the uncertainty in the relationship, and a and b are model parameters (or constants) estimated using a regression analysis for the seismic demand model in the transformed logarithmic space in the following form.

$$\ln\big(D(IM)\big) = \ln(a) + b \cdot \ln(IM) + \ln(\varepsilon) \qquad (6.3)$$

The estimates of a and b from the transformed demand model in Eq. (6.3), denoted by $\hat{a}$ and $\hat{b}$, are unbiased estimators. The other assumption in the demand model of Eq. (6.3) is the homoscedasticity property (Gardoni et al. 2002) which implies that the model variance $\beta_{D|IM}^2$ is independent of IM or equivalently, the coefficient of variation of the error term in Eq. (6.2) is uniform. From Eq. (6.3), the natural logarithm of the median demand for a given IM, $\lambda_{D|IM}$, is found as

$$\lambda_{D|IM} = \ln(\hat{a}) + \hat{b} \cdot \ln(IM) \qquad (6.4)$$

The assumption that the demand follows a lognormal distribution with respect to the IM is applied to all demand measures associated with critical components such as the acceleration of electrical devices or the relative displacement of conduits. Assuming that the dispersion of seismic demand parameters is independent of the IM in the logarithmic scale, the uncertainty in the seismic demand $\beta_{D|IM}$ in Eq. (6.1) is determined as the logarithmic standard deviation of errors in fitting the demand models, expressed in Eq. (6.5), where n denotes the total number of samples.

$$\beta_{D|IM} = \left[\sum_{i=1}^{n} (\ln(D_i) - \lambda_{D|IM})^2 \Big/ (n-2) \right]^{\frac{1}{2}} \tag{6.5}$$

PSDMs are developed for demand measures on various components of switchboard cabinets. Generally interstory drift, displacement, or stress are commonly adopted and important response measures for structural elements in buildings, but previous studies have shown that the acceleration response can be a critical indicator for evaluating the response of frequency-sensitive components such as electrical components (NUREG, 1987). Therefore, the acceleration response is considered to be a critical engineering demand parameter in this research. Table 6.2 details the response measures used to assess the behavior of various components considered in this study, including deformation of fasteners, global frame drift, relative displacement of conduits, and accelerations at locations where devices are attached.

Table 6.2 Critical components demand measures

Demand measure	Abbreviation	Units
Acceleration at electrical devices		
Top front	A_{tf}	g
Middle rear	A_{mr}	g
Screw deformation	Δ_s	mm
Global drift	δ	Ratio (mm/mm)
Total displacement at conduits	Δ_T	mm

6.3.2   Intensity Measures (IM)

Common intensity measures that have been used in seismic fragility analyses are peak ground acceleration (PGA) or spectral acceleration (PSA). Both of these traditional IMs have benefits and drawbacks when applied to electrical equipment. PGA is an accurate indicator of the peak acceleration in the time history, but it is difficult to derive the correlation with the input data for a fragility function of a frequency-sensitive component. Spectral acceleration (PSA_{Tn}) at a certain period is a better indicator for frequency-sensitive components, but it may not be practical to assess the fragility of complex switchboard cabinets, as the large number of devices affixed in a switchboard cabinet can have different sensitive frequencies. That is, the fundamental frequency of the structure of electrical equipment may differ substantially from the other devices attached to the structure. Therefore, the average spectral acceleration (PSA_{Avg}) is suggested to complement the disadvantages of PGA and PSA_{Tn}. (NUREG, 1987). It is obtained by dividing the area under a portion of the response spectrum curve (g-value vs.

frequency on a regular scale) by the corresponding frequency band, which is the frequency range of interest for the particular equipment as shown in Figure 6.5. Using the average spectral acceleration ensures that the response accelerations can be discussed in the frequency band of interest according to IEEE Standard 693 (2005). Generally, the electrical equipment of an indoor substation is assumed to have a frequency range of 4~16Hz unless otherwise specified.
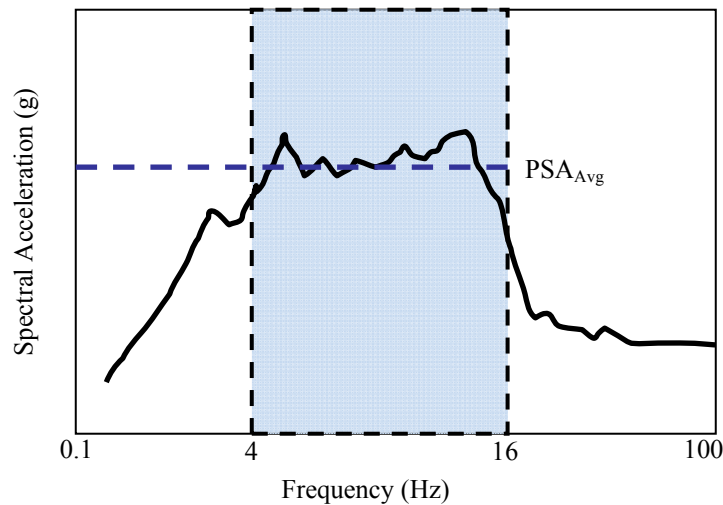
Figure 6.5 The Average Spectral Acceleration

Other commonly adopted IMs are peak ground velocity (PGV) and peak ground displacement (PGD) as shown in Table 6.3. It must be noted that PGV and PGD are the velocity and displacement computed by integrating the ground acceleration histories.

Table 6.3 Intensity measures

Intensity Measure	Definition	Units
PGA	Peak ground acceleration	g
PGV	Peak ground velocity	mm/sec
PGD	Peak ground displacement	mm
PSA_{Tn}	spectral acceleration at 10 Hz	g
PSA_{Avg}	Average spectral acceleration at 4-16 Hz	g

Having described the commonly adopted IMs, it is imperative to identify the optimal IM to describe and characterize PSDMs. Optimality of IMs requires them to satisfy certain essential properties. Giovenale et al. (2004) suggested that sufficiency, efficiency, and hazard computability characterize an optimal IM, while Luco and Cornell (2002) and Padgett et al. (2008) added the practicality and the proficiency measures, respectively, to complement the aforementioned properties. These properties will further serve as a validation for the strength and accuracy of the power law assumption of the PSDM. Figure 6.6 shows a sample PSDM for the explanation of these properties.

For the efficiency of IMs, the logarithmic standard deviation of the seismic demands is commonly used. A lower value of the dispersion ($\beta_{D|IM}$) indicates more efficient IM, as it reduces the variation in the estimated demand for a given IM value and at the same time maintains a constant variability over the entire range of the chosen IM. As previously mentioned, in this study it is assumed that the dispersion has the homoscedasticity property with respect to IMs.

Sufficiency of IMs ensures the applicability of total probability theorem in probabilistic seismic demand analysis (PSDA). Sufficiency refers to the property where

an IM is independent of ground motion characteristics such as magnitude (M) and epicentral distance (R). Figure 6.4 already showed that IMs such as PGA, PSA_{Tn}, and PSA_{Avg} are independently distributed in various range of moment magnitude (M).

Practical IMs show the dependence of the demand upon the IM level. For the practicality, the slope ($\hat{b}$), described in Eq. (6.3) and Figure 6.6 is a good indicator of this dependence. A higher value of b indicates that the IM is more practical, and a lower value of b presents that there is a negligible dependence of the demand upon the IM, thereby indicating an impractical IM.

Proficiency is a composite measure of efficiency and practicality. This property is derived by rearranging the terms in the formulation presented in Eq. (6.1) after substitution by Eq. (6.4). The term in the denominator in the formulation given in Eq. (6.6) is defined as modified dispersion, ζ, and is a measure of proficiency. A lower value of ζ indicates a more proficient IM thereby indicating a lower uncertainty in the demand model by the choice of the IM.

$$P(LS < D|IM) = \Phi \left(\frac{\ln(\text{IM}) - \dfrac{\ln(\lambda_{LS}) + \ln(\hat{a})}{\hat{b}}}{\dfrac{\sqrt{\beta_{D|IM}^2 + \beta_M^2 + \beta_{LS}^2}}{\hat{b}}} \right) \tag{6.6}$$

$$\zeta = \frac{\sqrt{\beta_{D|IM}^2 + \beta_M^2 + \beta_{LS}^2}}{\hat{b}} \tag{6.7}$$
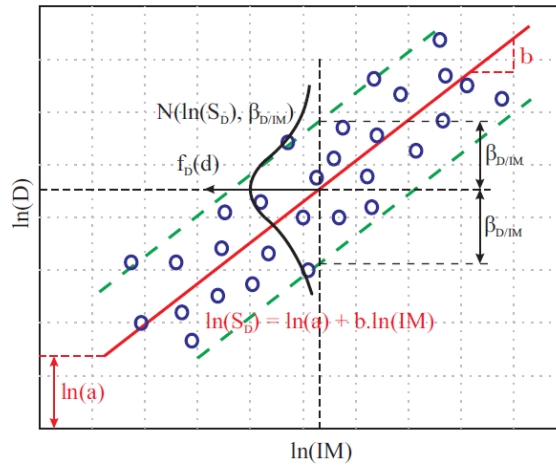
Figure 6.6 Probabilistic Seismic Demand Model

Considering these factors, the most appropriate IM for evaluation of electrical equipment such as switchboard cabinets is evaluated from among the suggested intensity measures given in Table 6.3. For this purpose, PSDMs for the displacement at the top of the cabinet can be developed for all of the considered IMs using nonlinear time history analysis results of the restrained FE models for the 60 ground motions. The correlations between the IMs and the simulation results are generated using the linear regression model described in Eq. (6.3). Table 6.4 and Figure 6.7 show PSDMs for the displacement at top level of switchboard cabinets (Δ_T) using the five different IMs. The displacement response at the top level is the one of demand parameters suggested in section 6.3.1. Since the conduits are connected to the top surface of cabinets, Δ_T induces the physical damage to the connectivity from conduits to cabinets and causes operational failure as well.

As shown in Table 6.4, based on the displacement response at the top level of the switchboard cabinets, the optimal IM is spectral acceleration at 10Hz (PSA$_{Tn}$). Table 6.4

shows that the value of b is the highest; R^2 is also close to 1; both $\beta_{D|IM}$ and ζ are the smallest among the IMs. In contrast, PGA, PGV and PGD were poorly correlated with demand (Δ_T).

Table 6.4 Effective intensity measures

	PGA	PGV	PGD	**PSA$_{Tn}$**	PSA$_{Avg}$
$\hat{a}$	1.27	-0.03	1.20	1.13	1.05
$\hat{b}$	0.73	0.23	-0.12	**0.96**	0.93
R^2	0.56	0.08	0.05	**0.94**	0.88
$\beta_{D|IM}$	0.37	0.54	0.55	**0.14**	0.19
ζ	0.51	2.32	-4.56	**0.14**	0.21

Figures 6.4 (a)-(e) help in visualizing the optimality comparisons between IMs. The two blue lines above and below the mean response in the logarithmic space indicate the mean conditional demand plus and minus one standard deviation. The vertical distance of these lines from the logarithmic mean demand is related to the R^2 and $\beta_{D|IM}$ of each model. The slope ($\hat{b}$) shows the practicality of IMs, and ζ is defined with $\beta_{D|IM}$ and $\hat{b}$ as explained in Eq. (6.7). Note that PSA$_{Tn}$ shows a very good agreement with the linear regression model; its dispersion is small; and its slope is steeper than other models. Therefore, PSA$_{Tn}$ is chosen as the optimal IM and is used in this study to investigate the possible trends that may exist between the response of the switchboard cabinets and the IMs.

Figure 6.7 PSDMs characterizing the displacement demand at top level in front to back direction (Δ_T) in the restrained model

Figures 6.4 (a)-(e) help in visualizing the optimality comparisons between IMs. The two blue lines above and below the mean response in the logarithmic space indicate the

mean conditional demand plus and minus one standard deviation. The vertical distance of these lines from the logarithmic mean demand is related to the R^2 and $\beta_{D|IM}$ of each model. The slope $(\hat{b})$ shows the practicality of IMs, and ζ is defined with $\beta_{D|IM}$ and $\hat{b}$ as explained in Eq. (6.7). Note that PSA_{Tn} shows a very good agreement with the linear regression model; its dispersion is small; and its slope is steeper than other models. Therefore, PSA_{Tn} is chosen as the optimal IM and is used in this study to investigate the possible trends that may exist between the response of the switchboard cabinets and the IMs.

6.3.3   PSDMs from Component Responses in Switchboard Cabinets

This section presents the PSDMs for several components affecting the vulnerability of switchboard cabinets. The seismic responses of cabinets are computed using the finite element (FE) models presented in the previous chapters, which include three different boundary conditions: (1) restrained model that represents a fully fixed condition without any deformation at the support, (2) anchored model that includes bolted connections with nonlinear force-deformation relationships connecting the switchboard cabinets to the ground, and (3) unrestrained model that represents a free-standing cabinet without any restraint. Using nonlinear time history analysis, the seismic responses of each model are estimated, and the maximum responses of critical components of interest in these models are collected to aid in the development of PSDMs. The critical components in the switchboard cabinets and their response measures are the total displacement at the top level where conduits are connected to cabinets, absolute acceleration at two locations: top front and middle rear of electrical devices in the front-back and vertical directions, global

frame drift for the physical damage to cabinets, and screw deformation for minor physical damage. From the discussion in the previous section, it was concluded that acceleration based intensity measures PGA, PSA_{Tn}, and PSA_{Avg} would be the most appropriate intensity measures to model demand parameters of switchboard cabinets. However, PGV can be an alternate IM for PSDMs of response acceleration and screw deformation of unrestrained models. Consequently these IMs are used in the subsequent sections to describe the seismic behavior of various components of switchboard cabinets.

6.3.3.1 PSDMs - Restrained Models

Probabilistic seismic demand models of critical components in restrained switchboard cabinets are developed using the nonlinear time-history analysis (NTHA) results for 60 ground motions. Tables 6.5 to 6.7 present the characteristics of the PSDMs in terms of the intercept ($\hat{a}$), slope ($\hat{b}$), and associated dispersion ($\beta_{D|IM}$) for PGA, PSA_{Tn}, and PSA_{Avg} as IMs, respectively. Higher values of $\hat{b}$ indicate more practical IMs, and lower values of $\beta_{D|IM}$ mean more effective IMs. Therefore, it is observed that PSA_{Tn} is a more practical and effective IM than others for the PSDMs of restrained models.

Based on $\hat{b}$ values, response acceleration measures in vertical direction (A_{tf}^{V} and A_{mr}^{V}) and screw deformation (Δ_s) are less dependent on the IMs (less practical), with horizontal ground excitation. PSDMs of accelerations in both front-back and vertical directions have high values of dispersion in comparison to Δ_T or δ.

Table 6.5 Statistics of the estimated parameters of demand models using PGA

Response measure		$\hat{a}$	$\hat{b}$	$\beta_{D|IM}$
Total displacement at conduits: Δ_T (mm)		1.27	0.73	0.37
Acceleration at electrical devices (Front-Back Dir.)	Top front: A_{tf}^H (g)	0.79	0.71	0.70
	Middle rear: A_{mr}^H (g)	0.59	0.71	0.70
Acceleration at electrical devices (Vertical Dir.)	Top front: A_{tf}^V (g)	-0.28	0.38	1.50
	Middle rear: A_{mr}^V (g)	-0.90	0.34	1.38
Global drift: δ (mm/mm)		-6.46	0.73	0.37
Screw deformation: Δ_s (mm)		-0.53	0.30	0.51

Table 6.6 Statistics of the estimated parameters of demand models using PSA$_{Tn}$

Response measure		$\hat{a}$	$\hat{b}$	$\beta_{D|IM}$
Total displacement at conduits: Δ_T (mm)		1.13	0.96	0.14
Acceleration at electrical devices (Front-Back Dir.)	Top front: A_{tf}^H (g)	0.63	0.90	0.63
	Middle rear: A_{mr}^H (g)	0.42	0.84	0.65
Acceleration at electrical devices (Vertical Dir.)	Top front: A_{tf}^V (g)	-0.33	0.61	1.47
	Middle rear: A_{mr}^V (g)	-0.95	0.49	1.37
Global drift: δ (mm/mm)		-6.61	0.96	0.37
Screw deformation: Δ_s (mm)		-0.59	0.39	0.49

Table 6.7 Statistics of the estimated parameters of demand models using PSA$_{Avg}$

Response measure		$\hat{a}$	$\hat{b}$	$\beta_{D|IM}$
Total displacement at conduits: Δ_T (mm)		1.05	0.93	0.19
Acceleration at electrical devices (Front-Back Dir.)	Top front: A_{tf}^H (g)	0.55	0.85	0.65
	Middle rear: A_{mr}^H (g)	0.35	0.81	0.66
Acceleration at electrical devices (Vertical Dir.)	Top front: A_{tf}^V (g)	-0.38	0.57	1.48
	Middle rear: A_{mr}^V (g)	-1.00	0.46	1.37
Global drift: δ (mm/mm)		-6.68	0.93	0.19
Screw deformation: Δ_s (mm)		-0.62	0.39	0.49

Figure 6.8 shows the correlation of seismic response measures and their PSDMs. The PSDMs characterizing the top displacement, Δ_T, and total drift, δ, as shown in Figures 6.8(a) and 6.8(f), show excellent applicability of the power law assumption in characterizing the respective component response measures. This is depicted by the higher slope and reduced dispersion values. The PSDMs of accelerations in both front-back and vertical directions have high values of dispersion. The PSDMs of response accelerations at two locations in the front-back direction (A_{tf}^{H} and A_{mr}^{H}) are more dependent on the IMs than those in the vertical direction (A_{tf}^{V} and A_{mr}^{V}). Without any lateral seismic effects, the vertical accelerations should be close to 0g, but their values vary depending on the characteristics of ground motions and their local mode shapes.
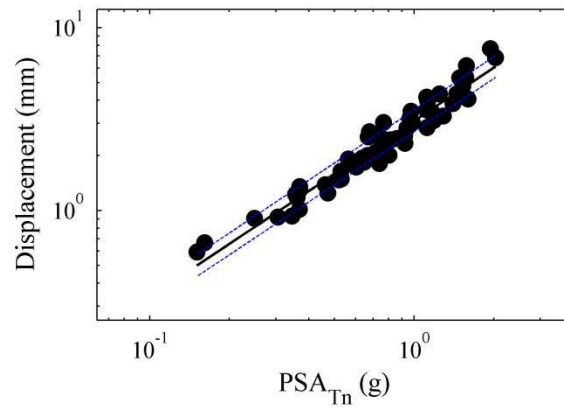
(a) Δ_T (mm)

Figure 6.8 PSDMs describing component responses in restrained models using PSA_{Tn} as the intensity measure (continued on next page)

(b) A_{tf}^{H} (g)

(c) A_{mr}^{H} (g)

(d) A_{tf}^{V} (g)

(e) A_{mr}^{V} (g)

(f) δ (mm/mm)

(g) Δ_{s} (mm)

Figure 6.8 PSDMs describing component responses in restrained models using PSA_{Tn} as the intensity measure

153
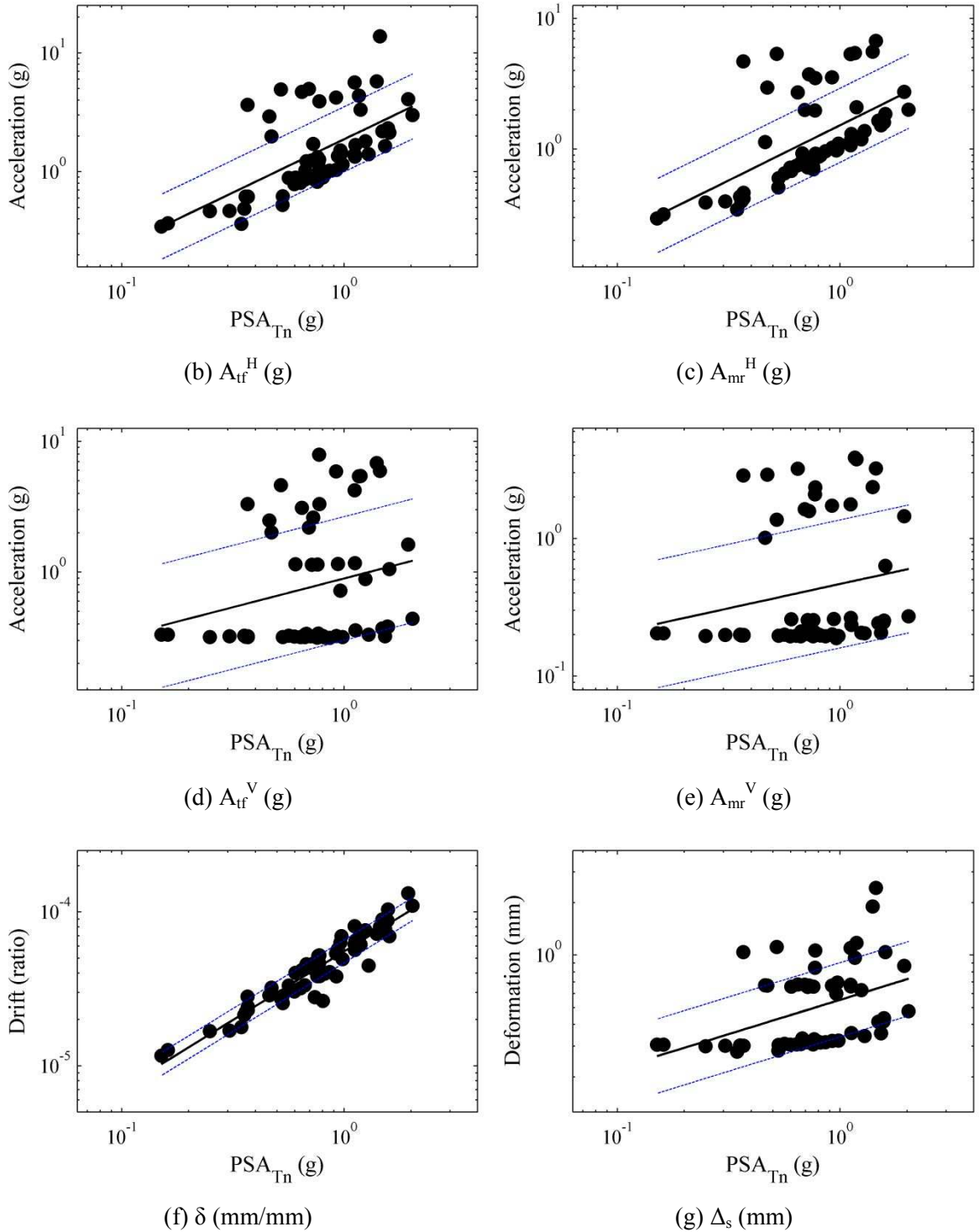
6.3.3.2 PSDMs - Anchored Models

PSDMs of components in anchored switchboard cabinets are developed using the NTHA described in previous sections. The critical response measures described in the previous section are considered in the development of PSDMs of anchored models. Tables 6.8 through 6.10 present the characteristics of the PSDMs for PGA, PSA_{Tn}, and PSA_{Avg} as IMs, respectively. Based on higher values of $\hat{b}$ and lower values of $\beta_{D|IM}$, PSA_{Avg} is an appropriate IM for anchored models.

As in the case of restrained models, the PSDMs characterizing top displacement, Δ_T, shown in Figure 6.9 (a) and total drift, δ, shown in Figure 6.9 (f), show good linear fit of the respective component responses with respect to IM in the lognormal space. Their slopes are higher, and dispersions are relatively low values. On the other hand, acceleration responses in both front-back and vertical directions and screw deformation have higher values of dispersion compared to those in the restrained models described in the previous section, and are less practical.

Table 6.8 Statistics of the estimated parameters of demand models using PGA

Response measure		$\hat{a}$	$\hat{b}$	$\beta_{D|IM}$
Total displacement at conduits: Δ_T (mm)		2.55	1.39	0.49
Acceleration at electrical devices (Front-Back Dir.)	Top front: A_{tf}^{H} (g)	0.98	0.95	0.67
	Middle rear: A_{mr}^{H} (g)	0.71	0.76	0.60
Acceleration at electrical devices (Vertical Dir.)	Top front: A_{tf}^{V} (g)	0.91	0.81	0.72
	Middle rear: A_{mr}^{V} (g)	2.30	1.06	0.89
Global drift: δ (mm/mm)		-0.82	1.27	0.96
Screw deformation: Δ_s (mm)		-5.19	1.39	0.49

Table 6.9 Statistics of the estimated parameters of demand models using PSA_{Tn}

Response measure		$\hat{a}$	$\hat{b}$	$\beta_{D|IM}$
Total displacement at conduits: Δ_T (mm)		2.19	1.57	0.30
Acceleration at electrical devices (Front-Back Dir.)	Top front: A_{tf}^H (g)	0.75	1.10	0.61
	Middle rear: A_{mr}^H (g)	0.44	0.62	0.66
Acceleration at electrical devices (Vertical Dir.)	Top front: A_{tf}^V (g)	0.73	1.03	0.63
	Middle rear: A_{mr}^V (g)	1.97	1.01	0.91
Global drift: δ (mm/mm)		-1.12	1.54	0.84
Screw deformation: Δ_s (mm)		-5.54	1.57	0.30

Table 6.10 Statistics of the estimated parameters of demand models using PSA_{Avg}

Response measure		$\hat{a}$	$\hat{b}$	$\beta_{D|IM}$
Total displacement at conduits: Δ_T (mm)		2.08	1.60	0.25
Acceleration at electrical devices (Front-Back Dir.)	Top front: A_{tf}^H (g)	0.67	1.13	0.59
	Middle rear: A_{mr}^H (g)	0.41	0.69	0.64
Acceleration at electrical devices (Vertical Dir.)	Top front: A_{tf}^V (g)	0.66	1.07	0.61
	Middle rear: A_{mr}^V (g)	1.91	1.07	0.89
Global drift: δ (mm/mm)		-1.23	1.52	0.85
Screw deformation: Δ_s (mm)		-5.65	1.60	0.25

(a) Δ_T (mm)

Figure 6.9 PSDMs characterizing component responses in anchored models using PSA_{Avg} as the intensity measure (continued on next page)

(b) A_{tf}^{H} (g)

(c) A_{mr}^{H} (g)

(d) A_{tf}^{V} (g)

(e) A_{mr}^{V} (g)

(f) δ (mm/mm)

(g) Δ_s (mm)

Figure 6.9 PSDMs characterizing component responses in anchored models using PSA_{Avg} as the intensity measure

6.3.3.3 PSDMs - Unrestrained Models

As in the previous cases, PSDMs describing component responses in unrestrained switchboard cabinets are also developed using NTHA. Unlike the PSDM interpretations for restrained and anchored models described before, the trends observed in the case of unrestrained models are different. Tables 6.11 and 6.12 present the characteristics of the PSDMs developed using PSA_{Tn} and PGA as IMs. While the PSA_{Tn} performs better as an IM in comparison to PGA based on the high slope ($\hat{b}$) values of total displacement at top (Δ_T) and total drift (δ), the dispersions obtained in this case are much higher when compared to restrained and anchored models. Accordingly, the PSA_{Tn} is not a practical IM for PSDMs of accelerations and screw deformation due to negative values of slope. The PGV shows better practicality but still the values of slope are not high.

Table 6.11 Statistics of the estimated parameters of demand models using PSA_{Tn}

Response measure		$\hat{a}$	$\hat{b}$	$\beta_{D|IM}$
Total displacement at conduits: Δ_T (mm)		3.47	2.44	1.07
Acceleration at electrical devices (Front-Back Dir.)	Top front: A_{tf}^H (g)	1.26	-0.40	0.84
	Middle rear: A_{mr}^H (g)	1.66	-0.56	0.78
Acceleration at electrical devices (Vertical Dir.)	Top front: A_{tf}^V (g)	0.09	-0.61	0.82
	Middle rear: A_{mr}^V (g)	-0.63	-0.53	0.89
Global drift: δ (mm/mm)		-6.14	1.30	0.44
Screw deformation: Δ_s (mm)		0.37	-0.54	0.48

Table 6.12 Statistics of the estimated parameters of demand models using PGV

Response measure		$\hat{a}$	$\hat{b}$	$\beta_{D|IM}$
Total displacement at conduits: Δ_T (mm)		-2.61	1.43	1.43
Acceleration at electrical devices (Front-Back Dir.)	Top front: A_{tf}^{H} (g)	1.06	0.09	0.87
	Middle rear: A_{mr}^{H} (g)	1.26	0.15	0.83
Acceleration at electrical devices (Vertical Dir.)	Top front: A_{tf}^{V} (g)	0.22	0.01	0.85
	Middle rear: A_{mr}^{V} (g)	-0.52	0.01	0.87
Global drift: δ (mm/mm)		-9.05	0.68	0.71
Screw deformation: Δ_s (mm)		0.62	-0.02	0.57

As expected, PSDMs of total displacement response and drift are in good agreement with regression lines with respect to PSA_{Tn} despite higher dispersion than other two models. PSDMs of acceleration measures (A_{tf}^{H}, A_{mr}^{H}, A_{tf}^{V}, and A_{mr}^{V}) and screw deformation (Δ_s) are developed using PGV; this relationship is characterized by high values of dispersion, as shown in Figures 6.10(b) through 6.10(e). It is found that horizontal and vertical accelerations of unrestrained models are weakly dependent on IMs such as PGA, PSA_{Tn}, PSA_{Avg}, PGV, and PGD.
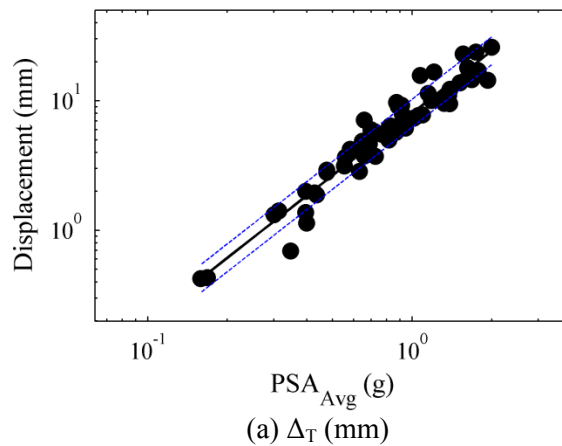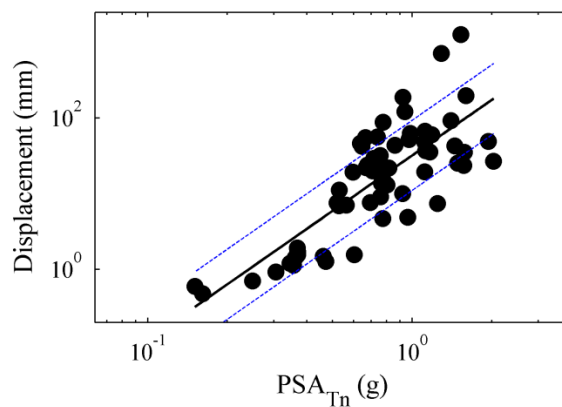

(a) Δ_T (mm)

Figure 6.10 PSDMs characterizing component responses in unrestrained models using PSA_{Tn} and PGV as the intensity measure (continued on next page)
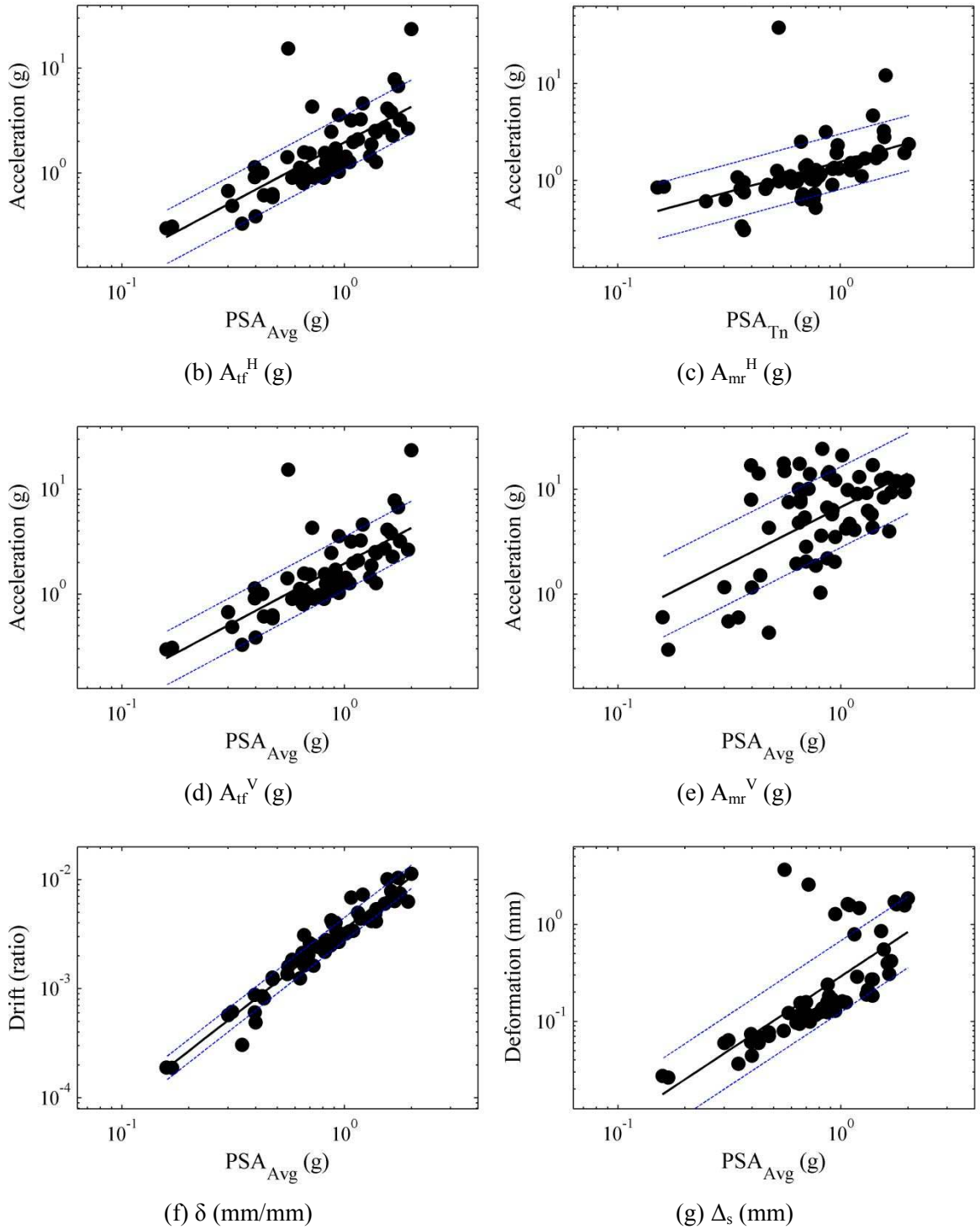
(b) A_{tf}^H (g)

(c) A_{mr}^H (g)

(d) A_{tf}^V (g)

(e) A_{mr}^V (g)

(f) δ (mm/mm)

(g) Δ_s (mm)
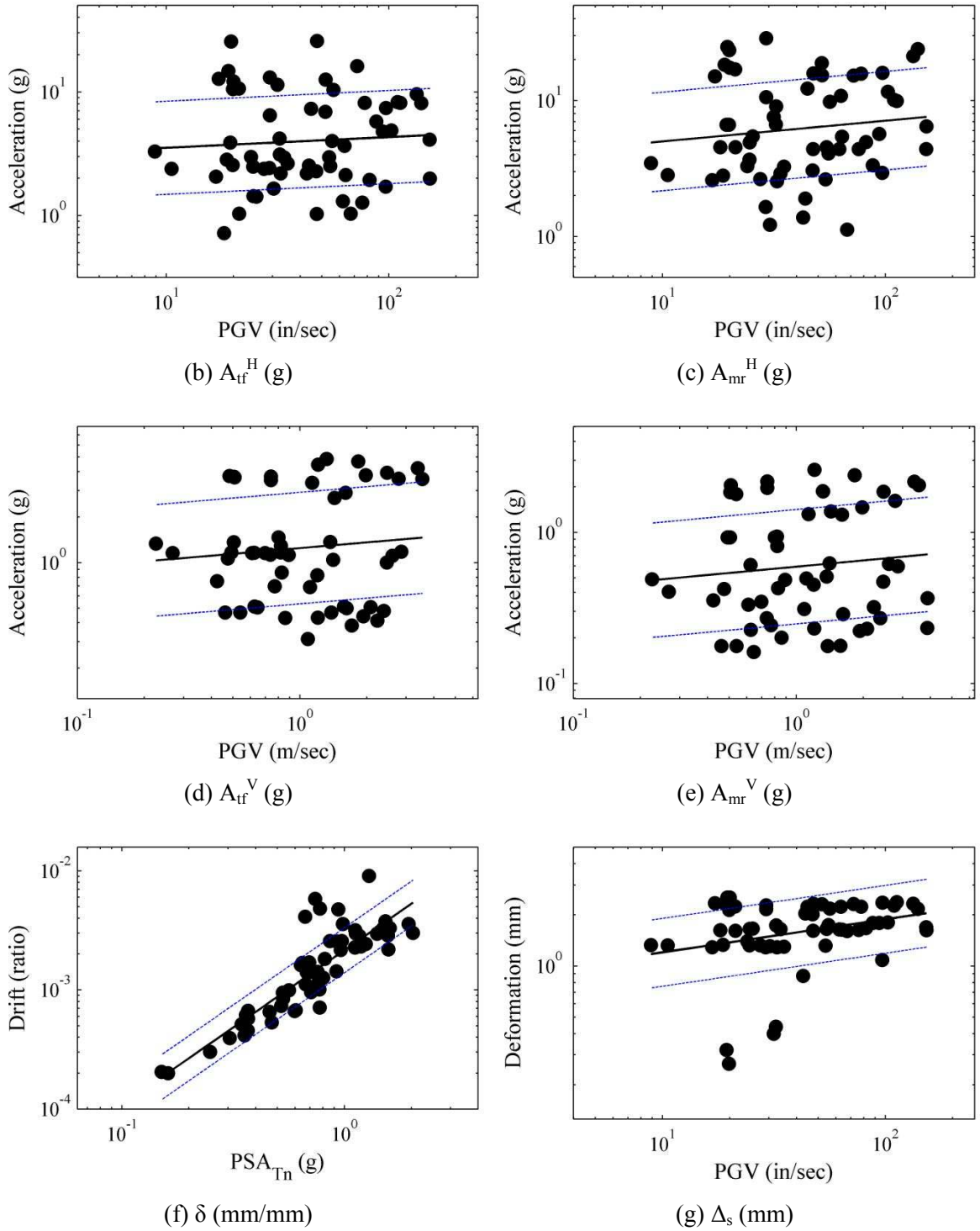
Figure 6.10 PSDMs characterizing component responses in unrestrained models using PSA_{Tn} and PGV as the intensity measure

6.3.3.4 Comparison of PSDMs of Anchored, Restrained and Unrestrained Models

This section presents the comparison of PSDMs characterizing similar component responses in the three models: Restrained, Anchored, and Unrestrained. To facilitate comparison, PSDMs are developed using spectral acceleration (PSA_{Tn}) at a frequency of 10Hz (period of 0.1 sec) and PGV as the IMs. Figure 6.11 shows the PSDM for total displacement at the top of the cabinet where conduits are connected to switchboard cabinets. As described in Chapter 5, the total displacements (Δ_T) of the unrestrained models are larger than the respective displacements in anchored and restrained models as the IM increases. However, the dispersion of displacement demand in unrestrained models is much higher than that exhibited by anchored and restrained models. The total displacements of unrestrained models at low levels of PSA_{Tn} are close to those of the restrained model. When PSA_{Tn} exceeds around 0.5g, however, Δ_T of unrestrained model increases drastically and exceeds that of the anchored model; this increase is accompanied by high values of dispersion.
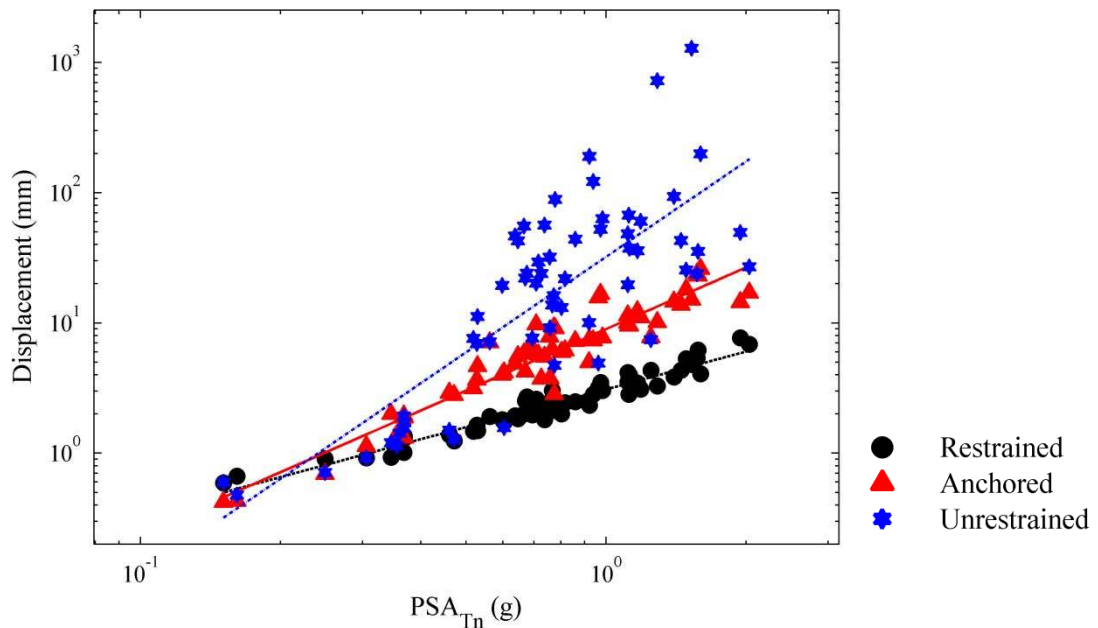
Figure 6.11 Comparison of PSDMs describing displacement Δ_T (front-back dir.) in three models using PSA_{Tn} as the intensity measure

Figure 6.12 shows the comparison of PSDMs describing global drift (δ) of switchboard cabinets. As shown in Figure 6.11, the total displacement of the unrestrained model exceeds that of the anchored model. However, in terms of global drift given in Figure 6.12, the trend is reversed. This is attributed to the sliding behavior observed in the unrestrained model as described in Chapter 5, while the total displacement of anchored model is governed by rocking behavior. Therefore, the response drift of anchored models is larger than that of other two models, while the dispersion of the unrestrained model is much higher than that of the other two models.
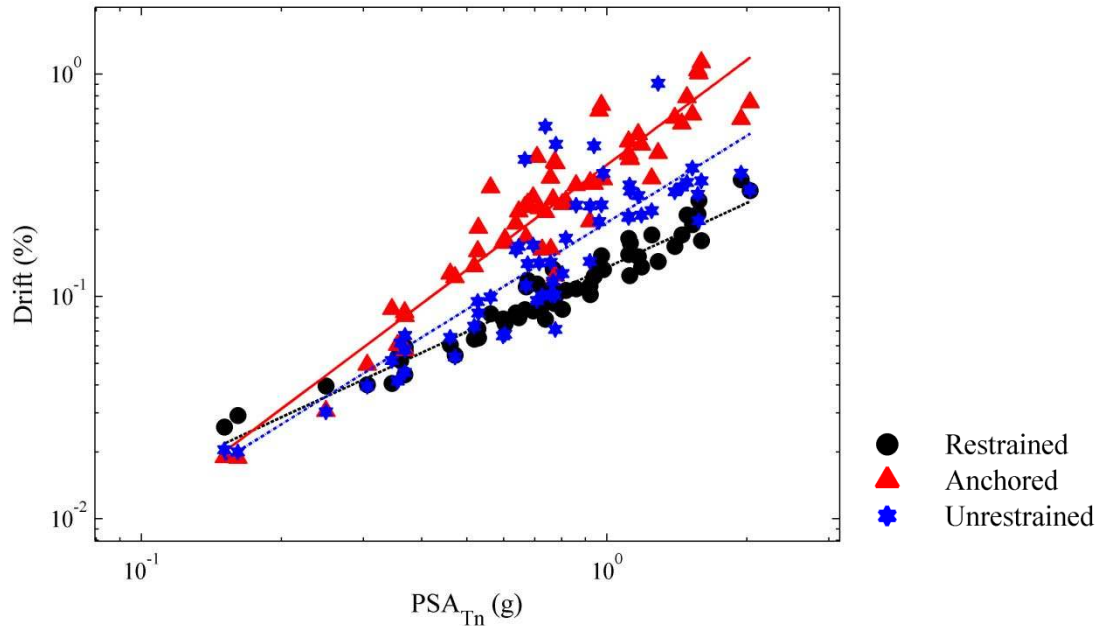
Figure 6.12 PSDMs describing global drift (δ) of the three models using PSA_{Tn} as the intensity measure

Figures 6.13 and 6.14 show the response accelerations at the top level of the three models in horizontal (front to back) and vertical directions respectively using PGV as the intensity measure. In both these figures, it is observed that the dispersions of all models in both directions are relatively large. In Figure 6.13, the horizontal accelerations of anchored and restrained models are relatively independent of the IMs, while those of unrestrained models are weakly correlated to IMs. As previously mentioned, the vertical accelerations without horizontal ground motion effect should be close to 0g, but their values fluctuate according to the horizontal ground motions and their local mode shapes. As shown in previous figures, the seismic responses of unrestrained models show high levels of dispersion, and their vertical accelerations are much higher than those of the other two models. As a result, electrical equipment which is vulnerable at high

acceleration levels should be restrained in order to improve the performance of vertical and horizontal acceleration as well as to reduce the uncertainty.
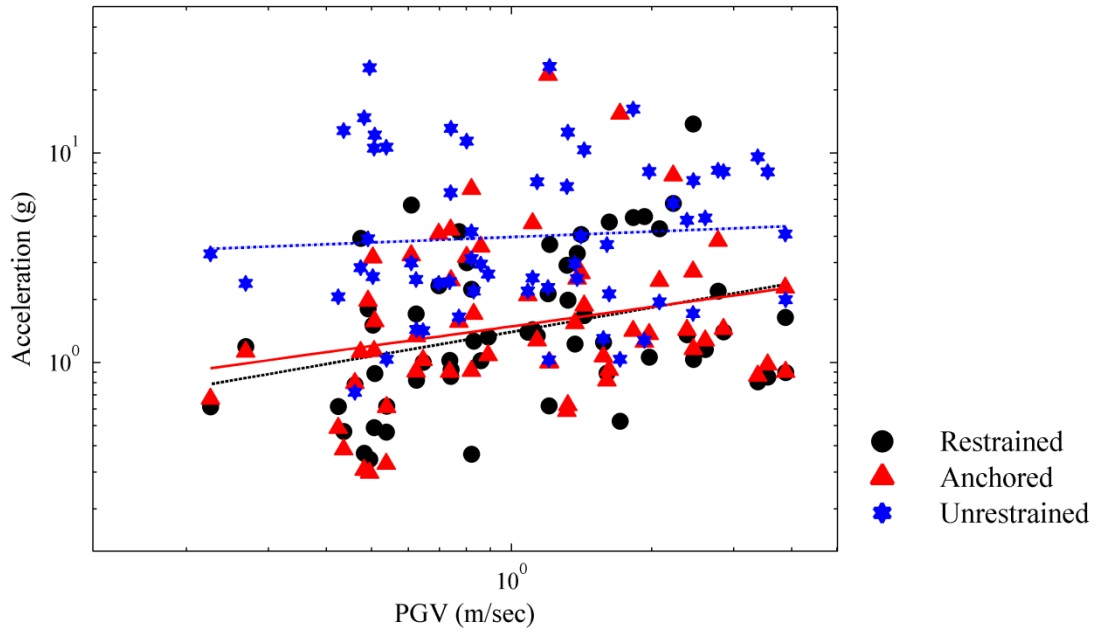
Figure 6.13 PSDMs describing acceleration (A_{tf}^H) in three models using PGV as the intensity measure
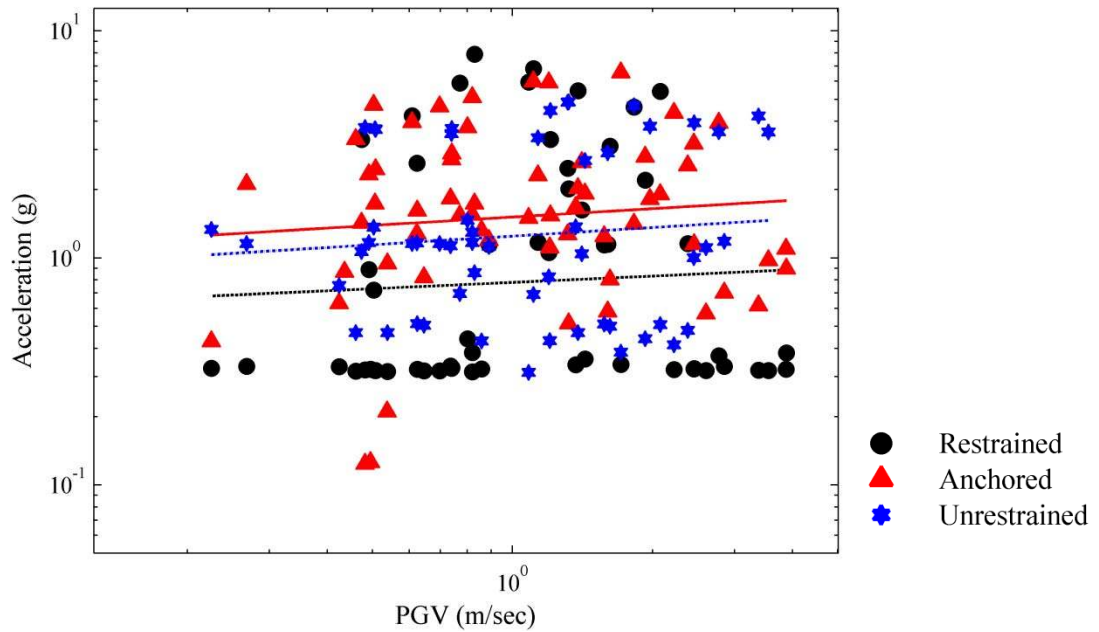
Figure 6.14 PSDMs describing acceleration (A_{tf}^V) in three models using PGV as the intensity measure

Figure 6.15 show the PSDMs of screw deformation obtained using the three models involving different support conditions. As described in the previous chapters, the yield deformation is about 2 mm. The maximum deformation of the screws in the unrestrained models reaches the yield deformation when subjected to most of the ground motions in the suite.
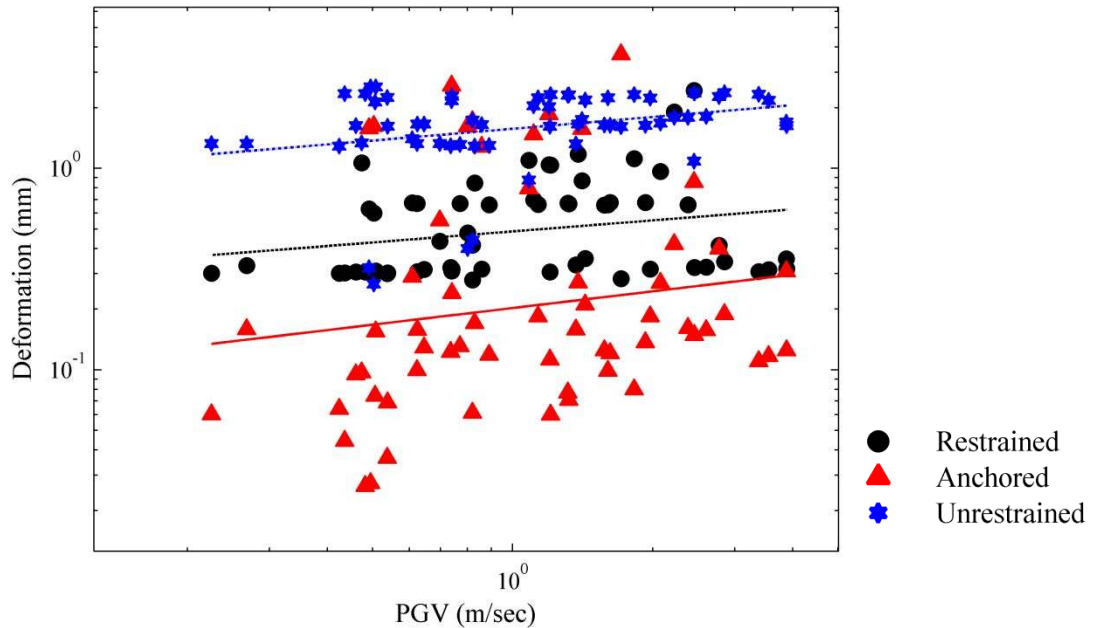
Figure 6.15 PSDMs characterizing screw deformation (Δ_s) in three models using PSA_{Tn} as the intensity measure

6.4 Closure

A methodology for developing probabilistic seismic demand models of electrical cabinets was presented in this chapter. The proposed method was used to describe the behavior of switchboard cabinets with different boundary conditions under various intensities of input ground motions.

The probabilistic seismic demand models (PSDMs) of different components of switchboard cabinets were generated by computing their nonlinear responses to a suite of ground motions that represent the uncertainty in seismic characteristics such as magnitude, distance and frequency content. The nonlinear time history analyses were performed using finite element models with three different boundary condition cases representing anchored, restrained and unrestrained conditions at the base. Several intensity measures (IMs) such as peak ground acceleration (PGA), spectral acceleration at 0.1 sec period (PSA_{Tn}), average spectral acceleration (PSA_{Avg}) for the frequency range of 4-16Hz, peak ground velocity (PGV), and peak ground displacement (PGD) were.

1. PSA_{Tn} was identified as the most practical and efficient IM for response displacement and drift across all three boundary conditions models. However, it was found that PGV was a more efficient IM for response acceleration of the unrestrained model.

2. PSDMs of total displacement (ΔT) at the top of the cabinet, as well as drift (δ) between top and base, were well represented in all three cases by linear regression models. The response measures are dependent on PSA_{Tn}, and their dispersions were found to be very small. Total displacements in the unrestrained model were larger than those of the anchored model, but global drifts in the unrestrained model were smaller than those of the anchored model due to sliding behavior.

3. PSDMs of absolute accelerations were developed at two locations in both horizontal and vertical directions. The dispersions of response acceleration in all models were larger than those of the response displacements or global

drifts. PSDMs of horizontal and vertical accelerations in restrained and anchored models were relatively dependent on PSA_{Tn}, PSA_{Avg}, and PGA, in contrast to the case of the unrestrained models where there was negligible dependence on the IM.

4. As PGA, PSA_{Tn}, or PSA_{Avg} increase, expected physical damage on restrained, anchored, and unrestrained models proportionally increase based on the total displacement and global drift. The malfunction probability of switchboard cabinets due to high accelerations also increases, as IMs increase. However, vertical and horizontal response accelerations in restrained and anchored models are characterized by large uncertainty exhibited by high values of dispersion.

5. The uncertainty associated with every seismic response measure of the unrestrained model is significant and the local part of this model can reach high response accelerations at lower PGAs. In addition, the horizontal and vertical response accelerations of this model are rarely dependent on PGA, PSA_{Tn}, or PSA_{Avg} which are the most commonly adopted intensity measures for electrical equipment.

6. Use of restrained boundary conditions reduced the seismic vulnerability of electrical equipment and also minimized the uncertainty of seismic behaviors such as displacement, drift, and vertical and horizontal accelerations.

CHAPTER VII

SUMMARY AND CONCLUSIONS, IMPACT, AND FUTURE WORK

7.1   Summary and Conclusions

The seismic performance of switchboard cabinets in building power distribution systems has been examined in previous studies in order to assess the seismic vulnerability and possible damage states of these cabinets in buildings and public service facilities. These studies have pursued different approaches: empirical data and surveys, shake table testing, and numerical models. However, the studies carried out to date do not address the wide range of switchboard cabinets used in buildings, nor do they consider the complex interactions between components within the cabinets.

The present study has provided simplified nonlinear numerical models based on the finite element method for use in investigating the seismic behavior of switchboard cabinets. First, their dynamic characteristics such as fundamental frequencies and mode shapes were determined using linear modal analysis. It was shown that the presence of steel plates which enclose the cabinet framework significantly increased the fundamental frequencies of the cabinets so that they behaved similar to a steel box. The local modes of these steel plates influenced the fundamental frequencies of cabinets, and the properties of significant overall modes were determined by the superposition of global and local modes. It was also found that the switchboard fundamental frequencies are sensitive to the stiffnesses of the bolted connections in the frames as well as to the

support boundary conditions at the base of the cabinets. The support boundary conditions played an important role in the determination of global behavior of relatively rigid electrical switchboard cabinets characterized by high fundamental frequencies.

In order to consider the highly nonlinear behavior of electrical switchboard cabinets at the base supports, numerical models using rigid bodies for the cabinet but having geometrically and materially nonlinear boundary conditions were developed. These numerical models were capable of capturing the various motions of both restrained and unrestrained cabinets, including resting, sliding, rocking, pounding, and up-lift. Numerical models of switchboard cabinets were validated by comparing the results of time history dynamic analysis to analytical solutions. It was observed that numerical models are more versatile because they can be used to study a range of cabinets having complicated geometry, eccentric connections and different support locations for equipment enclosed within the cabinet. These models were extended to anchored models which behave nonlinearly under seismic effects.

Combining the finite element models of switchboard cabinets and nonlinear support boundary conditions, comprehensive nonlinear numerical models were developed for use in the assessment of the dynamic behavior of the cabinets during seismic excitation. Three different boundary conditions at the base of switchboard cabinets were considered: (1) fully restrained, which represents a fully fixed condition without any deformation at the support; (2) anchored, which includes bolted connections with nonlinear force-deformation relationships connecting the switchboard cabinets to the ground; and (3) unrestrained, which represents a free-standing cabinet without any restraint. These models with different support boundary conditions were analyzed using nonlinear time

history analyses. The seismic responses from the three models were computed and compared using response measures including displacement, acceleration, drift, and deformation. As the amplitude of horizontal excitation increased, seismic response of anchored models entered the nonlinear range and their overall behavior changed significantly. It was observed that the vertical and horizontal response accelerations of anchored models greatly increased when very small deformations occurred at the location of anchor bolts. In addition, the total displacement of the unrestrained model was larger than the corresponding displacement in restrained and anchored models due to its sliding behavior, but the global drift of the anchored model was the largest due to the dominance of rocking behavior in its response. Because the response measures of all three models were dependent on the characteristics of ground motion time histories, a large number of ground motions representing various earthquake effects were required to investigate the seismic performance of these models.

In order to analyze the seismic performance of the three different nonlinear models, their probabilistic seismic demand models (PSDMs) were generated incorporating their nonlinear responses and a suite of ground motion time histories. This approach was presented as a methodology for possible use in future studies; an exhaustive vulnerability analysis was not conducted in this research program. Uncertainties in seismic demand are significant, and accordingly only uncertainties in the seismic demand were considered. Sixty sets of ground motions selected by the SAC Project (1997) were used to study responses of the numerical models. Seismic demands were characterized by several intensity measures (IMs), and the spectral acceleration (PSA_{Tn}) with a period of 0.1 seconds was identified as the most practical and efficient IM for response displacement

and drift across all three boundary conditions models. However, it was found that peak ground velocity (PGV) was a more efficient IM for acceleration response of the unrestrained model. Based on PSDMs for several components in the three models, it was found that total displacement at the top level of the cabinets and global drift could be well represented by linear regression models due to their high dependency on IMs and lower dispersions. It was observed that PSDMs of horizontal and vertical accelerations in restrained and anchored models were relatively correlated with PSA_{Tn}, average spectral acceleration (PSA_{Avg}), and peak ground acceleration (PGA), in contrast to the case in unrestrained models where the demand models are only weakly dependent on these IMs.

This study also provided a methodology for quantification of the seismic performance and uncertainty of the three models in terms of engineering demands such as total displacement, global drift, absolute acceleration in vertical and horizontal directions, and deformation of fasteners. As PGA, PSA_{Tn}, or PSA_{Avg} increase, expected physical damage to restrained, anchored, and unrestrained models increases proportionally based on the total displacement and global drift. The probability of malfunction of switchboard cabinets due to high accelerations also increases, as IMs increases. However, vertical and horizontal response accelerations in restrained and anchored models are characterized by large uncertainty exhibited by high values of dispersion. It was found that the uncertainty associated with every seismic response measure of the unrestrained model is significant and that local parts of this model can reach high response accelerations at lower PGAs. It was further observed that the horizontal and vertical response accelerations of this model are weakly dependent on PGA, PSA_{Tn}, or PSA_{Avg}, which are most commonly adopted intensity measures for electrical equipment. Based on the probabilistic seismic demand

analysis of the three models, it was observed that the use of fully restrained boundary conditions significantly reduced the seismic demands of electrical switchboard equipment as well as minimized the uncertainty of its seismic responses. However, further studies are needed to investigate the seismic performance of other types of cabinets with various boundary conditions.

7.2   Impact

This research provided a detailed and rigorous approach to evaluate the seismic response of electrical switchboard cabinets using numerical models. A methodology for developing probabilistic seismic demand models of electrical cabinets was also presented. The primary contribution of the research is the development of simplified numerical models of typical electrical cabinets, which can be used in future studies concerned with seismic vulnerability assessment of essential electrical equipment and electrical systems. Additional contributions of the research are as follows:

- This study provides a comprehensive framework within which the seismic behavior of electrical switchboard equipment can be evaluated. This framework starts with the introduction and description of the essential equipment in building electrical power systems and explains possible seismic damage to this equipment. The shortcomings of previous studies are highlighted and advanced finite element models are developed to utilize the efficacy of dynamic analysis procedures in their response prediction. The study also presents ways to analyze their dynamic responses and characterize them using probabilistic seismic demand models.

171

Seismic demand models provide a viable option to understand the dynamic behavior of electrical equipment and to define the correlation between the dynamic behavior of switchboard cabinets and the characteristics of earthquakes.

- Practical, computationally efficient, and versatile numerical models of switchboard cabinets are generated in this study in contrast to most of the previous research in this area. Use of these simplified models will result in significant reduction in the computational time required for a nonlinear time history analysis. A novel feature of these models is that they capture the critical nonlinear behavior of switchboard cabinets by including nonlinear force-deformation behavior of joint connections, which play a predominant role in dictating their dynamic response.

- Nonlinear time history analysis (NTHA) of the switchboard cabinets was performed using an expanded suite of ground motions with varying characteristics including magnitude, fault distance and frequency content. Through this analysis, the seismic response of components of interest in switchboard cabinets can be estimated using various engineering demand parameters such as total displacement, absolute acceleration, relative drift, and deformation of fasteners which are the best indicators of potential damage and vulnerability of electrical equipment.

- This study provides an enhanced understanding of the seismic behavior of switchboard cabinets using both linear and nonlinear dynamic analyses. While previous work has focused on the dynamic behavior of rigid bodies or the linear modal analysis of electrical cabinets, this study utilized both linear modal analysis

and nonlinear time history analysis of cabinets with highly nonlinear support boundary conditions in order to investigate the total seismic behavior of electrical cabinets under various conditions.

- The seismic behavior of cabinets having a full range of different support boundary conditions (fully restrained, partially restrained, and unrestrained) was considered in this study. In order to validate numerical results for cabinets having this range of boundary conditions, highly nonlinear numerical models were developed for use in NTHA, and the results were compared with analytical solutions for both sliding and rocking behaviors. These analyses included geometric as well as material nonlinearities. The models were used to quantify the effectiveness of a variety of restraint conditions used for electrical equipment when subjected to various seismic effects. Fully fixed, anchored with slight deformation, and unrestrained base conditions were considered in these studies.

- Through the probabilistic seismic demand analysis with a large number of ground motion time histories, this study evaluated the most practical and effective intensity measures for different demands on electrical equipment considering different boundary conditions. Results suggest that peak ground acceleration, spectral acceleration with a specific period, and average spectral acceleration, which are the most commonly used intensity measures, may not be practical or effective for the horizontal and vertical response accelerations of unrestrained models.

7.3   Future Work

The insights gained over the course of this research program suggest additional research in the following areas would be fruitful:

- The switchboard cabinets considered in this study are typical configurations from one manufacturer. Future studies should consider other configurations and types and characterize their seismic behavior. Such studies will provide an expanded database for use in the seismic vulnerability assessment of electrical equipment encompassing its diversity and complexity.

- This study considered one common type of anchor details for support boundary conditions. Consideration of other practical and varied details at the support boundaries such as welding, clipping, or bolting would be a useful expansion of this study of seismic behavior of not only electrical equipment but also other nonstructural components such as mechanical equipment.

- Future experimental studies should consider the use of system identification techniques to determine stiffnesses of linear connection. This approach is likely to lead to optimal agreement between the numerical models and shake table testing.

- Using the expanded database of seismic vulnerabilities of individual electrical equipment, seismic vulnerability assessment of the entire electrical system in buildings, hospitals, or public service facilities should be evaluated under various earthquake scenarios. This more comprehensive approach would provide a more reliable vulnerability analysis with uncertainties quantified in a proper and rigorous approach rather than one based only on expert opinion.

- The uncertainties from PSDMs in Chapter6 focused on seismic actions manifested by the response spectra. Future works would be more detailed uncertainty studies in cabinet and component vulnerabilities under known ground motions. The uncertainties would consider not only the mechanical characteristics of cabinets but also their functional capacity from component to system levels. In addition, a determined excitation such as a deterministic sine sweep test would strengthen the uncertainty studies of cabinets.

APPENDIX

A.1.   The Location of Screw Connections

The location of screw connections in FE models of the switchboard cabinets that are described in Chapters 3 and 5 are shown in Figure A.1. For each screw connection, nonlinear axial force-deformation and shear force-deformation relationships are considered. The initial stiffness of these models and their nonlinear force-deformation relationships are described in detail in Chapters 3 and 5 respectively.
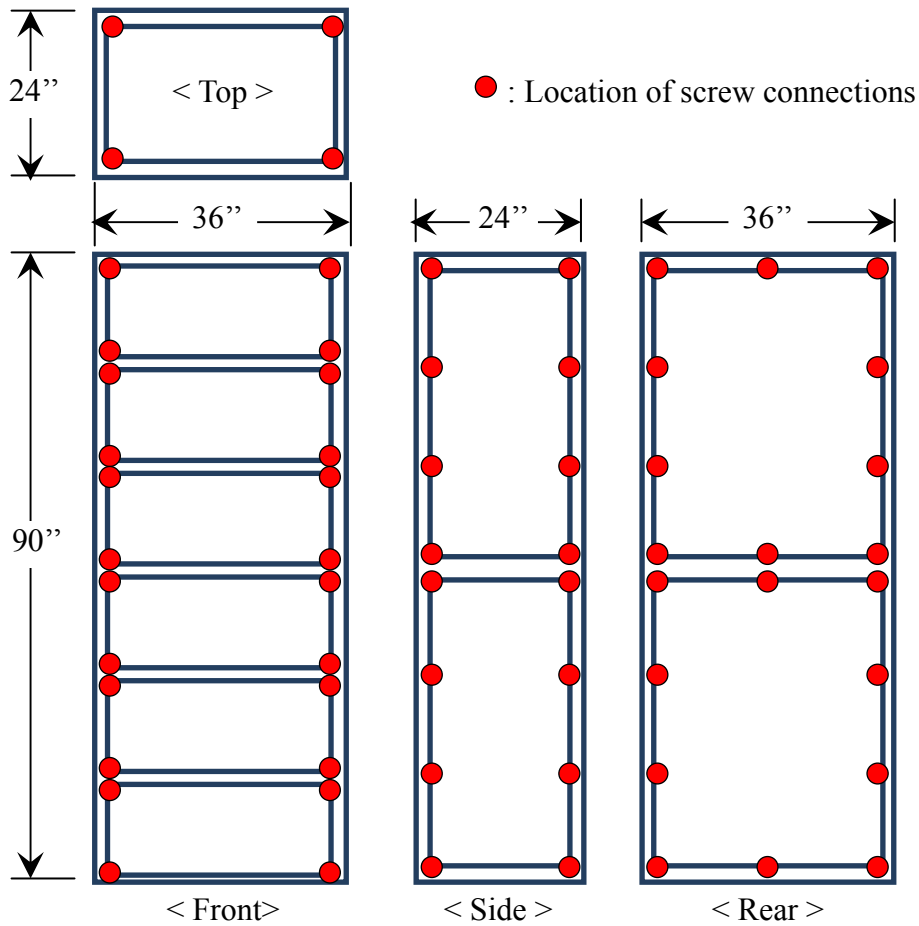
Figure A.1 Locations of screw connections

A.2.   The Discretization of the Plates in Cabinets

The discretization of top, front, side, and rear plates of cabinets in the FE models is shown in Figure A.2. As mentioned in Chapter 3, the top plate and side plats are divided into twenty-four shell elements, front plates are divided into twelve elements, and rear plates are divided into thirty-six shell elements with six elements per each edge.
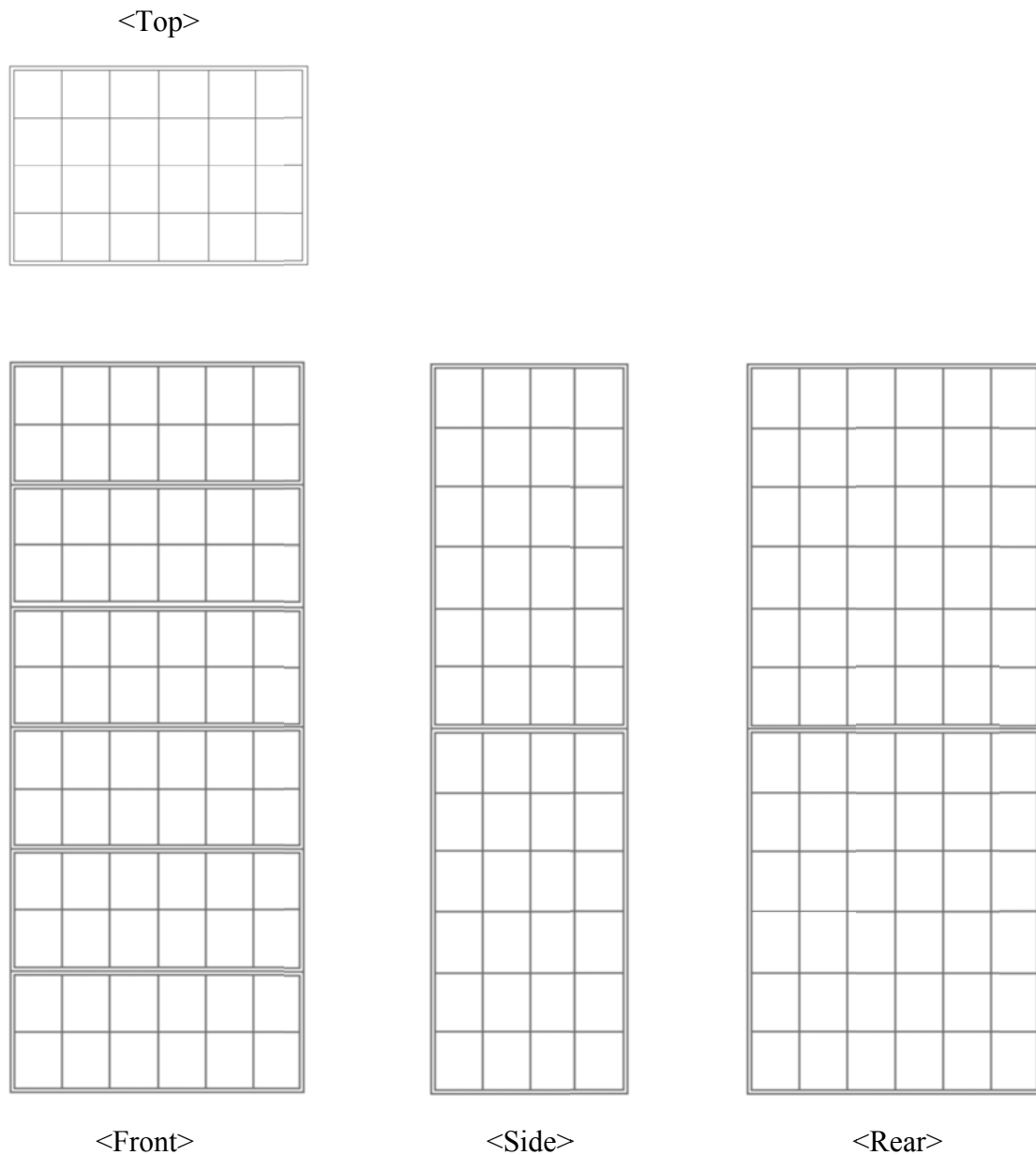
<Top>

<Front>   <Side>   <Rear>

Figure A.2 Discretization of top, front, side, and rear plates of cabinets in the FE models

A.3. The Change in the Fundamental Frequencies of Cabinets with Change in the Stiffness of the Connections

AISC (2005) provides moment-rotation (M-θ) relationships of various steel beam-column connections. These relationships are proposed by Salmon and Johnson (1980), and Bjorhovde, et al. (1987, 1990), and they are explained with three types as shown in Figure A.3. Type 1 (full rigid) connections are required to carry an end moment greater than or equal to 90% of the full fixity end moment of the beam and not to rotate more than 10% of the simple span rotation. A Type 2 (pinned) connection is allowed to resist an end moment not greater than 20% of the full fixity end moment and rotate at least 80% of the simple span beam end rotation. A Type 3 (partially rigid) connection lies between the limits of the Type 1 and Type 2 connections.
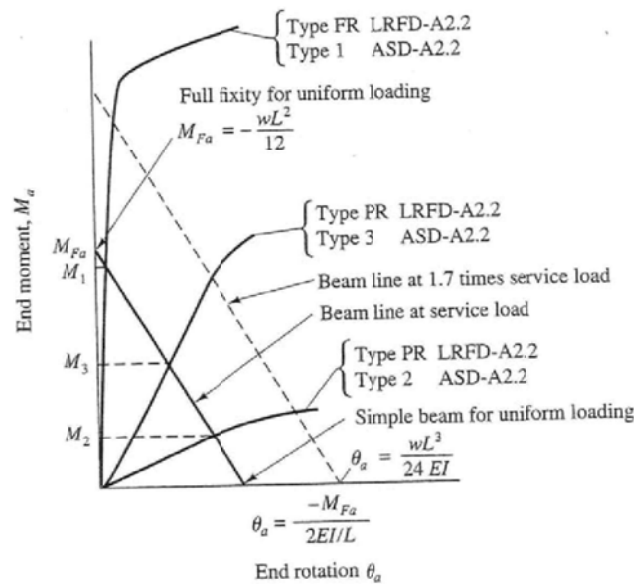

Figure A.3 Moment-rotation curves (AISC, 2005)

In order to investigate the effect of the initial stiffness of beam-column connections on the fundamental frequency of cabinets, several FE models which are described in Chapter 3 are analyzed with various values of rotational stiffness, k. The values of the rotational stiffness are chosen such that the connection behavior ranges from the fully

rigid connection to pinned connection behavior. Figure A.4. shows the beam to column connection and identifies the orthogonal axes about which the connection moments are defined. The coupling stiffness about the x-axis is assumed as rigid based on the analysis of detailed connection models in Chapter 5, while the coupling stiffnesses about the y- and z-axes are treated as variable parameters in the FE models.
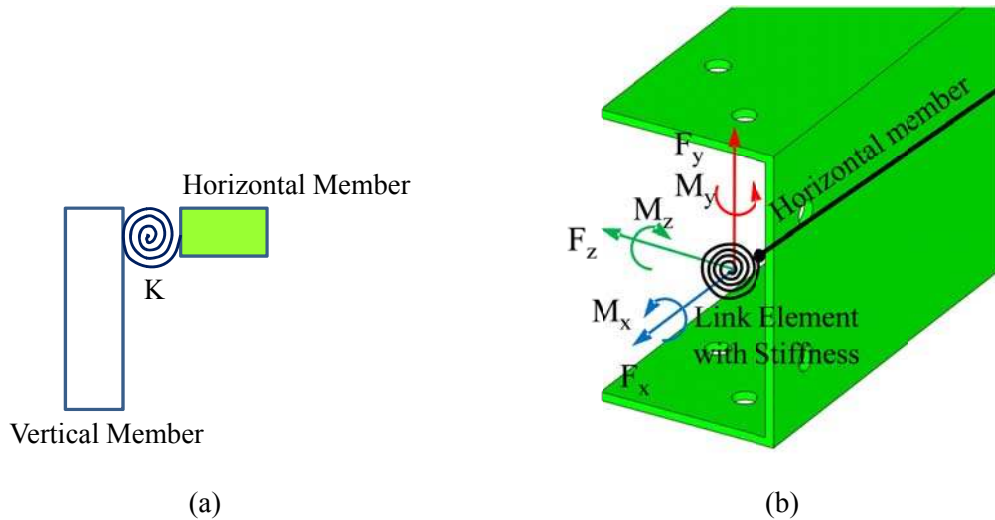
Figures. A.4 Stiffness of beam to column connection

In order to evaluate the effect of the finite rotational stiffnesses about the y and z axes, a connecting rotational spring of stiffness k is introduced in the FE model and the stiffness is defined in terms of a dimensionless parameter, K, as $k=K\cdot\frac{EI}{L}$ where EI is the bending stiffness and L is the length of the horizontal member. Thus K defines the relative rotational stiffness of the spring to the bending stiffness of the horizontal beam. Table A.1 presents the values of dimensionless rotational stiffness which is applied to all the beam-column connections in the FE models along with the corresponding equivalent k values and the resulting fundamental frequencies of the cabinet that are found using modal analysis. Figure A.5 illustrates the effect of rotational stiffness on the fundamental frequency of the cabinet. The figure shows clearly that the fundamental frequency is most sensitive to rotational stiffness in the range $0 < K < 2$ or from zero to about two

times the rotational stiffness of the horizontal beams. While this study considered only a single parameter, K, a more realistic analysis should consider different values of K for each connection axis throughout the structural model.

Table A.1 Fundamental Frequencies of Stiffnesses of Connections

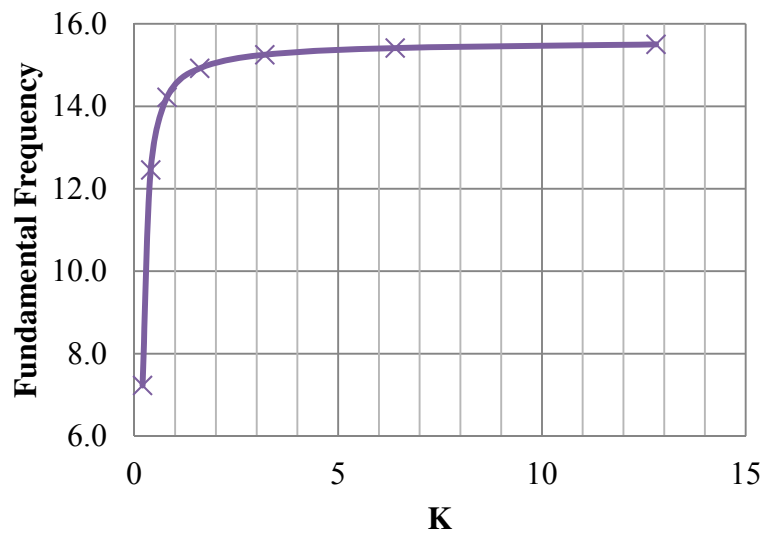| K (dimensionless)	0.2	0.4	0.8	1.6	3.2	6.4	12.8
$k_{Mz} = K*EIz/L$ (kip*inch/rad)	135	269	539	1077	2155	4309	8618
$k_{My} = K*EIy/L$ (kip*inch/rad)	28	56	112	224	449	898	1796
Fundamental Frequncy (Hz)	7.2	12.5	14.2	14.9	15.2	15.4	15.5

Figure A.5. The correlation of rotational stiffness and fundamental frequency of cabinet

181

REFERENCES

American Institute of Steel Construction (AISC). (2005). *Steel Construction Manual*, 14th Edition.

American Iron and Steel Institute (AISI). (2007). North American Standard for Cold-Formed Steel Framing-General Provisions, AISI S200–07.

Aslam, M,. Scalis, D., Godden, W.G., (1980) "Earthquake Rocking Response of Rigid Bodies", Journal of the Structural Division, Vol. 106, No. 2, February 1980, pp. 377-392

ATC − Applied Technology Council (1985), "Earthquake Damage Evaluation Data for California," Report ATC-13, Applied Technology Council, Redwood City, CA.

ATC − Applied Technology Council (2007), "Guidelines for Seismic Performance Assessment of Buildings," Report ATC-58, Applied Technology Council, Redwood City, CA.

BNL NUREG Report 52007, 1987, "Seismic Fragility of Nuclear Power Plant Components (Phase II)", Long Island, New York

Christopher Rojahn et al., 1985, ATC-13 Earthquake Damage Evaluation Data for California, Applied Technology Council

Constantinou, M.C., Tsopelas, P., Kasalanati, A., and Wolff, E.D. (1999). "Property modification factors for seismic isolation bearings". Report MCEER-99-0012, Multidisciplinary Center for Earthquake Engineering Research, State University of New York.

Cornell, C. A., Jalayer, F., Hamburger, R. O., Foutch, D. A., 2002. "Probabilistic basis for the 2000 SAC Federal Emergency Management Agency steel moment frame guidelines." Journal of Structural Engineering, 128(4), 526–533.

European Convention for Constructional Steelwork (ECCS). (2009). The testing of connections with mechanical fasteners in steel sheeting and sections, ECCS TC7 TWG 7.10, Mem Martins, Portugal.

Federal Emergency Management Agency (FEMA), 2011. "Reducing the Risks of Nonstructural Earthquake Damage." Report No. FEMA- E74, Washington D.C., NY.

Filatrault, A and Matt, H. (2006), "Seismic Response of High Voltage Electrical Transformer-Bushing Systems," Jounal of Structurl Engineering, pp. 287-295

Garcia, D.L., Soong, T.T., (2003), "Sliding fragility of block-type non-structural components. Part 1: Unrestrained components", Earthquake Engineering & Structural Dynamics, Volume 32, Issue 1, pages 111–129,

Garcia, D.L., Soong, T.T., (2003), "Sliding fragility of block-type non-structural components. Part 2: Restrained components", Earthquake Engineering & Structural Dynamics, Volume 32, Issue 1, pages 131–149,

Gatscher, J.A., McGavin, G.L., Caldwell, P.J., 2012, "Earthquake Protection of Building Equipment and Systems", ASCE, Reston, VA

Gatscher, J.A., Caldwell, P.J., Bachman, R.E., and Littler, S.R.(2004), "Seismic qualification testing of nonstructural components and equipment," Proceedings of the 2004 Structures Congress - Building on the Past: Securing the Future, 2004, pp. 841-852

Giovenale, P., Cornell, A. C., Esteva, L., 2004. "Comparing the adequacy of alternate ground motion intensity measures for the estimation of structural responses." Earthquake Engineering and Structural Dynamics, 33(8), 951-979.

Goodno, B. J., Craig, J. I., Hur, J-. E., Gould, N., Feser, E., Navarro, C., and Spencer, B. F., (2007). "Nonstructural Seismic Evaluation of the MLGW Operations Center", Internal Report, Mid-America Earthquake Center, University of Illinois, Urbana, IL.

Goodno, B. J., Gould, N. C., Caldwell, P., Gould, P. L., (2011), "Effects of the January 2010 Haitian Earthquake on Selected Electrical Equipment", Earthquake Spectra, Volume 27, No. S1, pages S251–S276.

Gupta, A., Rustogi, S. K., and Gupta, A. K. (1999). "Ritz vector approach for evaluating incabinet response spectra." Nuclear Engineering and Design, 190(3), 255–272.

Hancock, G., Murray, T., and Ellifritt, D. (2001). "Chapter 9: Connections" Cold-Formed Steel Structures to the AISI Specification, Marcel Dekker, Inc, New York.

International Code Council (2010), ICC-ES AC 156, "Acceptance Criteria for Seismic Certification by Shake-Table Testing of Nonstructural Components"

IEEE Standard 693-2005, (2005), "IEEE Recommended Practice for Seismic Design of Substations," The Institute of Electrical and Electronics Engineers

Llambias, J. M., Sevant, C. J., and Shepherd, D. J. (1989). ''Nonlinear response of electrical cubicles for fragility estimation.'' Trans. 10th Int. Conf. on Structural Mechanics in Reactor Technology, Anaheim, Calif., 893–897.

Luco, N., Cornell, A. C., (2007). "Structure-specific scalar intensity measures for near-source and ordinary earthquake ground motions." Earthquake Spectra, 23(2),357-392.

Makris, N. and Zhang, J. (2001) "Rocking Response of Anchored Blocks Under Pulse-Type Motions." Journal of Engineering Mechanics, ASCE, 127(5), 484-493.

Makris, N. and Zhang, J. (1999), "Rocking Response and Overturning of Anchored Equipment under Seismic Excitations," PEER Reprot, Pacific Earthquake Engineering Research Center, College of Engineering, University of California, Berkeley

Melchers, R. E. (2002), Structural Reliability Analysis and Prediction, Second Edition, John Wiley & Sons, Inc., New York.

NUREG - U.S. Nuclear Regulatory Commission (2006), "Recommendations for Revision of Seismic Damping Values in Regulatory Guide 1.61," NUREG/CR-6919, BNL-NUREG-77174-2006, Office of Nuclear Regulatory Research, Washington, DC

NUREG - U.S. Nuclear Regulatory Commission (1987), "Seismic Fragility of Nuclear Power Plant Components [PHASE II]," NUREG/CR-4659, BNL-NUREG-52007, Vol. 2-4, Department of Nuclear Energy, Brookhaven National Laboratory, Long Island, NY

Padgett, J. E., Nielson, B. G., DesRoches, R., (2008), "Selection of optimal intensity measures in probabilistic seismic demand models of highway bridge portfolios." Earthquake Engineering and Structural Dynamics, 37(5), 711-725.

Porter, K., Johnson, G., Sheppard, R., and Bachman, R., (2010), "Fragility of mechanical, electrical, and plumbing equipment", Earthquake Spectra 26, 451–472.

Porter, K.A., Kiremidjian, A.S., and LeGrue, J. S.(2001), "Assembly-Based Vulnerability of Buildings and Its Use in Performance Evaluation," Earthquake Spectra, Vol. 17, No. 2, pp.291-312.

Porter,K.A. (2005) "A Taxonomy of Building Components for Performance-Based Earthquake Engineering", PEER 2005/03, Pacific Earthquake Engineering Research Center, Richmond, CA

Rex, C. and Easterling, S. (2003). "Behavior and modeling of a bolt bearing on a single plate." Journal of Structural Engineering, ASCE, 129(6), 792-800.

Rustogi, S., and Gupta, A., (2004). "Modeling the Dynamic Behavior of Electrical Cabinets and Control Panels: Experimental and Analytical Results.", Journal of Structural Engineering, ASCE, 130(3),511-519.

SAC Joint Venture Steel Project Phase 2, (1997) , "Project Title: Develop Suites of Time" Histories, Pasadena, California

Salmon, C.G. and Johnson, J.E.,(2009), Steel Structures: Design and Behavior (4th Edition), Harper Collins College Publishers

Shampine, Lawrence F.; Reichelt, Mark W. (1997), "The Matlab ODE Suite", SIAM Journal on Scientific Computing 18 (1): 1–22

Shenton, H. W. (1996), "Criteria for initiation of slide, rock, and slide rock rigid body modes." Journal of Engineering Mechanics, ASCE, 122(7),690-693.

Shinozuka, M., and Masri, S., 2003, Seismic Risk Assessment of Nonstructural Components in Hospitals, ATC-29-2, Applied Technology Council

Shome, N., and Cornell, C. A. (1999), "Probabilistic seismic demand analysis of nonlinear structures." Reliability of Marine Structures Rep. No. RMS-35, Dept. of Civil and Environmental Engineering, Stanford Univ., Stanford, CA.

Szilard, R. (2004), "Theories and Applications of Plate Analysis: Classical Numerical and Engineering Methods", John Wiley

Taghavi, S., and Miranda, E., (2003). Response Assessment of Nonstructural Building Elements, PEER 2003/05, Pacific Earthquake Engineering Research Center, Richmond, CA

Taniguchi, T (2002). "Non-linear response analyses of rectangular rigid bodies subjected to horizontal and vertical ground motion Earthquake Engineering and Structural Dynamics, 31(8), 1481-1500

Uang, C., Sato A., Hong J., and Wood K. (2010), Cyclic testing and modeling of cold-formed steel: special bolted moment frame connections. ASCE, 136(8), pp 953-960.

Wen, Y. K., Ellingwood, B. R., and Bracci, J. M. (2004), "Vulnerability functions." Mid-America Earthquake Center, Univ. of Illinois, Technical Rep. No. DS-4, Champaign, Ill.

Whittaker, A. S., Fenves, G. L., and Gilani, A. S.J. (2007), "Seismic Evaluation and Analysis of High-voltage Substation Disconnect Switches," Engineering Structures, Vol. 29, pp. 3538–3549

Wyle Test Report 55636R08, (2008), "Seismic Testing on QED-2 & Speed-D Switchboard Configurations", Huntsville, Alabama

Yim, C., and Chopra, A., (1985), "Simplified earthquake analysis of multistory structures with foundation uplift." Journal of Structural Engineering, 111(12), 2708–2731.